SURFACE MODIFICATIONS OF THE ALUMINA CERAMIC FOR BIOMEDICAL APPLICATIONS

A Thesis

Presented to

the Graduate School of

Clemson University

In Partial Fulfillment

of the Requirements for the Degree

Master of Science

Materials Science and Engineering

---

by

Baris Kokuoz

August 2005

Advisors: Dr. Sarit B. Bhaduri and Dr. A. Cuneyt Tas

August 5, 2005

To the Graduate School:

This thesis entitled "Surface Modifications of the Alumina Ceramic for Biomedical Applications" and written by Baris Kokuoz is presented to the Graduate School of Clemson University. I recommend that it be accepted in partial fulfillment of the requirements for the degree of Master of Science with a major in Materials Science and Engineering.

S. Bhaduri

Sarit B. Bhaduri, Thesis Advisor

We have reviewed this thesis
and recommend its acceptance:

Igor A. Luzinov

Burtrand I. Lee

Burtrand I. Lee

A. Cuneyt Tas

A. Cuneyt Tas

Accepted for the Graduate School:

Gill Brunch Barnett

ABSTRACT

Surface of implant material is in direct contact with body environment. Therefore, successful implantation requires compatibility between physical and chemical properties of the surface and the body environment.

Bioinert ceramic materials (e.g. Alumina and Zirconia) provide unique properties such as high wear and corrosion resistance as well as the mechanical strength. Surface modification of these materials, either chemically or physically, is a suitable way to increase the biological acceptability of the material in the human body, without trading off bulk properties.

Alumina has been used for orthopedic and dental restorations for several decades. In the present study, Alumina surfaces were modified both physically and chemically to increase osseointegration and possibility of fixation.

The first approach was physical alteration of the surface by a simple etching process to introduce micron and nano-size surface irregularities to increase the available surface area for improved cell attachment. As a result of chemical etching, a thin film formation (sodium β-alumina) that enhances surface response to the biomimetic coating procedure in Simulated Body Fluid (SBF) was also observed

The second approach was directly coating alumina surfaces with a bioactive layer, such as Hydroxyapatite (HA). A novel method was introduced to achieve high quality HA coating on alumina surfaces. This method includes direct pyrolysis of the coating sol at relatively low temperatures. Resulting coatings (Ca-P coating) were also subjected to

biomimetic coating procedures to achieve bone-like apatitic coatings on alumina surfaces. Both physically and chemically modified surfaces were cell cultured with osteoblast-like cells to evaluate the effect of modifications.

TABLE OF CONTENTS

Table of Contents (Continued)

LIST OF TABLES

LIST OF FIGURES

List of Figures (Continued)

CHAPTER I

INTRODUCTION

1. Biomaterials

National Institutes of Health has formally defined a biomaterial to be "any substance other than a drug, or combination of substances, synthetic or natural in origin which can be used for any period of time as a whole or as a part of the system which treats, augments, or replaces any tissue, organ or function of the body" [1]. The uses of biomaterials include replacement of a body part that has lost function due to disease or trauma, to assist in healing, to improve function, and to correct abnormalities [2].

There are many factors, which influence implant biocompatibility such as implant size, morphology, chemical composition, porosity, surface texture, surface wettability and/or hydrophilicity, surface roughness, and surface charge.

For a material to be considered biocompatible, any undesirable reactions (such as fibrous encapsulation) that may develop at the blood/material or tissue/material interface must be minimal. This requires a biomaterial to interact as a natural material in the presence of blood and tissue. It might be much easier to define what a biomaterial should not be. A biomaterial should not cause thrombosis which is the formation or presence of a thrombus (a clot of coagulated blood attached at the site of its formation) in a blood vessel. It should not destroy and sensitize the cellular elements of blood or cause adverse

immune responses. An implant material should not alter plasma proteins (including enzymes) so as to trigger undesirable reactions, like malignant tumor or cyst formation. Lastly, it should not produce any toxic and allergic responses by the host tissue [3]. Most of the implant materials do not satisfy the above conditions completely, with the exception of calcium phosphates (CaP). This special case of calcium phosphates will be discussed later on Bioceramics section.

When a foreign material is placed into a biological environment, certain reactions take place between host and material. No synthetic material will be completely harmonious with the living environment; however, materials have different levels of reactivity. Implantable materials all have inherent morphological, chemical, and surface qualities, which cause responses from the surrounding biological environment.

There are three major types of biomaterials in terms of interfacial response of tissue: "nearly inert materials", "materials with controlled reactive surfaces", and "resorbable materials" [4].

When a bioinert material is used, a thin fibrous tissue typically encapsulates the implant to separate it from the host tissue. Bioinert materials are thus attached to the host only through mechanical interlocking. The fibrous tissue causes the lack of adhesion between the host and implant that results in motion of the tissue-implant interface under stress or deformation. Movement at the biomaterial-tissue interface eventually leads to deterioration in function of the implant or of the tissue at the interface or of both [5].

A surface reactive biomaterial is designed to form chemical bonds at the implant/host interface rather than minimize it. After implantation in the host, surface reactive materials form strong bonds with nearby tissue [6].

In contrast, a resorbable biomaterial is designed to be replaced ultimately by regenerating tissues, eliminating the original interface altogether [4].

The ultimate aim is to produce such implant materials that are able to imitate natural response upon implantation. Among various applications, bone substitutes are particularly challenging due to the chemical complexity and dynamic nature of the bone. Human bones consist of organic and inorganic portions with little amount of water. In that sense, bones are composite materials. Mineral portion of human bone is usually referred to as calcium hydroxyapatite (HA), having the chemical formula of $Ca_{10}(PO_4)_6(OH)_2$. In fact, biological apatite differs from pure HA in many ways. Bone mineral is non-stoichiometric, calcium-deficient (with respect to stoichiometric hydroxyapatite), poorly crystalline, carbonated, and contains small amounts of substitute atoms and groups. The more appropriate chemical formula for the bone mineral is $Ca_{10-x+v}Na_y(HPO_4,PO_4)_{6-x}(CO_3)_x(OH)_{2-x+v}$ for Na, K, and/or Mg inclusions and substitution of CO_3^{2-} for PO_4^{3-} or OH^- with the presence of Ca vacancies [7].

The design of bone substitute materials has to account for the biological activity of the body. Bones undergo constant remodeling, with the skeletal tissue being continuously resorbed and re-deposited in order to maintain skeletal integrity, shape and mass in unison with the biomechanical forces. Bone remodeling takes place primarily through three types of cells: "osteoblasts", "osteoclasts", and "osteocytes". Osteoblasts are responsible for bone mineral deposition. Thereby, they are also known as bone making cells. Osteoclasts are large multinucleate cells found in growing bone that resorb bony tissue. Osteocytes are branched cells embedded in the matrix of bone tissue, which orchestrate osteoblast and osteoclast activity. The continuance of normal bone integrity

and mass depends on interactions between osteoblasts, osteoclasts and osteocytes to keep the processes of bone resorption and formation in balance. Ideally, for a material to be used as a bone substitute, it has to take part in bone remodeling, has to maintain its mechanical properties during the remodeling process, and has to resorb in a controlled manner. If all the above criteria are satisfied, the result is the newly remodeled bone [8], with the disappearance of the original implant material.

The wide variety of biomaterials used for clinical applications can be divided into three categories based on chemical structure: "metals", "ceramics", and "polymers".

2. Bioceramics

A wide range of ceramic materials are currently used in biomedical applications, from chemically pure oxides, such as alumina, to the chemically complex bone-like calcium phosphates. [9]. Bioceramics can be categorized by their degree of chemical reactivity. Oxide ceramics are often used for their relatively inert behavior. At the other extreme, resorbable bioceramics are highly reactive in the physiological environment. Finally, surface reactive materials have intermediate reactivity and are designed to provide direct bonding.

Three broad categories of bioceramics based on chemical reactivity with the physiological environment have been defined by Hulbert *et al.* as illustrated in Figure 1.1 [10].

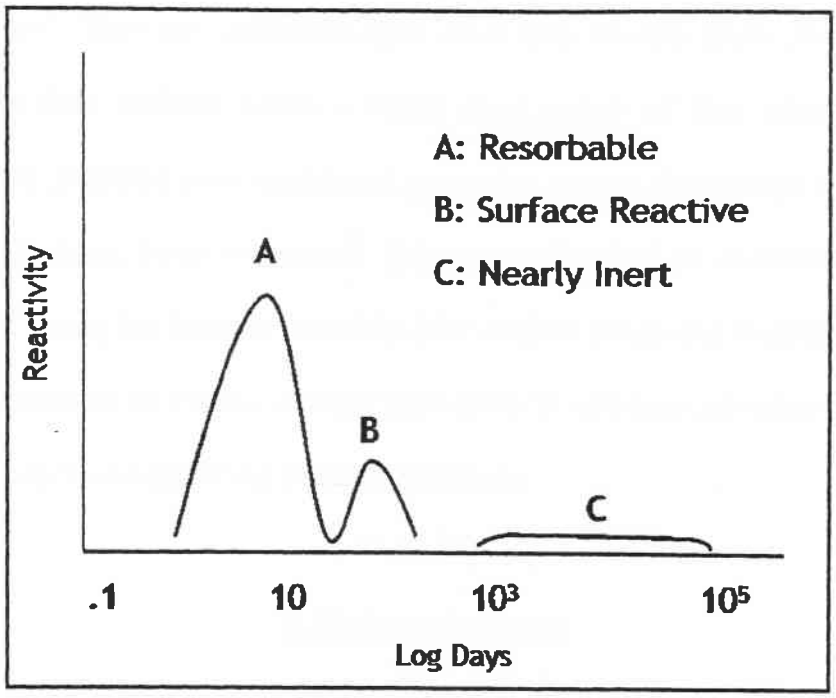

Fig. 1.1 Reactivity of Bioceramics in Physiological Conditions.

Relatively inert bioceramics, such as alumina and zirconia, tend to exhibit low levels of reactivity which peak on the order of 10^4 days. Surface reactive bioceramics, such as hydroxapatite (HA) and Bioglass®, have a substantially higher level of reactivity peaking on the order of 100 days. Resorbable bioceramics, as an example TCP (tricalcium phosphate, $Ca_3(PO_4)_2$), have even higher levels of reactivity peaking on the order of 10 days.

Calcium phosphates (CaP's) are biocompatible, nontoxic, resorbable, cause no inflammatory response, and have excellent osteoconductive ability [11]. In other words, calcium phosphates do not cause the formation of fibrous encapsulation observed as a result of the precautionary immune system response to numerous cytotoxic substances

when implanted. They are osteoconductive since they readily allow for *in vivo* bone formation on their surfaces within a rather short period of time after implantation. However, their inherited poor mechanical properties restrict their usage in load-bearing applications such as, bone substitutes. This eventually lead to extensive research on mechanically strong but bioinert materials (like surface processed titanium or nano-size alumina) as implants or various coating procedures to combine advantages of bioactive surfaces and mechanically strong substrate materials.

3. Bioinert Ceramics

Bioinert ceramics maintain their physical and mechanical properties while they are in the host, and they do not take part in the bone remodeling processes. They resist corrosion and wear under physiological conditions. Examples of relatively bioinert ceramics are dense and porous alumina, zirconia, and single phase calcium aluminates. Bioinert ceramics are typically used as structural-support implants [12]. Some of these are bone plates, dental implants, bone screws, and femoral heads.

3.1 Alumina (Al_2O_3)

High purity alumina has been used for biomedical devices because of its high strength and hardness values compared to other bioceramics. These superior mechanical properties make Al_2O_3 useful for load bearing applications, such as orthopedic and dental

implants. Table 1.1 presents some important mechanical properties of compact human bone, sintered hydroxyapatite and alumina for comparison.

To achieve osseointegration (bone ingrowth), an implanted ceramic must have an interconnected porosity, of 55 to 70%. Interconnected porosity together with pore sizes of 100-200 μm, allow osteoblasts to grow over and into the pores, leading to osteoid formation that can mineralize within the pores. It is a well known fact that with increased porosity, i.e. partially dense ceramic, mechanical properties of ceramic materials decline drastically. Thus, one has to be careful with the values shown in Table 1.1 since they are for fully sintered and dense ceramics, which may never find any biomedical applications or use due to their lack of required porosity.

For decades researchers have been investigating the biocompatibility of alumina in every aspect. Evaluation of biocompatibility is made to provide assurance that the final product will be safe for human use and perform as intended. *In vitro* (Latin: 'within glass') tests based on cell culture is the simplest and inexpensive method to analyze cytotoxicity, sensitization, systematic toxicity, and genotoxicity (mutagencity) which are associated with biocompatibility [17].

It is generally accepted that alumina undergoes no chemical change during long term exposure to the physiological environment. Several studies reported that alumina is non-cytotoxic [18-19] and do not cause any toxic reactions or mutation [20]. One another method of determining the biocompatibility of the candidate materials is to examine *in vitro* osteoblast attachment on those materials. Direct and tight attachment of bone on the materials is the main prerequisite for long-term clinical success of these implants. Bone formation depends mainly upon the metabolic activities of osteoblast cell. *In vitro* test

results using osteoblast-like cells showed well attachment and proliferation of cells on alumina surfaces [21]. Moreover, formation of contiguous cell layer with intimate cell-to-cell contacts was also observed on dense alumina samples [22].

Table 1.1 Mechanical Properties of Sintered, Non-porous Hydroxyapatite, Alumina and Human Compact Bone

	HA (ref. 13,14)	Al_2O_3 (ref. 15,16)	Compact human bone
Tensile Strength, MPa	38	250-300	49
Compression Strength, MPa	120	3450-4000	133
Hardness (HV), GPa	3.0-7.0	12.0-26.5	
Young's Modulus (*E*), GPa	35-120	380-406	17.0-18.9
Fracture Toughness, (K_{Ic}), $MPa.m^{1/2}$	0.8-1.2	3.0-4.1	2-12

Another important factor in determining the acceptance of implants is the plasma protein adsorption capacities [23]. After implantation, proteins immediately adsorbed on to the surface of the biomaterial. Thus, adherence of cells depends on the adsorption of plasma proteins.

In spite of the fact that numerous *in vitro* tests for durability and biocompatibility, as well as animal investigations, are undertaken before clinical use of implant devices,

In spite of the fact that numerous *in vitro* tests for durability and biocompatibility, as well as animal investigations, are undertaken before clinical use of implant devices, pathological analysis of explanted devices and long term histological evaluations help in the determination of their safety and efficiency. Long-term effects of alumina components and their performance were reported by Mittlemeier *et al.*, Dorlot and Piattelli *et al.* [24-26]. All these reports indicated successful implantation of both orthopedic and dental alumina components even under cyclic loading.

Cell behavior on biomaterial surfaces depends on implant cell interactions correlated with surface properties. Roughness, texture, chemical composition, charge and morphology strongly affect cellular responses in contact with the implant [27]. Increased surface roughness is associated with better cell adherence, higher bone-implant contact and improved biomechanical interaction [28]. Therefore, the effect of increased surface roughness on cell proliferation and activity was investigated and presented in Chapter 2. A chemical etching procedure to obtain rough surfaces is also described in detail in this chapter. Although, several reports indicated the effect of smaller grain size may have a positive effect on cell proliferation on alumina surfaces, it is beyond the scope of this study. Additionally, to test bioactivity and the apatite-inducing ability, the roughened alumina surfaces were soaked in synthetic body fluid (SBF) for a period of one week. The details of SBF soaking are given in Chapter 2.

4. Coatings

Although increasing the available surface area improves cell proliferation and enhances cell attachment, alumina still remains bioinert. As indicated above, HA is biocompatible and bioactive in human body. It rapidly interactes into human body and will bond to bone chemically. However, poor mechanical properties restrict its usage in bulk form for load-bearing applications such as orthopedics and dentistry. Coating hydroxyapatite onto mechanically strong materials is a promising solution to this problem. Thus, HA can exploit the biocompatibility and bone bonding properties, while the metallic or ceramic materials have the required mechanical properties. They benefit from the hydroxyapatite, which provides a bioactive layer for bone to bond contact and anchors the implant and transferring load to skeleton. Some techniques that have been used are summarized in Table 1.2. Among the techniques outlined in Table 1.2, thermal spraying/plasma spraying is the only commercially available method for producing HA coatings. The effect of high temperature procedures to the coating quality was outlined in section 3.1.

Hydroxyapatite coating using sol-gel process has several advantages. High purity coatings are processed at low temperatures, variety of starting chemical and small grain formations increasing the surface area can be count as the advantages of sol-gel process. However, long processing times (i.e. 24 hours or longer) are required to obtain high purity coatings and desired thickness. Chapter 3 investigates the possibility of forming HA coating on smooth alumina surfaces employing a similar process to sol-gel. This new

approach eliminates the long processing times by direct deposition of the coating on the surface.

Biomimetic coating is an *in situ* process to deposit an apatite layer on the surfaces of implants which is chemically similar to bone mineral under physiological conditions (at 37°C and pH 7.4). The coating medium is generally referred as simulated body fluid (SBF) [29]. Ca-P coating grown from a fluid at physiological conditions preserves the carbonated nature of apatitic phase since hydrogen carbonate groups cannot be maintained in the system temperatures higher than 650°C. Moreover, magnesium, sodium and potassium ions in SBF solutions are chemically incorporate into the structure of Ca-P coatings. Since coating procedure is taken place in fluid medium and ion concentrations are very similar to human blood plasma, Na^+, K^+, Mg^{2+}, CO_3^{2-}, HPO_4^{2-} and water are readily incorporate into the Ca-P coating [30]. Unlike high temperature methods (e.g. plasma spraying), biomimetic coating application deposits non-stiochimetric, carbonated, defective and poorly crystalline apatite which is similar to the bone mineral.

Chapter 3 also includes the conversion of HA coating obtained by direct deposition technique on dense alumina substrates into bone-like apatitic phase using SBF solutions. A detailed *in vitro* evaluation of crystalline hydroxyapatite coatings versus bone like apatitic phases was also included in Chapter 3.

Table 1.2 Comparison of Applicable Thickness, Advantages and Disadvantages of Different Coating Methods for Biomedical Applications.

Method	Applicable Thickness (μm)	Advantages	Disadvantages
Electrophoretic [31]	1-100	• Rapid deposition • Can coat complex shapes	• High temperature sintering • Non--uniform coating thickness
Thermal Spray [32,33]	10-1000	• High deposition rates • Inexpensive	• High temperatures induce decomposition • Can not coat complex shapes
Sputter Coating [34,35]	0.2-1	• Uniform coating thickness on flat surfaces	• Low deposition rate • Expensive • Time consuming
Sol-gel (spin and dip-coating) [35]	0.1-1000	• High quality coating • Low temperature processing	• Maximum applicable coating thickness • Time consuming (if multiple times application required)

References

[1] D. W. Friedman, P. J. Orland, R. S. Greco, "Biomaterials: An historical perspective," Implant Biology, R. S. Greco (ed.), CRC Press, Florida, pp. 1-11 (1994)

[2] J. B. Park, R. S. Lakes, "Introduction to Biomaterials," Plenum Press, New York, pp. 1-5 (1992)

[3] R. S. Wilson, S. L. Cooper, "In vitro and in vivo test methods for assessing blood-compatibility," Polymeric Biomaterials, E. Piskin, A. S. Hoffman (ed.), Martinus Nijhoff Publishers, Dordrecth, pp. 29-40 (1986)

[4] L. L. Hench, E. C. Ethridge, "Biomaterials An interfacial approach," Academic Press, New York, pp. 1-17 (1982)

[5] L. L. Hench, "Bioceramics," Journal of the American Ceramic Society, 81 (7) 1705-1728 (1998)

[6] W. G. Billotte, "Ceramic Biomaterials," Biomaterials principles and applications, J. B. Park, J. D. Bronzino (ed.), CRC Press, Florida, pp. 21-55 (2003)

[7] L. L. Hench, J. Wilson, "An introduction to Bioceramics," Advanced Series in Ceramics, 1 144-146 (1993)

[8] A. C. Tas, "Participation of calcium phosphate bone substitutes in the bone remodeling process: Influence of materials chemistry and porosity," Key Engineering Materials, 264-268 1969-1972 (2004)

[9] J. K. Shackelford, "Bioceramics," Materials Science Forum, 293 99-106 (1993)

[10] S. F. Hulbert, L. L. Hench, D. Forbes, L. S. Bowman, "History of Bioceramics," Ceramics in surgery, P. Vincenzini (ed.), Elsevier Scientic Publishing Company, Amsterdam, 1983, pp. 3-33

[11] P. Ducheyne, Q. Qiu, "Bioactive ceramics: the effect of surface reactivity on bone formation and bone cell function," Biomaterials, 20 2287-2303 (1999)

[12] W.G. Billotte, "Biomaterials, principles and applications," J.B. Park (ed), CRC Press, 2003, pp. 21-53

[13] W. Suchanek, M. Yoshimura, "Processing and properties of hydroxyapatite-based biomaterials for use as the hard tissue replacement implants," Journal of Materials Research, 13 (1) 94-117 (1998)

[14] K. S. Katti, "Biomaterials in total joint replacement," Colloids and Surfaces B: Biointerfaces, 39 133-142 (2004)

[15] I. J. McColm, "Ceramic hardness," Plenum Press, pp. 255-264 (1990)

[16] W. H. Gitzen, "Alumina as a ceramic material," The American Ceramic Society, pp. 43-62 (1970)

[17] J.H. Braybrook, "biocompatibility assessments of medical devices and materials," John Wiley & Sons, pp. 119-120 (1997)

[18] M. Fini, G. Giavaresi, N. N. Aldini, P. Torricelli, G. Morrone, G. A. Guzzardella, R. Giardino, A. Krajewski, A. Ravaglioli, M. M. Belmonte, A .D. Bneits, G. Biagini, "The effect of osteopenia on the osteointegration of different biomaterials: histomorphometric study in rats," Journal of Materials Science: Materials in Medicine, 11 579-585 (2000)

[19] I. Dion, L. Bordenave, F. Lefebvre, R. Bareille, CH. Baquey, J. R. Monties, P. Havlik, "Physico-chemistry and cytotoxicity of ceramics," Journal of Materials Science: Materials in Medicine, 5 (1) 18-23 (1994)

[20] Y. Takami, T. Nakazawa, K. Makinouchi, J. Glueck, Y. Nose, "Biocompatibility of alumina ceramic and polyethylene as materials for pivot bearings of a centrifugal blood pump," Journal of Biomedical Materials Research, 36 381-386 (1997)

[21] Y. Josset, Z. Oum'Hamed, A. Zarrinpour, M. Lorenzato, J. J. Adnet, D. L. Maquin, "In vitro reactions of human osteoblasts in culture with zirconia and alumina ceramics," Journal of Biomedical Materials Research, 47 481-493 (1999)

[22] A. D. Benedittis, M. M. Belmonte, A. Krajewski, M. Fini, A. Ravaglioli, R. Giardino, G. Biagini, "In vitro and in vivo assessments of bone-implant interface: a comparative study," International Journal of Artificial Organs 22 516-521 (1999)

[23] T. A. Horbett, "Protein absorption on biomaterials, biomaterials: interfacial phenomena and applications," American chemical society, 233-44 (1982)

[24] H. Mittelmeier, J. Heisel, "Sixteen-years' experience with ceramic hip prostheses," Clinical Orthopedics and Related Research, 282 64-72 (1992)

[25] J M. Dorlot, "Long-term effects of alumina components in total hip prostheses," Clinical Orthopedics and Related Research 282 47-51 (1992)

[26] A. Piattelli, G. Podda, A. Scarano, "Histological evaluation of bone reactions to aluminum oxide dental implant in man: a case report," Biomaterials, 17 711-714 (1996)

[27] K. Anselme, "Osteoblast adhesion on biomaterials," Biomaterials 21 667-681 (2000)

[28] D. Buser, R. K. Schenk, S. Steinemann, J. P. Fiorellini, C. H. Fox, H. Stich, "Influence of surface characteristics on bone integration of titanium implants. A histomorphometic study in miniature pigs," Journal of Biomedical Materials Research 25 889-902 (1991)

[29] T. Kokubo, H. Kushitani, S. Sakka, T. Kitsugi, T. Yamamuro, "Solutions able to reproduce in vivo surface-structure changes in bioactive glass-ceramic," Journal of Biomedical Materials Research, 24 721-734 (1990)

[30] E. I. Dorozhkina, S. V. Dorozhkin, "Structure and properties of the precipitates formed from condensed solutions of the revised simulated body fluid," Jornal of Biomaedical Materials Research, 67A 578-581 (2003)

[31] W. V. Raemdonck, P. Ducheyne, P. D. Meester, "Auger electron spectroscopic analysis of hydroxyapatite coating on titanium," Journal of te American Ceramic Society, 63 381-384 (1986)

[32] L. Sun, C. C. Berndt, K. A. Gross, A. Kucuk, "Material fundamentals and clinical performance of plasma sprayed hydroxyapatite coatings: a review," Journal of Biomedical Materials Research, 58 570-592 (2001)

[33] Y. C. Tsui, C. Doyle, T. W. Clyne, "Plasma sprayed hydroxyapatite coatings on titanium substrates Part1: mechanical properties and residual stress levels," Biomaterials, 19 2015-2019 (1998)

[34] J. L. Ong, L. C. Lucas, "Post-deposition heat treatments for ion beam sputter deposited calcium phosphate coatings," Biomaterials, 15 337-341 (1994)

[35] W. L. Jaffe, D. F. Scott, "Total hip arthroplasty with hydroxyapatite-coated prostheses," The Journal of Bone and Joint Surgery, 78A 1918-1934 (1996)

CHAPTER II

CHEMICAL ETCHING OF ALUMINA IN MICROWAVE-MELTED NaOH BATHS

Abstract

Dense and sintered alumina (Al_2O_3) is chemically inert to most chemical (either acidic or basic) treatments. Two of the most commonly used etching processes used for alumina are (1) thermal etching in air or in corrosive gases, and (2) etching within hot or boiling acids. Surface roughened aluminas are expected to display an increased level of attachment to the host tissue, i.e., long bones and jaw bones. Properly roughened alumina components, with a reproducible surface texture, should find numerous new uses in fields such as dental restorative and orthodontic fields.

Dense alumina substrates were placed in NaOH pellets and heated in a microwave oven for five minutes. The technique developed in this study caused the initial dissolution of alumina grains, accompanied by erosion of the surface, as well as the formation of sodium aluminate phases (e.g. $NaAl_{11}O_{17}$) on the nanorough surfaces. Cavitation morphology and surface chemistry were studied by SEM and XRD. Mechanical properties of the samples were determined before and after the etching process. The effect of sodium aluminate phase for biomimetic coating applications was investigated. Cell culture tests were also performed.

1. Introduction

Cell behavior on biomaterial surfaces depends on implant cell interactions correlated with surface properties. Roughness, texture, chemical composition, charge and morphology strongly affect cellular responses in contact with the implant [1]. It is well known that surface geometry determines the interactions of proteins and cells with the implant surface [2]. In that sense, a high degree of osseointegration can be achieved by large implant surface. Increased surface roughness is associated with better cell adherence, higher bone-implant contact and improved biomechanical interaction [3,4]. Thus, a rough structure enlarging the surface area of implant leads to an improved bone bonding surface without depending on coating methods [5]. Pillar *et al.* suggested that an increased roughness promotes the bone-anchoring ability of implant by increasing the interlocking capacity of the surface. Therefore, a favorable stress distribution will be obtained by the functional loading of an implant at the interface [6]. Additionally, it is reported that an increased surface roughness promotes osteoblast function [7,8].

Alumina is currently used for orthopedic and dental implants because of its bio-inertness, non-cytotoxicity and high strength [9-11]. Moreover, long term follow-ups showed the success of alumina implant materials especially for hip prostheses [12,13]. Single crystal alumina oxide has also been used in dental implants with some success [14].

For several decades, researchers have been investigating the corrosion behavior and etching of alumina for high temperature refractory applications. Dense, sintered alumina is chemically inert to most chemical treatments, and presents difficulties to etch

its surface. The surface irregularities created by etching would enhance subsequent micromechanical or chemical bonding of the sintered alumina substrates. Two of the well-known etching processes used for alumina are: thermal etching in air [15] or in corrosive gases [16,17], and etching within hot or boiling hydrofluoric, sulfuric or phosphoric acid [18,19]. Etching of alumina with hot or molten alkaline salts using conventional techniques has been reported previously [20-22]. Earlier interest in etching alumina was generally for the usage of the electronic packing industry and surface finish applications. Test conditions were varied from hot alkaline salt baths to molten alkaline salts for periods of minutes to days. None of those studies include microwave assisted etching of alumina in alkaline baths.

The second part of the research investigates the possibility of bone-like apatite formation on the chemically and morphologically modified alumina surfaces. Bone consists of an organic compound (20-25% weight), an inorganic compound (70%) and a water component (5%). The organic compound is largely Type I collagen, but also includes bone cells (Osteoblast, Osteocyte and Osteoclast) and a small amount of noncollagenous protein. The inorganic portion of the bone and teeth consist of hydroxyapatite (HA), predominantly in the impure calcium phosphate (CaP) form. Having the chemical formula of $Ca_{10-x}(HPO_4)_x(PO_4)_{6-x}(OH)_{2-x}$, it is also known as calcium deficient hydroxyapatite. Besides magnesium, sodium, and potassium, the chief constituent of the hard tissues (bones) is the poorly crystalline, calcium deficient, carbonate containing apatite phase.

Simulated body fluid has the ability to mimic human blood plasma since ionic concentrations of both are almost identical (like TAS-SBF or r-SBF). Furthermore, these

supersaturated Ca-P solutions have the ability to coat suitable metal and ceramic surfaces with bone-like apatite under physiological conditions. Different from stoichiometric HA both morphologically and chemically, this type of coating greatly increases the osseointegration. Few studies have been conducted to combine the advantages of biomimetic coating under physiological conditions and mechanically strong and bioinert ceramics like alumina and zirconia. Li *et al.* compared apatite inducing abilities of hydrated silica, titania and alumina in SBF coating solutions. Although, apatite formation was observed on titania and hydrated silica samples, they reported insufficient apatite formation on alumina surfaces even after three weeks in simulated body fluid [23]. Uchida *et al.* investigated apatite inducing ability of zirconia/alumina nano-composite in SBF solution after the samples were chemically treated by NaOH at 95°C for four days. They concluded that Zr-OH groups on the composite serve as the sites for apatite nucleation rather than Al-OH groups. They claimed that the positively charged Al-OH surface inhibits the apatite nucleation in simulated body fluid with pH 7.4 [24].

One solution might be forming an intermediate layer, which increases the affinity of the surface. In that sense, sodium β-alumina might be a suitable candidate. Sodium ions can be released from the alumina surface into the surrounding body fluid and substitution of Na^+ ions with H_3O^+ and/or Ca^{2+} may be effective for the apatite nucleation on the alumina surfaces.

The present study can be divided into two parts. First part investigates the chemical alkali etching of alumina surfaces assisted by microwaves. Additionally, effect of surface roughness on osteoblast proliferation and function is also investigated. Second

part of the research investigates the effect of surface chemistry changes due to the formed etching by-products on biomimetic coating applications.

2. Experimental Section

99.8% purity α-alumina substrates were purchased from CoorsTek® (CoorsTek Inc. CO, USA). Chemical analysis of alumina was obtained from the manufacturer and shown in Table 2.1. Received substrates were cut into 1x1 cm square samples for the handling ease with a diamond saw. Samples degreased in acetone and cleaned with distilled water in an ultrasonic bath.

Etching process is as follows: (i) alumina samples were placed at the bottom of a Pyrex® glass beaker. (ii) Al_2O_3 sample was completely covered by 15 g NaOH pellets (Fisher Chemicals, NJ, USA). (iii) Reaction beaker was placed in a domestic microwave oven (Sunbeam SBM7700W, LG Electronics, NY, USA) and microwave radiated (mid-power setting, 450 W) until NaOH became molten. The required time for the most preferred morphology is determined as 4 minutes additional radiation after NaOH became molten. Samples were recovered in boiling water and cleaned with distilled water in an ultrasonic bath for 15 minutes.

2.1 Surface Morphology & Chemistry

Surface morphology of the as-received and etched samples was studied by Field Emission SEM (Hitachi 3500, Hitachi 4700, Hitachi Corp. Japan). A XDS 2000 (XRD, Scintag Corp. USA) equipped with a monochromated Cu K_α radiation source was used to characterize surface chemistry. The scanning parameters that were used are scan range (2θ): 5-45°, step size: 0.03°, step time: 10 s.

Table 2.1 Chemical Composition of Alumina Substrates

Constituent	Al_2O_3	SiO_2	Fe_2O_3	MgO	Na_2O
Weight Percent (%)	99.82	0.02	0.01	0.07	0.08

2.2 Surface Roughness

Surface roughness was measured using a non-contact surface profiler (Mikro Precision Instruments, MN, USA). Three-dimensional profiles were drawn and analyzed. Five measurements were taken from three separately prepared samples to show the reproducibility. The three-dimensional surfaces were digitized into 736X480 points. Ra (average roughness), Rq (mean square root roughness), and finally Rz (peak-to-valley roughness) values were measured.

2.3 Mechanical Properties

The effect of the etching process on fracture toughness was tested according to ASTM C 674-88. Three-point bend test samples were cut into rectangular pieces made precisely to scale with regard to height to width ratio. An Instron (Instron Corp. MA, USA) universal testing machine equipped with a data acquisition software package (DAX) was employed to test total of 20 controls and etched samples. Span length and crosshead speed were 10 mm. and 0.05 mm/sec., relatively. Modulus of rupture (MOR) values were calculated and reported.

2.4 Biomimetic Coating

The effect of surface modifications (roughness and surface chemistry) were investigated *in vitro* using simulated body fluid (SBF). The SBF solution was prepared as suggested by Tas [25]. The ion concentrations of the solution is given in Table 2.2 [25,26]. To accelerate the coating procedure, the values shown in Table 2.2 were multiplied by the factor of 1.50 in preparing the SBF-coating solutions. Samples were placed onto a 45° inclined stainless steel net platforms. The samples were above the precipitation settling range. This procedure conducted to prevent loosely attached precipitates on the surface that are mostly seen if the substrates placed at the bottom of the bottles. The bottles were then sealed tightly and kept at 37°C, replenishing the SBF solution every 48 hours during soaking period.

Table 2.2 Preparation of SBF Solution (1 L)

Order	*Reagent*	*Weight (g)*
1	NaCl	6.547
2	$NaHCO_3$	2.268
3	KCl	0.373
4	$Na_2HPO_4 \cdot 2H_2O$	0.178
5	$MgCl_2 \cdot 6H_2O$	0.305
6	$CaCl_2 \cdot 2H_2O$	0.368
7	Na_2SO_4	0.071
8	$(CH_2OH)_3CNH_2$	6.057 (Tris-buffer solution)

Ion	*Human Plasma*	*SBF (mM)*
Na^+	142	142
Cl^-	103	125
HCO_3^-	27	27
K^+	5	5
Mg^{2+}	1.5	1.5
Ca^{2+}	2.5	2.5
HPO_4^{2-}	1	1
SO_4^{2-}	0.5	0.5

Ref. [26]

2.5 Cell Culture

7F2 rat osteoblast cells (CRL-12557, American type culture collection, Rockville, MD) were grown on 75 cm^2 culture flasks at 37°C and 5% CO_2 in alpha minimum essential medium with 2 mM 1-glutamine and 1 nM sodium pyruvate without ribonucleosides and deoxyribonucleosides, augmented by 10% FBS. The culture medium was changed every other day until the cells reached a confluence of 90-95%, as determined visually with an inverted microscope. The cells then were passaged using trypsin (2.5 g/L) / EDTA (25mM) solution (Sigma-Aldrich). The obtained cells were then seeded at a concentration of 100,000 cells/per well on 1 cm^2 alumina samples for various assays. Cell viability assessment was performed after 72 hours and total protein amount measurements were done after 7 days in a 24 well cell culture plate. The medium replenished after day one and then every two days during the course of the experiment. After the prescribed time period for each test, substrates were rinsed in phosphate buffered saline to remove any non-adherent cells. For statistics, all experiments were carried out in triplicate where n=3.

Cell viability. After 72 hours, the numbers of live and dead cells were counted on the substrates. Followed by removing the unattached cells, the attached cells were collected by trypsinization with 0.5% mL/well trypsin-EDTA solution and were incubated for 10 minutes. After the cells were collected in a conical tube, 1 mL of media was added and centrifuged for 5 minutes at 1000 rpm. The pellet formed at the base was resuspended in 1 mL of media. Finally, trypan blue was added and the cells were counted

under light microscope. Only cells that stain blue deemed necrotic due to the plasma membrane damage.

Total protein. The total protein amount was measured using BCA™ Protein Assay Kit (Pierce Biotechnology Inc., Rockford, IL). A working reagent (WR) was prepared by mixing 50 parts of BCA™ reagent A with 1 part of reagent B (50:1, reagent A:B). 200 µl of the above-mentioned WR was added to each well and thoroughly mixed. Following mixing, the cell culture plate was covered and incubated at 37°C for 30 minutes. The absorbance at 562 nm was measured with the spectrophometer at room temperature. A standard curve was prepared by plotting the average blank-corrected 562 nm measurement for each BSA standard curve versus its concentration in µg/mL. Protein concentration of each sample was then determined by using this standard curve.

All cell culture experiments were performed at Department of Bioengineering, Clemson University.

3. Results & Discussion

Sodium hydroxide pellets were not dissolved in a solvent (i.e. water). Instead, the etching reaction started only when microwave energy was introduced to the system in an open environment and under normal room conditions. To speed up the process, NaOH was selected because of its low melting point (318°C) relative to KOH (360°C). Direct temperature measurements cannot be performed since microwaves greatly disturb signals and give false information. On the other hand, using a pyrometer in direct temperature measurements is not possible because no color change was observed during treatment

period. Even though temperature measurements could not be performed, the temperature range of the system might be estimated. As mentioned Pyrex® glass beakers were used as reaction beakers and the melting point of the glass is reported as the manufacturer to be 700°C. No deformation or softening of the beakers was observed. It is then reasonable to assume that the temperature range of the reaction was between 320°C to 700°C.

Dissolution behavior of Al_2O_3 in molten NaOH could be better understood by studying the Na_2O- Al_2O_3 binary phase diagram. Earlier reports of thermodynamic properties and phase diagram for the Na_2O- Al_2O_3 binary systems had been summarized and critically evaluated by Eriksson *et al.* [27] The Na_2O- Al_2O_3 phase equilibria data were also evaluated by DeVries and Roth [28]. Thermodynamic data (e.g. entropies, heats of formation, heat capacities, and activities) for the crystalline phases in the Na_2O-Al_2O_3 system was reported by Spear and Allendorf [29]. The alumina-rich portion of the Na_2O- Al_2O_3 binary system in Figure 2.1 shows that crystalline β''-Al_2O_3 (nominally, $NaAl_{11}O_{17}$ for perfect crystal structure) can form if molten NaOH reacts with α-alumina for Al_2O_3 mole fractions $X_{Al2O3} > 0.9$. The dissolution reaction can be written as follows;

$$11Al_2O_3 + 2NaOH(l) \rightarrow 2NaAl_{11}O_{17} + H_2O(g)$$

Furthermore, but very unlikely, molten NaOH may react with β''-Al_2O_3 to form β''-alumina where Al_2O_3 mole fractions 0.68 are $< X_{Al2O3} < 0.9$.

In order to confirm the above analysis, fine Al_2O_3 powder (Sigma-Aldrich Corp.) were treated similarly (ultrasonic cleaning with DI-water excluded) for further XRD analysis (Figure 2.2). The results revealed the formation of sodium β-alumina after

molten NaOH treatment. Although fully crystalline α-alumina peaks suppressed newly formed sodium β-alumina peaks, two new peaks were observed clearly at 8° and 16°. The hump within the 30-35° 2-theta range can be associated to the low crystallinity beta alumina where several mid-intensity peaks are located in this range according to tabulated X-Ray data (ICDD, PDF # 21-1096). Besides the XRD data, etched surfaces further examined using EDS to determine amorphous silicon presence on the surface due t corrosion of the Pyrex beakers and dissolution of Si. Elemental mapping results did not show presence of any amount of Si on the surface.

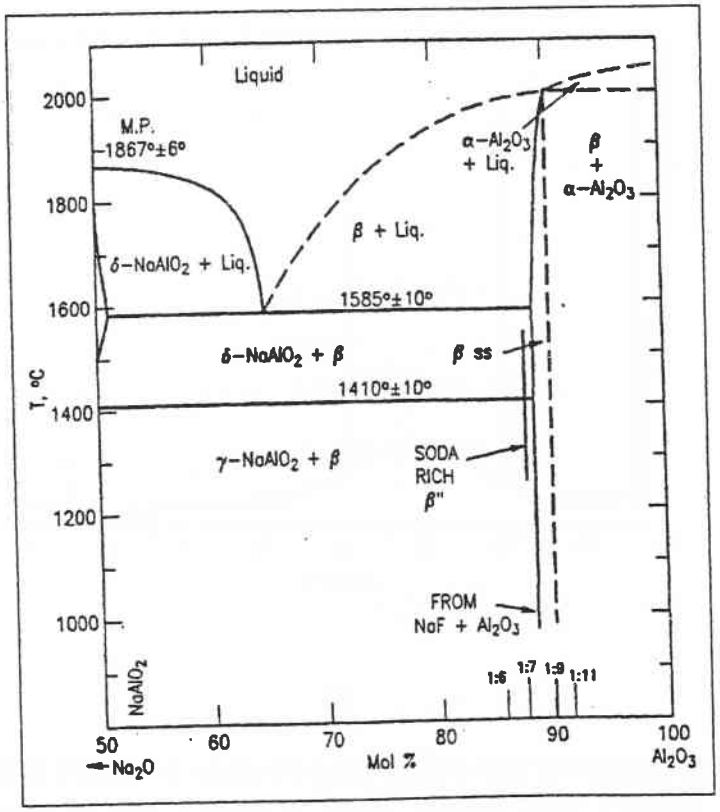

Figure 2.1 Alumina Rich Portion of N_2O-Al_2O_3 Binary Phase Diagram [28]

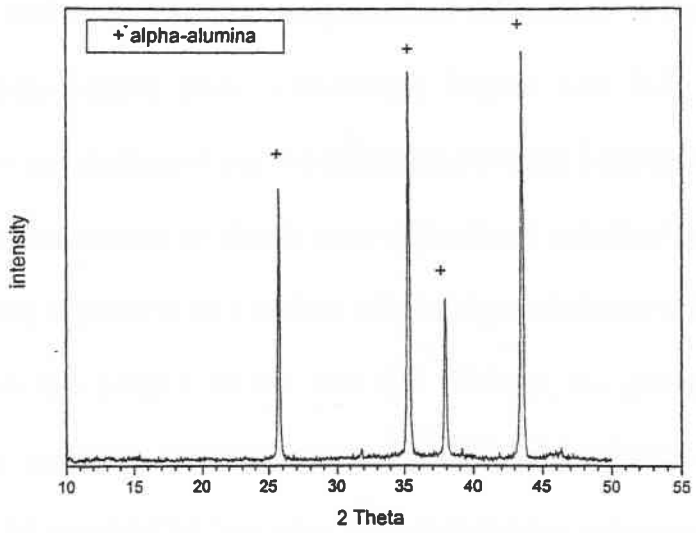

a)

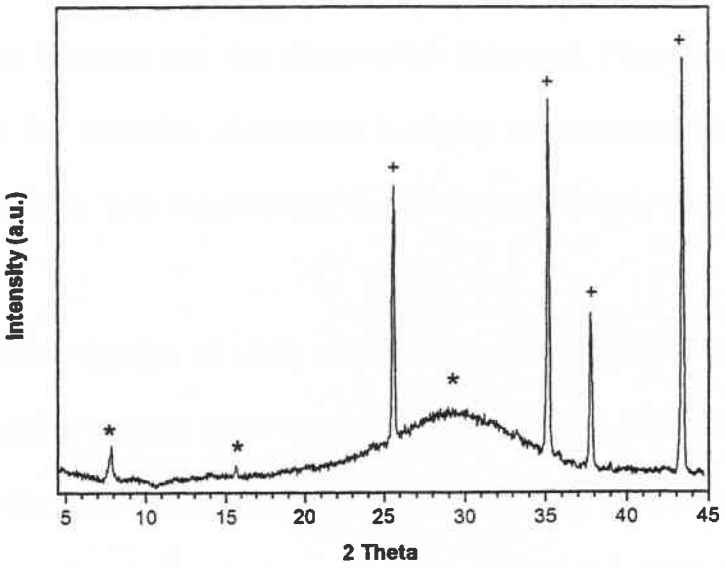

b)

Figure 2.2 a) XRD Pattern of Al_2O_3 Powder Prior to the Treatment Showing Single Phase Alpha Alumina. b) XRD Pattern of NaOH Treated Al_2O_3 Powder. (*) $NaAl_{11}O_{17}$, (+) α- Al_2O_3.

At temperatures higher than the melting point of NaOH, a chaotic alkaline melt formed and the molten NaOH vigorously attacked the surface of the ceramic (Figure 2.3 shows the alumina surface prior to treatment). Figure 2.4a, 2.4b, and 2.4d show the corroded surface morphology 4 and 8 minutes after NaOH became molten. 5-20 microns width cavity formations can be clearly seen with almost spherical geometry (Figure 2.4a and 2.4b). Etching appears to be a surface effect only because no etching was observed at any depth below the surface. In the first few seconds, the glassy phase at the grain boundaries was removed exposing the individual grains, further etching attacks the alumina grains. Molten NaOH, like other chemical etching techniques, etches selectively. It attacks grains with favorable orientations more readily, as can be seen in Figure 2.4c. Further etching causes new grains to be exposed under the surface (Figure 2.4d). A similar corrosion behavior was also observed by Sato *et.al.* They proposed formation of $Al(OH)^-_4$ phase for corrosion of alumina in highly concentrated NaOH solution [30]. They used relatively low temperatures (~160°C) and longer times compared to the present study.

The bending strength of Al_2O_3 corroded in molten NaOH is shown in Figure 2.5. The average flexural strength value was found to be 312 ± 31 MPa prior to the treatment and 215 ± 16 MPa after 4 minutes etching in molten NaOH. The average flexural strength value was decreased by 31% ± 2 after etching. The calculated weight loss of the samples measured before and after etching was found to be 0.35-0.5%. Although weight loss was less then 1%, large cavity formations on the surface greatly degraded the bending strength of alumina.

Roughness parameters were calculated and are presented in Table 2.3. Three-dimensional images showed that peak and valley formations are evenly distributed across the surface (Figure 2.6).

Several studies reported a good correlation between increased Ra value and bone anchorage [31, 32]. Li *et al.* evaluated implant removal torque for titanium implants placed in the alveolar crest of mini-pigs after 3 months. Two implants were compared: treated by either sandblasted and acid etched (SLA) or the machined and acid etched surface (MA). The surface with the highest Ra of Ti showed the highest anchorage and higher removal torque [33]. The results showed a strong correlation between Ra and the removal torque values. From a biomechanics view point, one can expect to have the same results for alumina surfaces with similar morphologies and roughness.

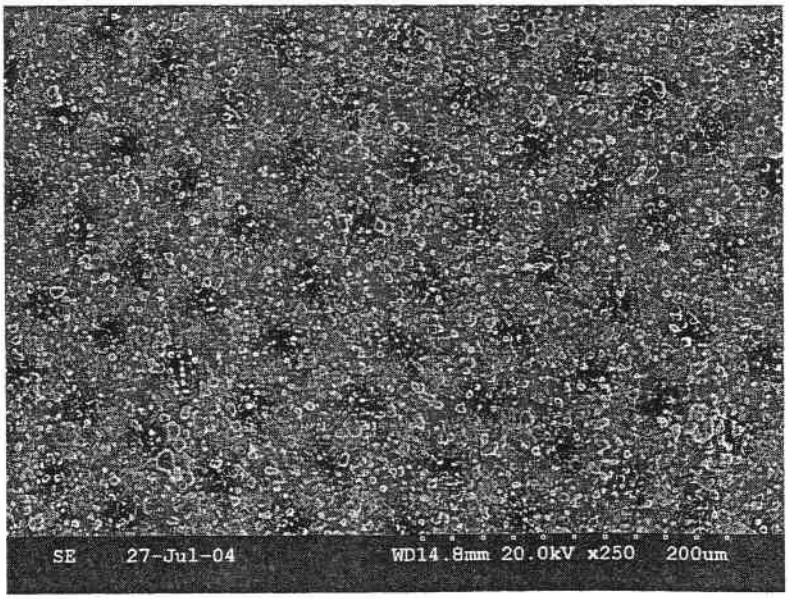

Figure 2.3 Alumina Surface prior to treatment

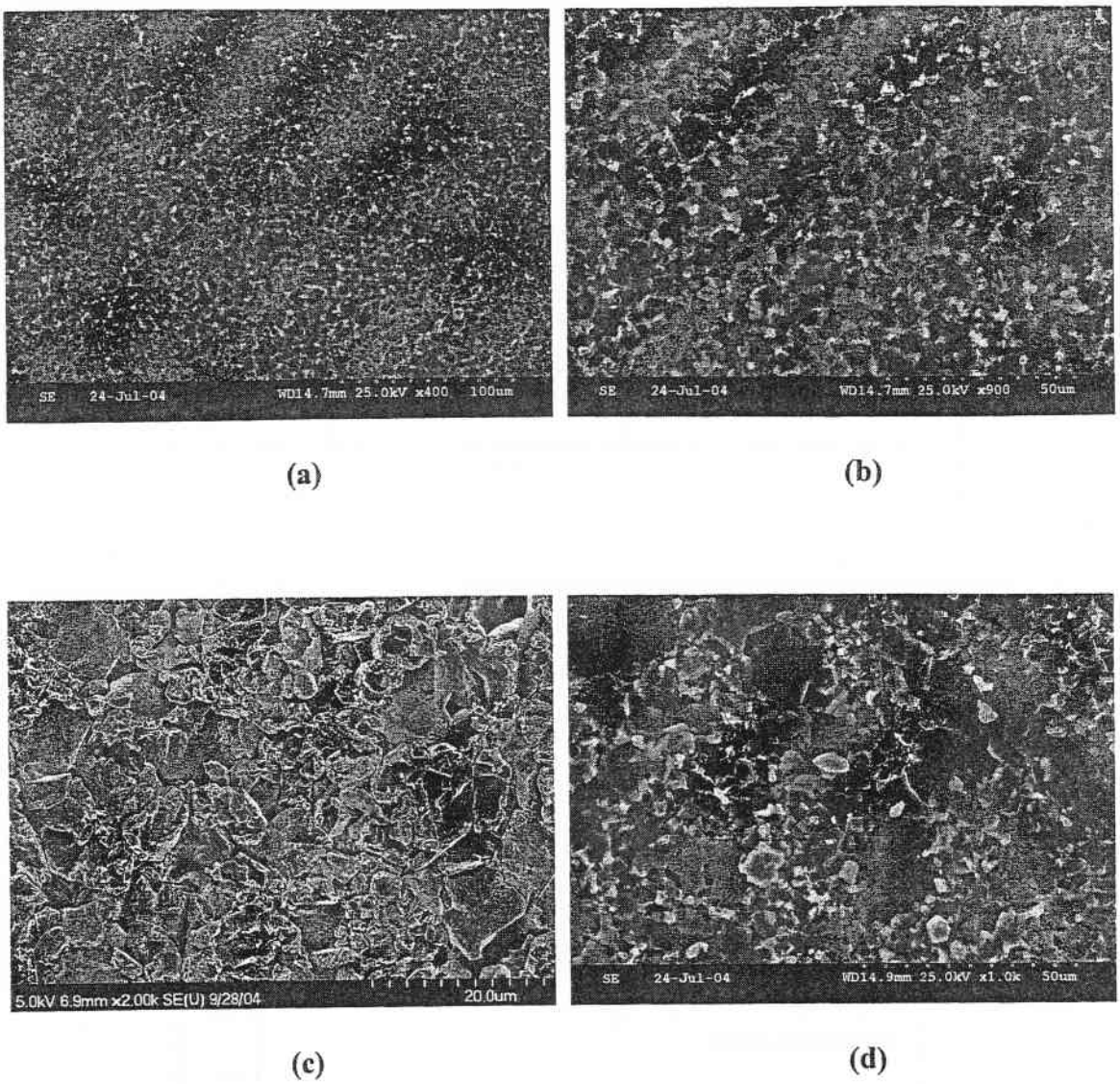

Figure 2.4 SEM Micrographs of (a) Surface Morphology after NaOH Etching 4 min. after NaOH Became Molten, (b) Higher Mag. Image of the Surface, (c) Dissolution of Individual Grains with Preferred Orientations 3 min. after NaOH Became Molten, (d) Surface Morphology 8 min. after NaOH Became Molten Exposing the New Grains Under Surface.

Table 2.3 Surface Roughness Values Before and After Etching.

	As-received Al_2O_3	Surface Etched
Ra (μm)	0.84±0.15	1.45±0.22
Rq (μm)	1.02±0.21	1.82±0.55
Rz (μm)	8.30±1.44	13.35±2.85

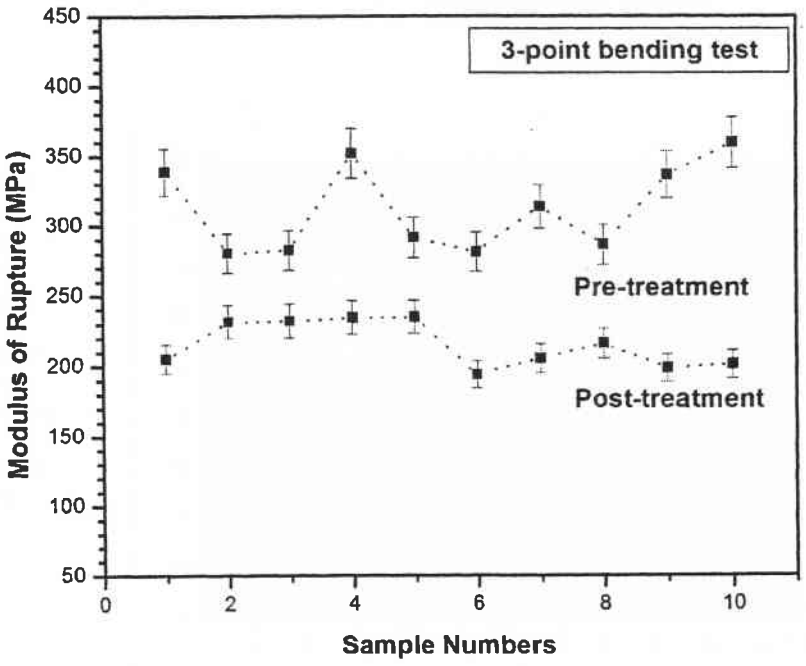

Figure 2.5 Results of 3-point Bending Test on Etched Surfaces.

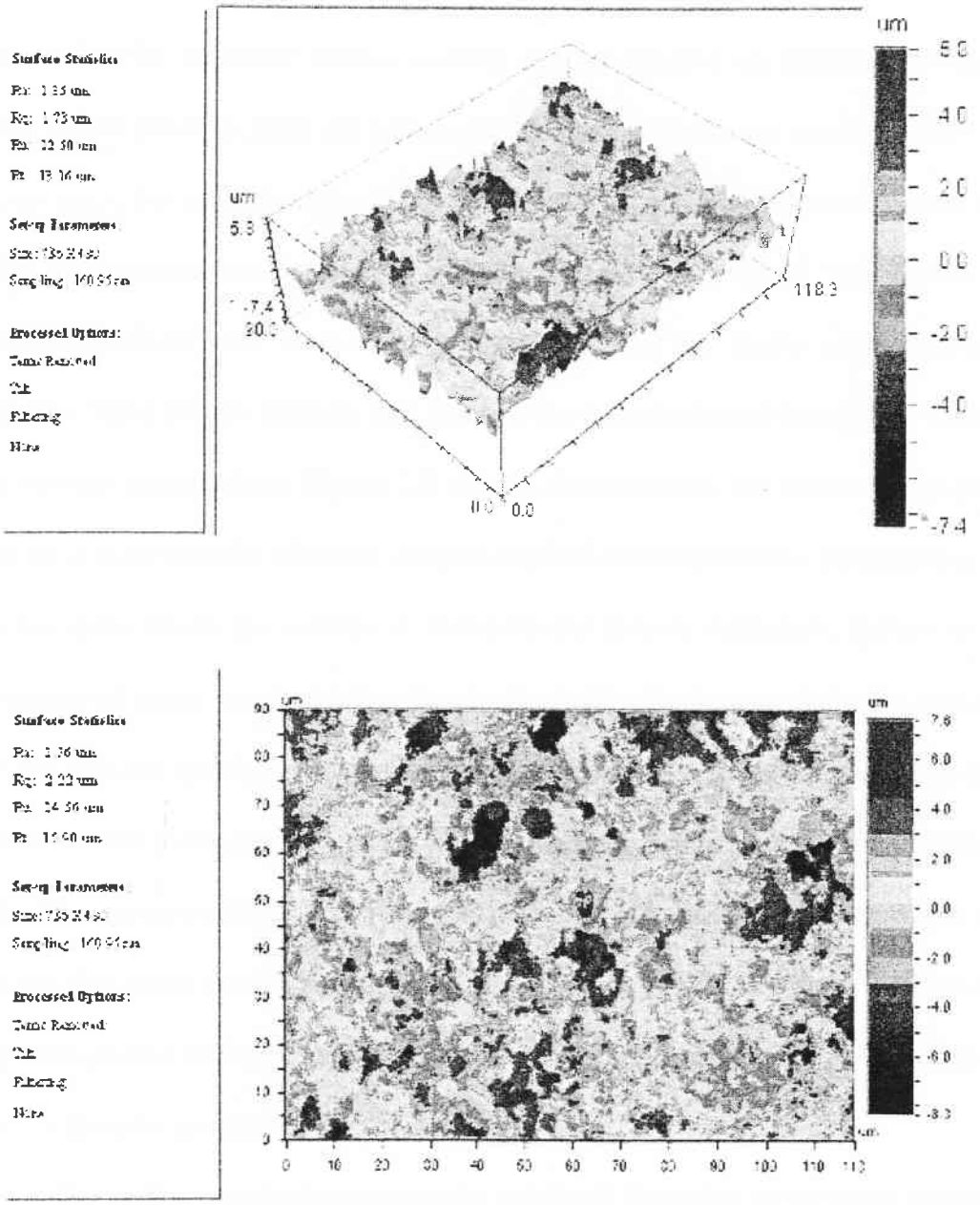

Figure 2.6 Surface Roughness Images

A similar anchoring trend was observed with the cell culture experiments. After three days of incubation, significantly more cells were attached to the etched surfaces compared to the smoother surface alumina control samples as indicated in Figure 2.7. These results possibly point out higher proliferation capacity on rough surfaces than on smooth ones. It is possible that a greater total surface area provided more contact area and higher proliferation on the etched surfaces. On the other hand, cell growth on the smoother surfaces may have already proliferated to the limits of the contact area available. SEM images indicate that most of the cells anchored themselves to the nano-size surface irregularities. Figure 2.8 clearly demonstrates the stress fibers (filipodia) associated with vinculin adhesion plaques attached to those surface irregularities and are actually going inside the cavities as shown by the arrows. Although, Hulbert *et al.* [34] demonstrated many years ago that the development of osteons required a minimum of 150 and 200 μm openings in ceramic materials, Karlsson *et al.* recently showed that pore sizes about the same size of cellular filipodia might function as anchoring points for the cells. Their cross-sectional TEM images demonstrated the filipodia ingrowths into the 200 nm size pores on a Whitman alumina membrane [35]. Our results indicate that not only nano-porous surfaces but also nanosize surface irregularities may serve as anchoring sites for the cells as well.

The surface rough alumina samples exhibited favorable *in vitro* cell response. The osteoblast like 7F2 cells on the rough surfaces expressed a higher cell activity than control samples (Figure 2.9). In particular, the cells on etched surface appeared to show a higher total protein concentration for both one and two weeks cultured samples than the cells on smooth surface, even though the difference was small. The result for the seven

days cell culture did not indicate a significant difference between two surfaces. On the other hand, at the end of second week, increased amount of total protein on both samples and a significant difference between the protein concentrations on the surfaces were observed. Interestingly, in the present study, the total protein concentrations on the both surfaces extended the limits of BCA assay kit (2000 μg/ml) at the end of second week which proved high metabolic activity. These results indicate a favorable cellular response on both surfaces and a higher activity on etched samples by modification of the surface physically as a result of NaOH treatment.

The success of biomimetic coatings is generally associated with the surface chemistry of the substrate material. For instance, titanium and its alloys receive a NaOH treatment that forms sodium titanate layers on the surface ($Na_2Ti_5O_{11}$) prior to the biomimetic coating step. Apatite inducing ability is directly related to subsequent Na^+ ion exchange with H_3O^+ ions during SBF soaking and formation of Ti-OH groups on the surface of Ti. The Ti-OH groups induced the apatite nucleation on the surface and apatite nuclei grew by consuming Ca^{2+} and $(PO_4)^{3-}$ ions from SBF [36]. A similar mechanism is also valid for ceramic materials. For example, hydrated forms of ceramic materials (e.g. SiO_2 and ZrO_2) which readily have abundant Si-OH and Zr-OH groups, can form bone-like apatite on their surfaces [37]. The presence of functional groups could have a great influence on the surface of an implant material to form an apatite layer in a living body.

Unsuccessful attempts to coat alumina in SBF solutions were believed to fail due to the positively charged alumina surfaces in SBF solution. The surface charge (zeta potential) of alumina is 0 at around pH 8. At pH values lower than 8, alumina surfaces become positively charged, decreasing the affinity of OH^- groups against Ca^{2+} and

$(PO_4)^{3-}$ ions [23]. One other factor can be the concentration of SBF solution. Li *et al.* used 1 X SBF in their experiments to investigate apatite inducing ability of alumina surfaces. However, 1 X SBF solutions are only slightly more supersaturated compared to calcium to phosphorus ratio of stoichiometric hydroxyapatite. This results in very slow nucleation and precipitation of calcium phosphates. For this reason, 1.5 X SBF solutions were commonly used to accelerate nucleation and precipitation reactions [38]. Another reason could be the carbonate ion concentration of Tas-SBF, which is almost 6.5 times higher than the 1 X SBF solution. Tas [25] and Dorozhkina *et al.* [39] separately showed that the increase of HCO_3^- ion concentration in a SBF solution increases the thickness and uniformity of the apatitic calcium phosphate coating. One of the above mentioned reasons or combination of them might lead to the failure of the earlier attempts.

In the present study, instead of low temperature (95°C) NaOH treatment, alumina surfaces were etched by molten NaOH. Figure 2.10 shows both kinds of surfaces, untreated and NaOH etched alumina, after being soaked 1.5 X SBF for one week. It can be seen that NaOH treated surface remarkable enhanced the apatite nucleation compared to untreated alumina surface. A thin, granular, nano-porous apatite layer nucleated on etched samples almost covering entire surface. However, on untreated surfaces, apatite formation was limited by physically attached lose precipitates. Although, it is not completely clear, the apatite nucleation on etched samples can be related to the presence of $NaAl_{11}O_{17}$. It is believed that sodium β-alumina thin film formed on the surface of etched samples, and it cannot be removed during washing due to the nano-rough surface. This thin film formation may acted similar to those sodium titanate layers on titanium surfaces, where Na^+ cat ions subsequently exchanged with H_3O^+ or Ca^{+2} ions.

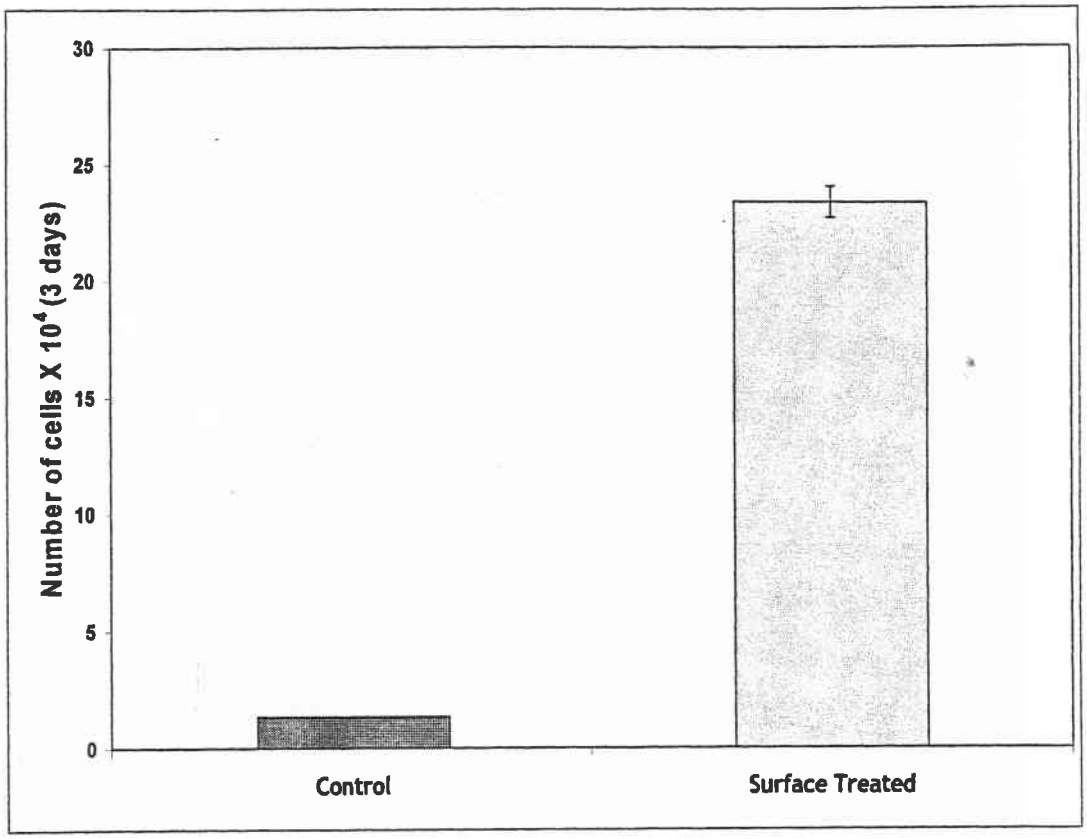

Figure 2.7 Cell Viability on Alumina Control and NaOH Etched Samples After 3 days.

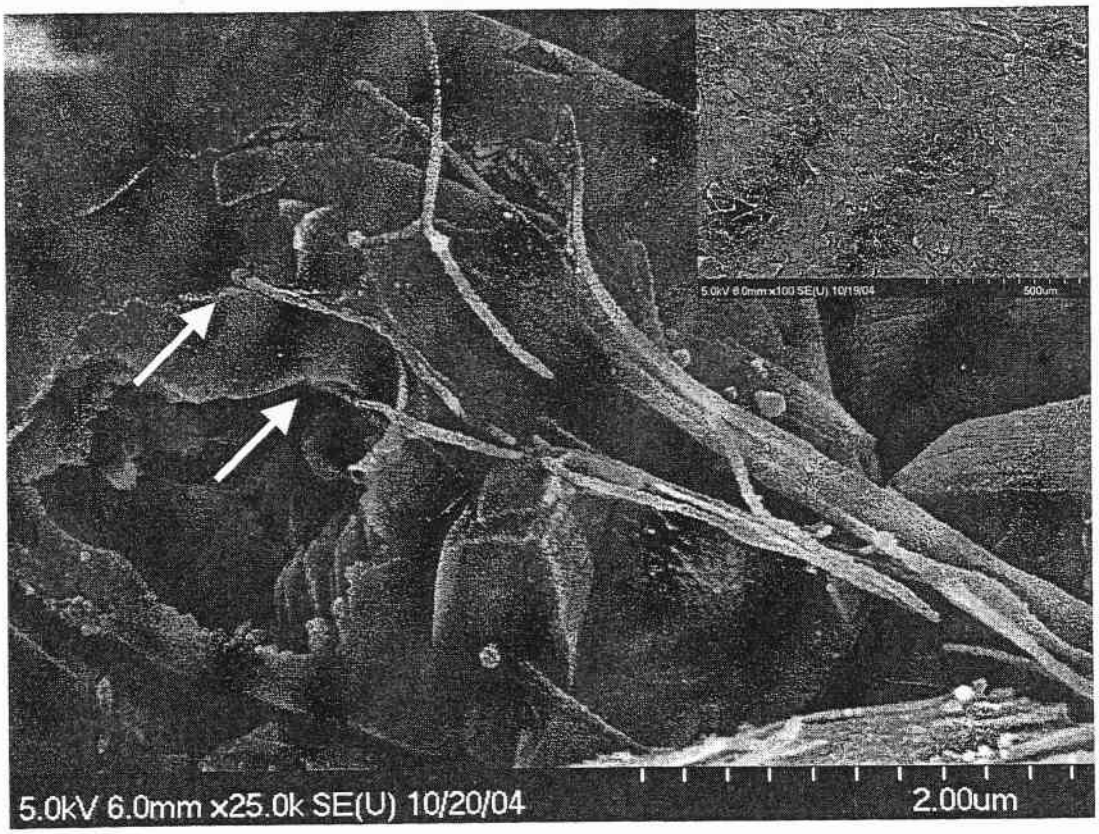

Figure 2.8 Stress Fibers Associated with Vinculin Adhesion Plaques Anchoring the Cell to the Nano-rough Surface. Inset is Low Magnification Image of Surface Covered with Osteoblasts.

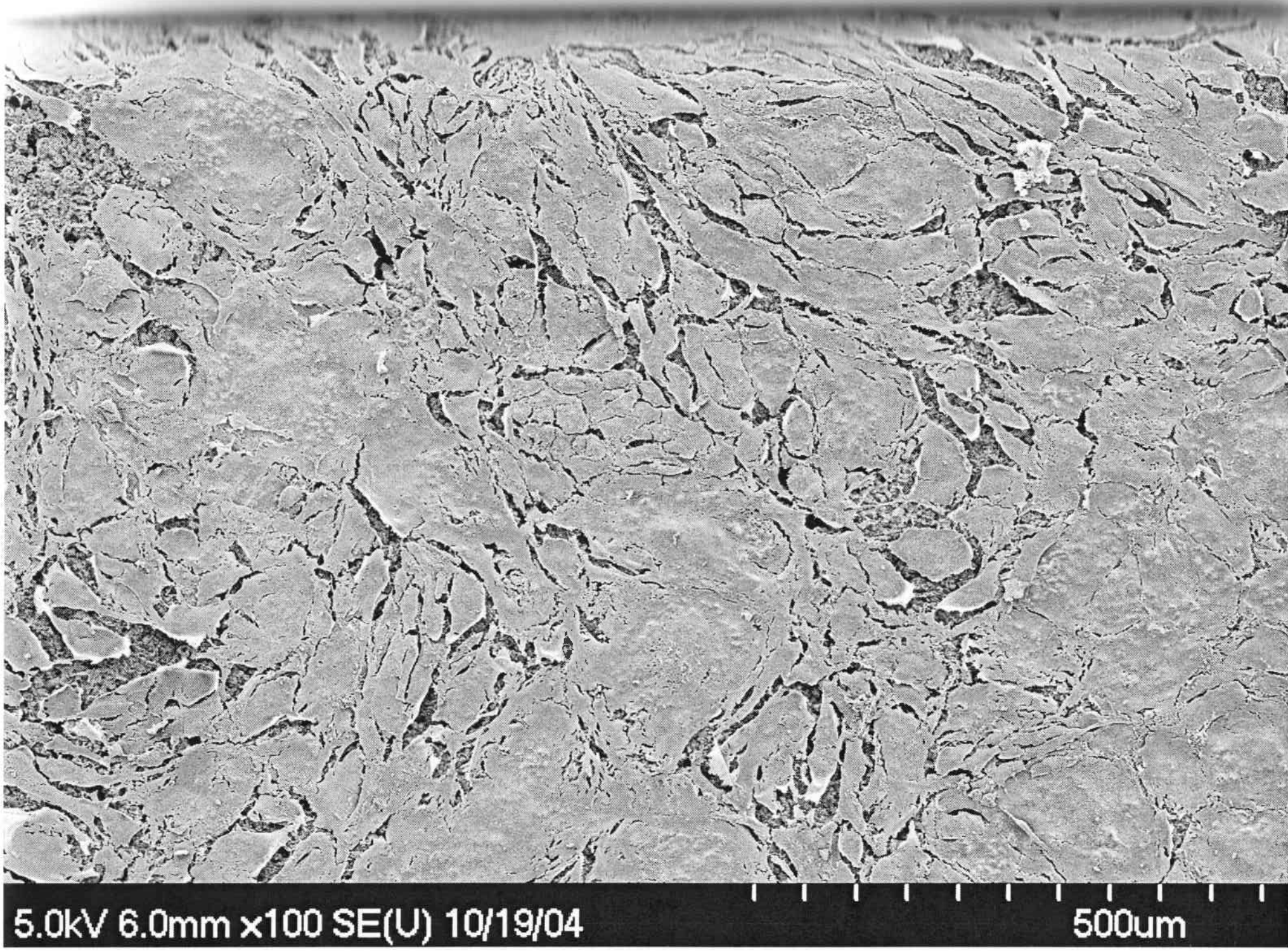
5.0kV 6.0mm x100 SE(U) 10/19/04
500um

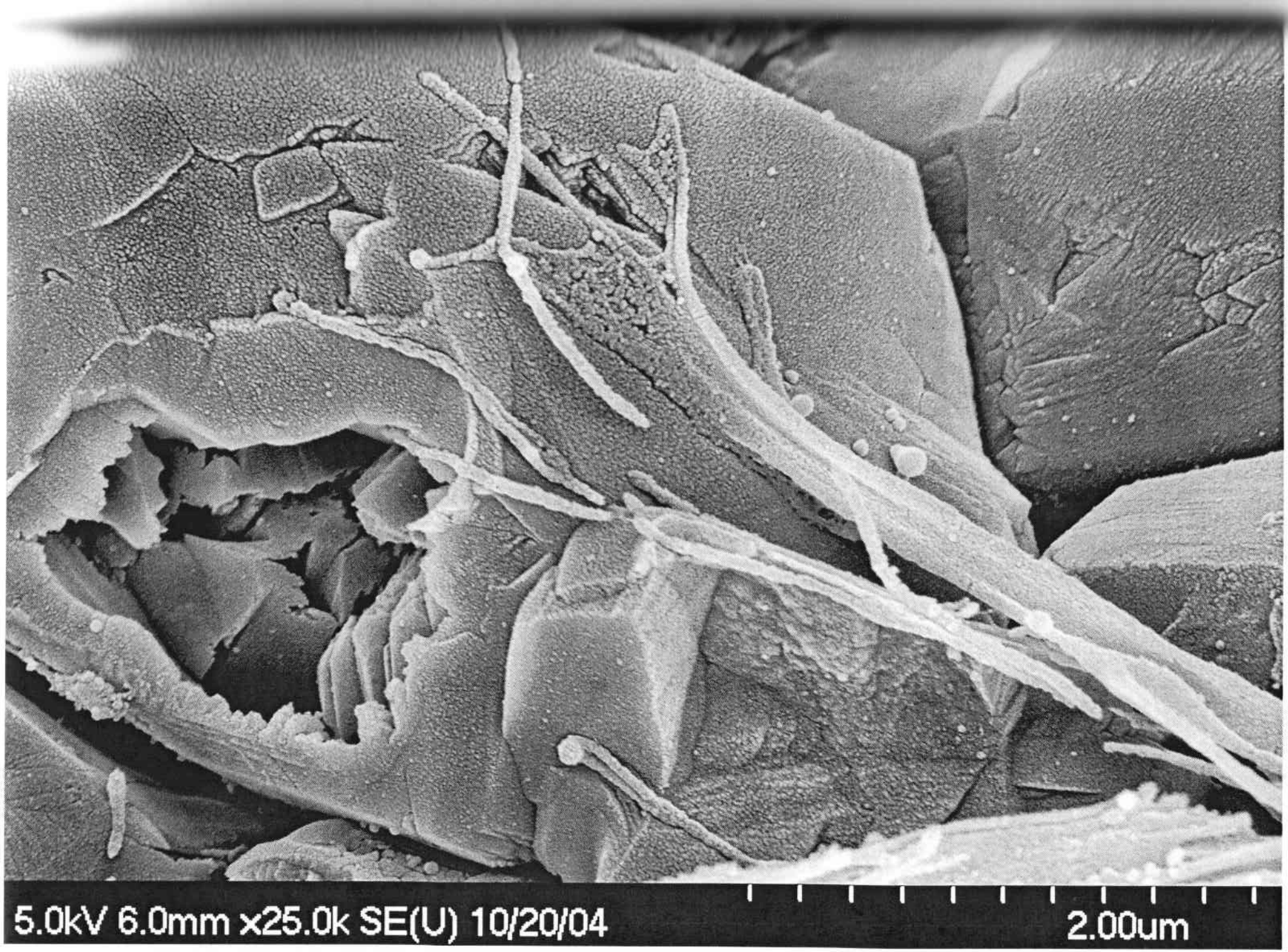
5.0kV 6.0mm x25.0k SE(U) 10/20/04
2.00um

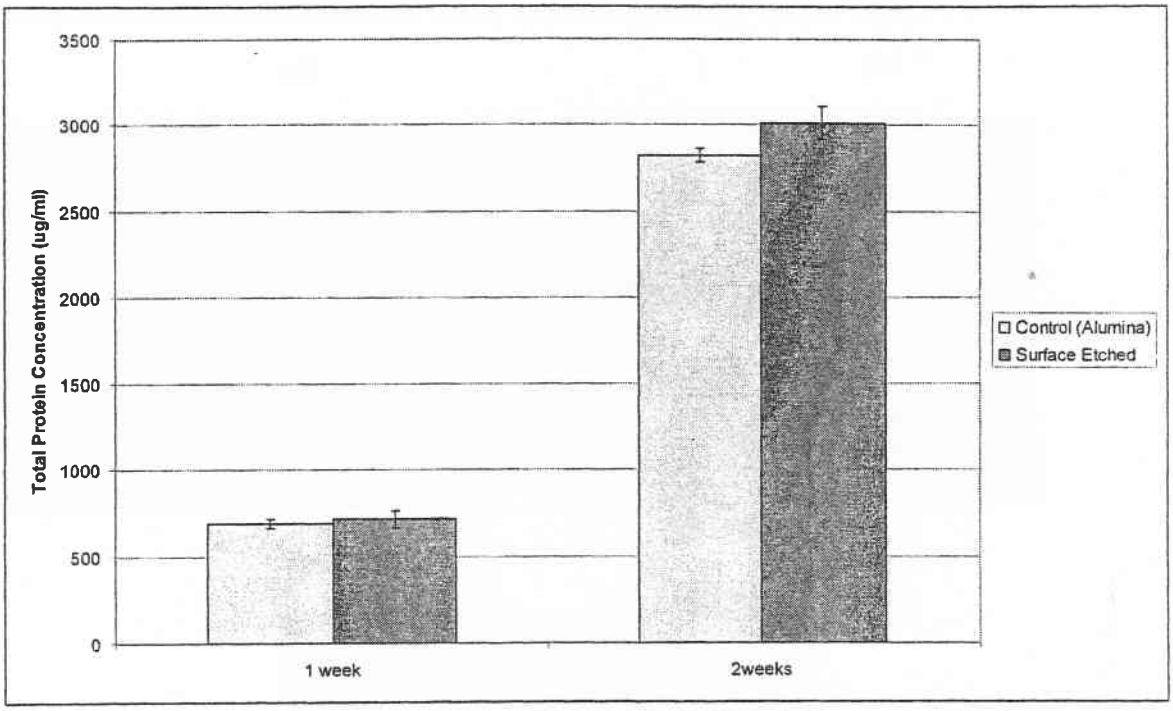

Figure 2.9 Total Protein Concentrations

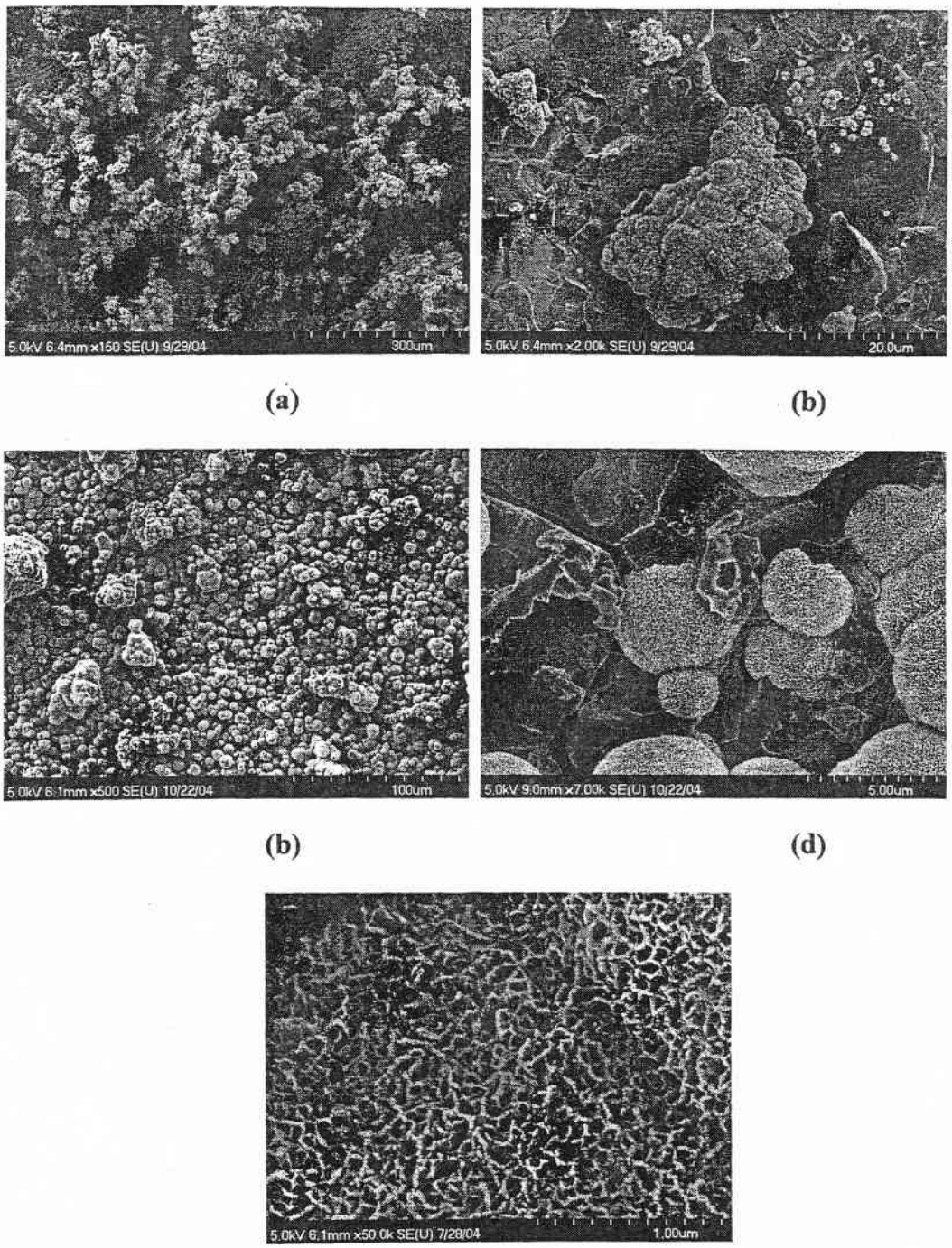

Figure 2.10 SEM Images of Untreated and NaOH Etched Samples Soaked Into SBF for 1 Week. (a) Low Mag. Image of Untreated Surface, (b) High Mag. Image of Untreated Surface, (c) Low Mag. Image of NaOH Etched Surface, (d) High Mag. Image of NaOH Etched Surface, (e) High Mag. Image of HA globule.

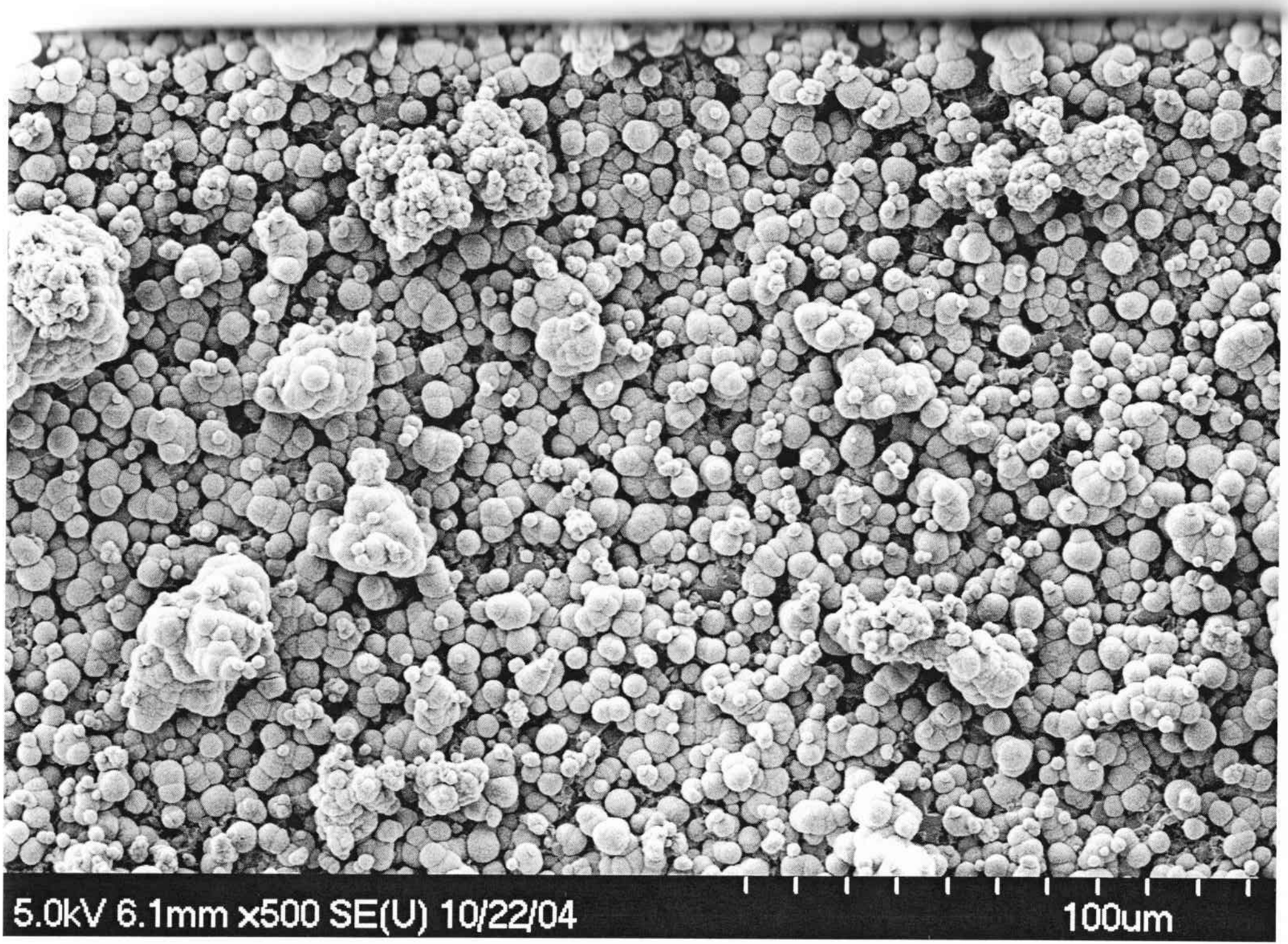
5.0kV 6.1mm x500 SE(U) 10/22/04
100um

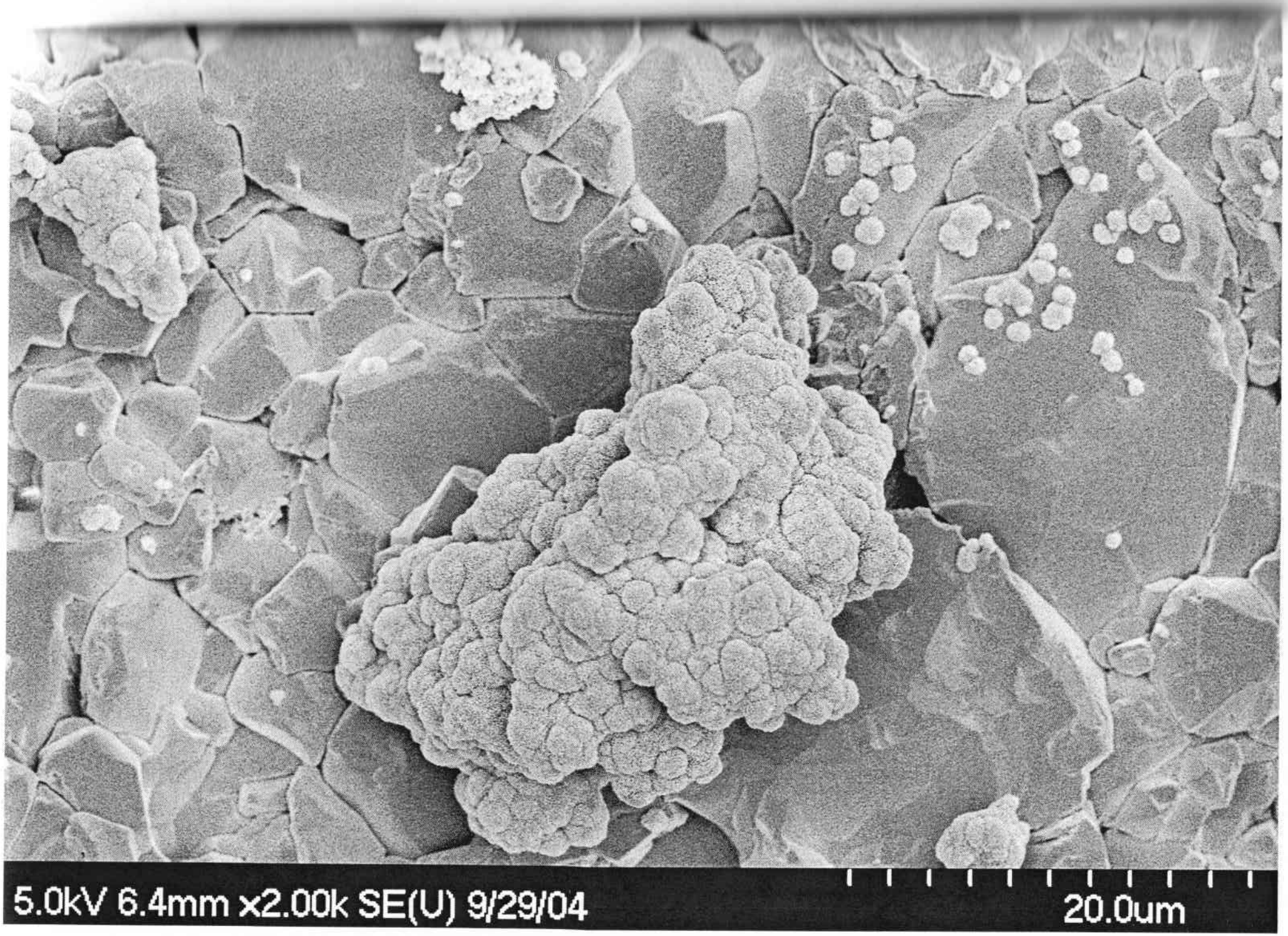
5.0kV 6.4mm x2.00k SE(U) 9/29/04
20.0um

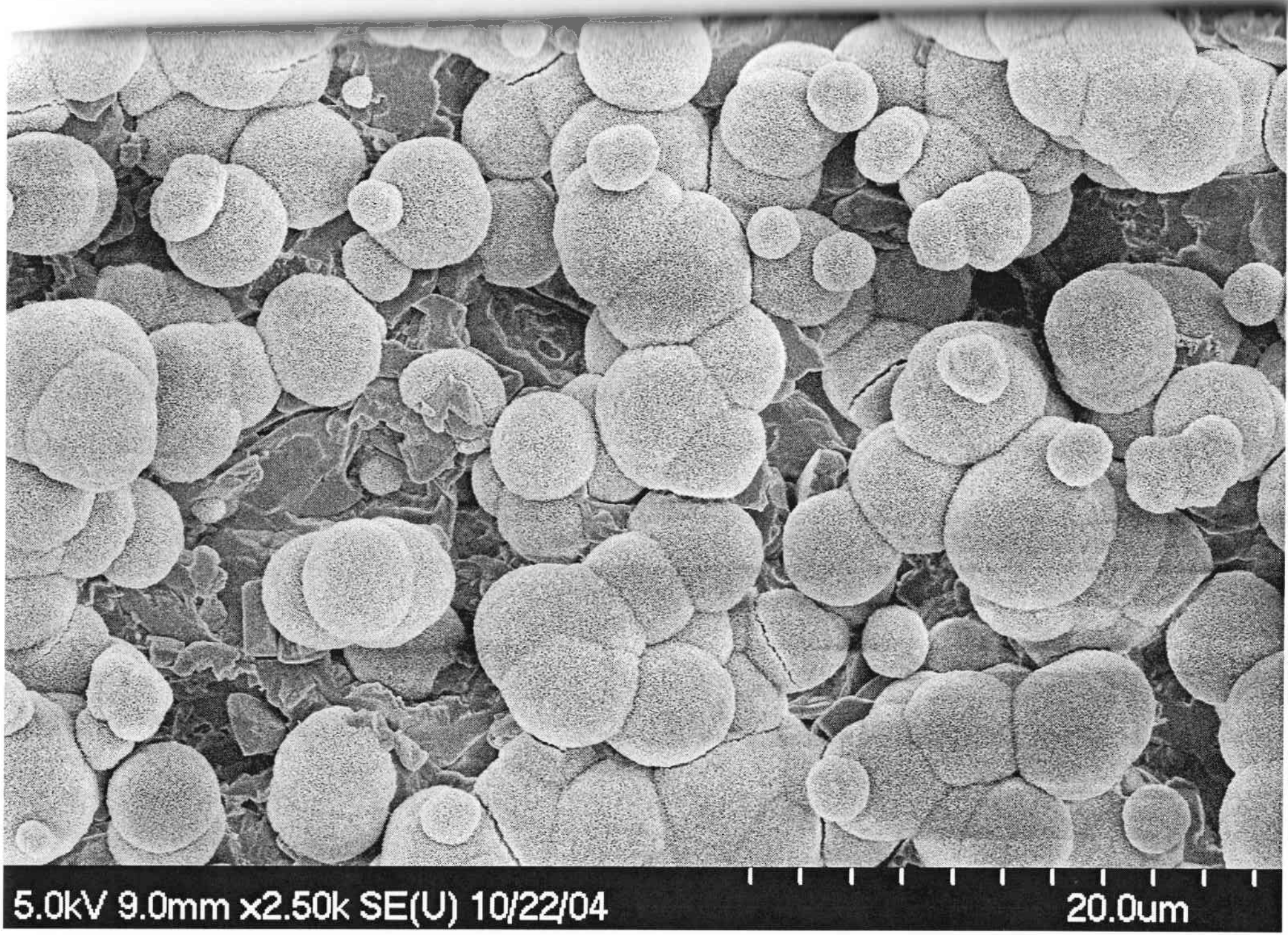
5.0kV 9.0mm x2.50k SE(U) 10/22/04
20.0um

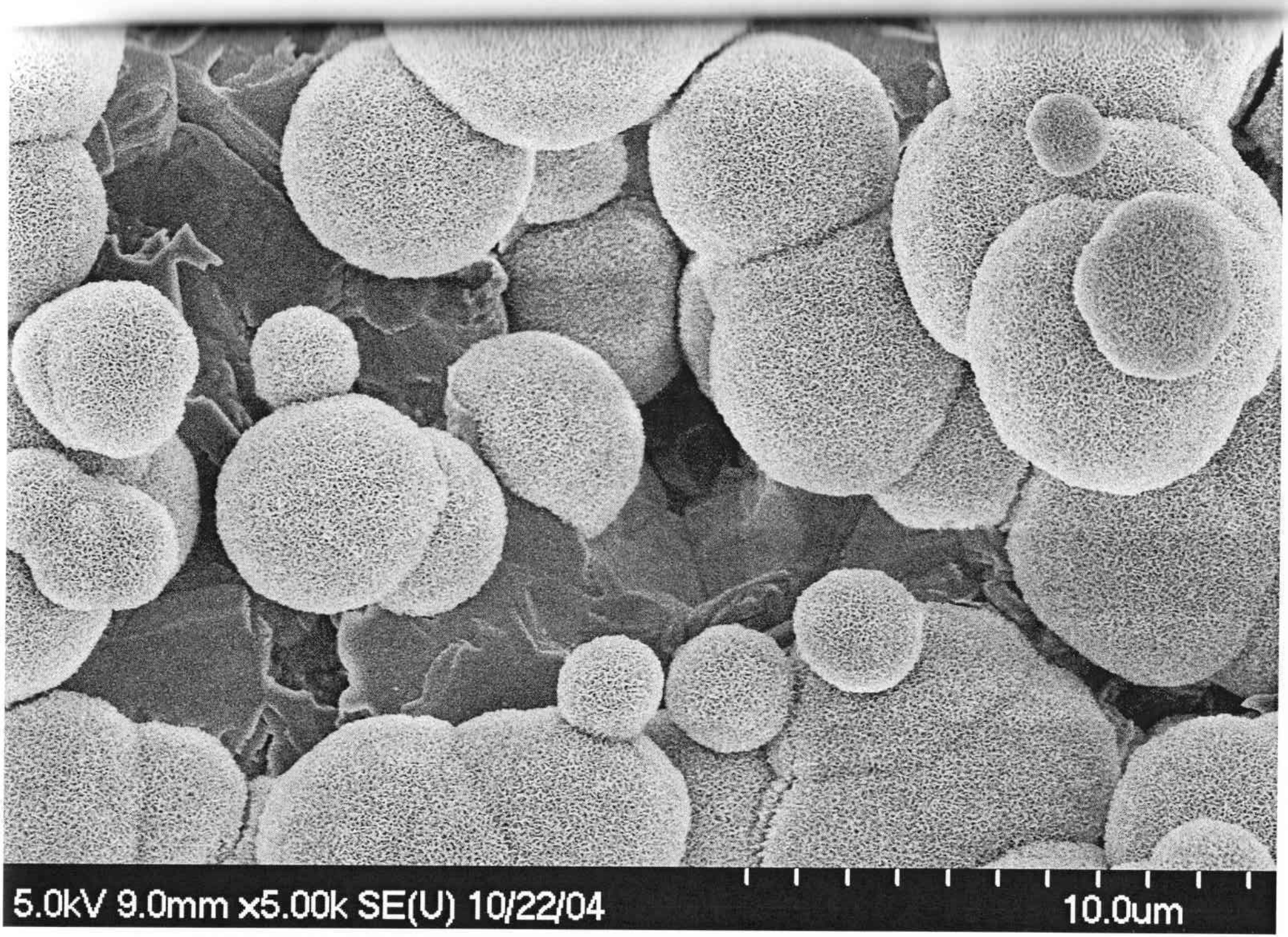
5.0kV 9.0mm x5.00k SE(U) 10/22/04
10.0um

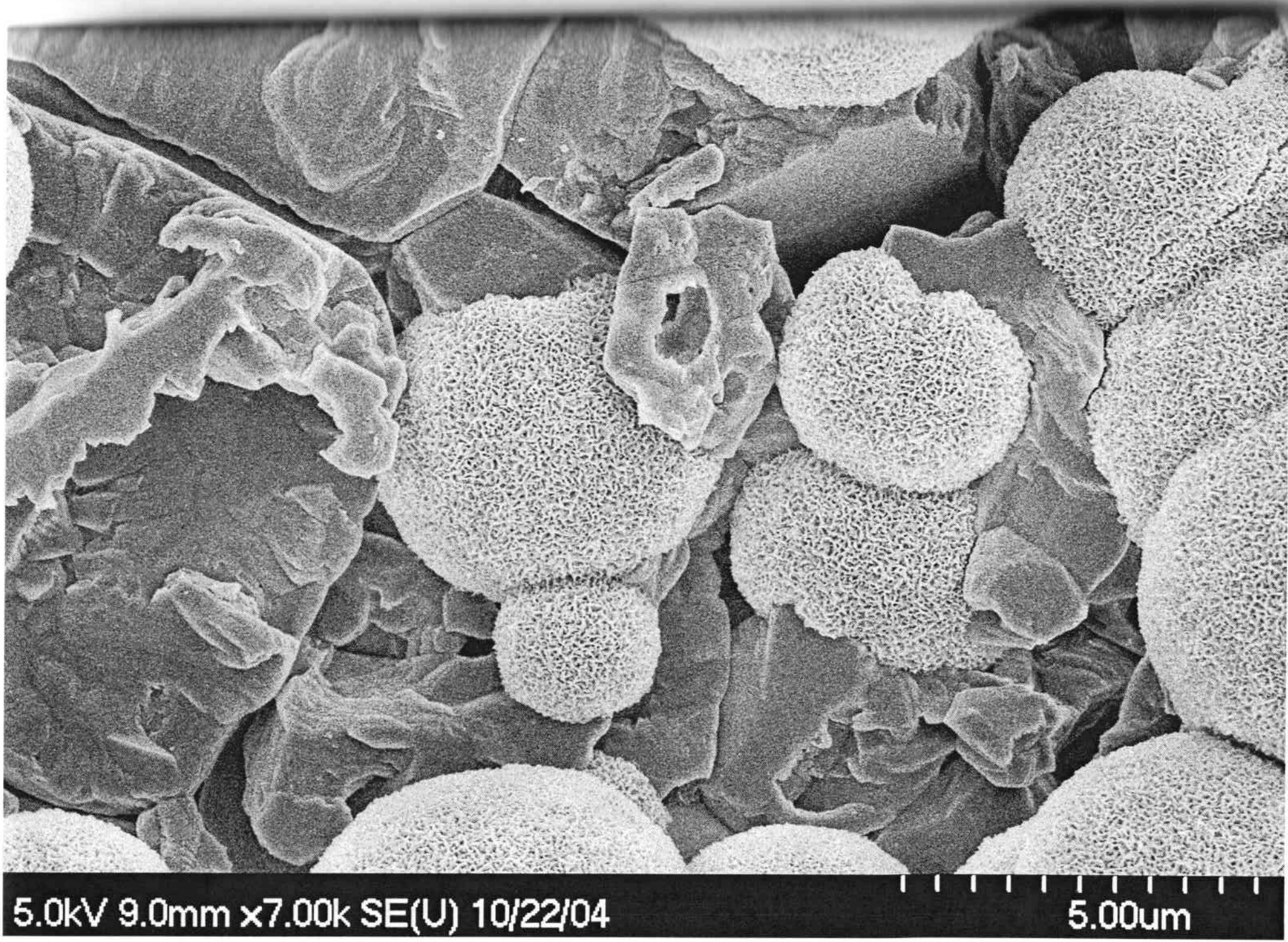
5.0kV 9.0mm x7.00k SE(U) 10/22/04
5.00um

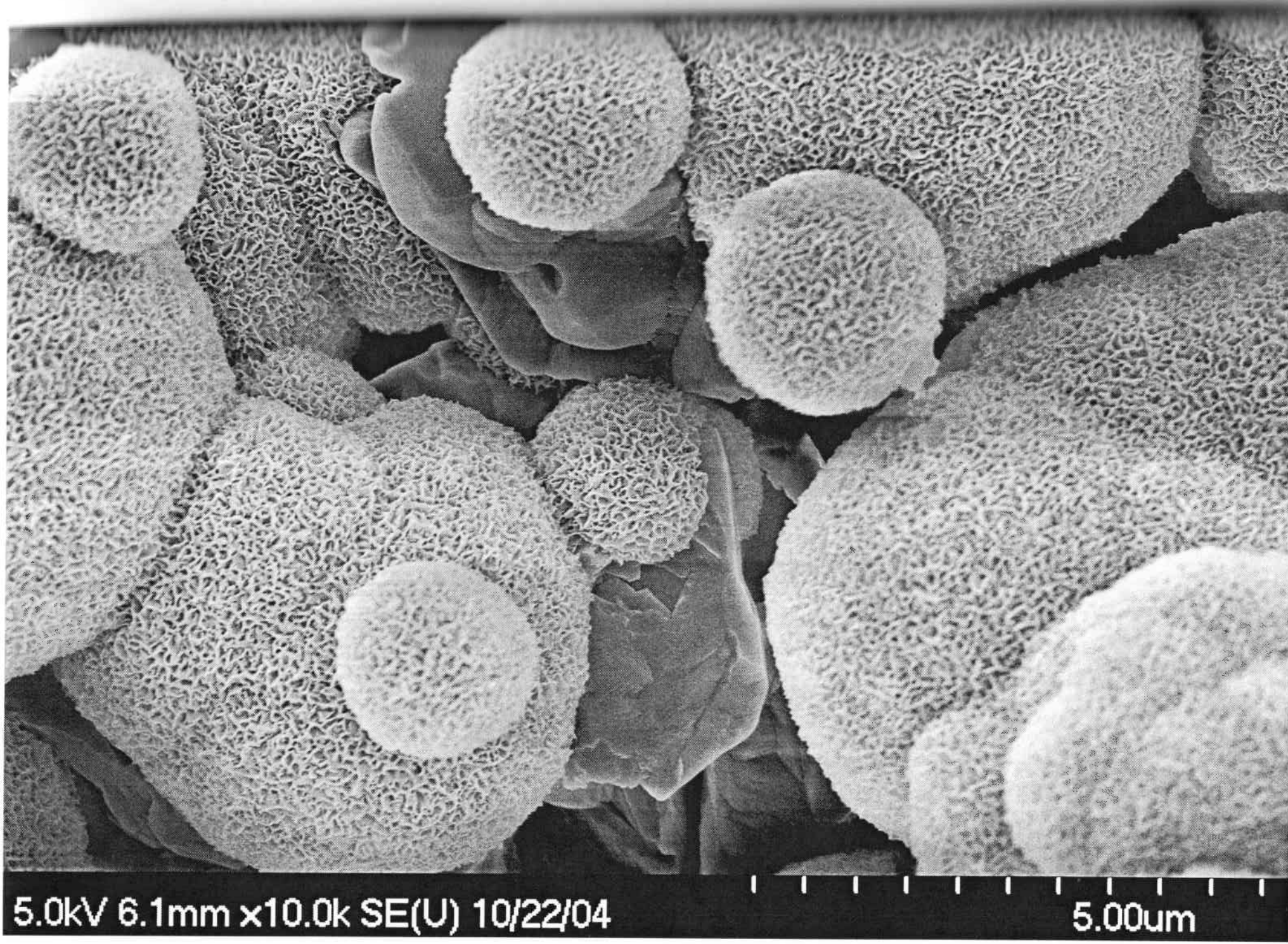
5.0kV 6.1mm x10.0k SE(U) 10/22/04
5.00um

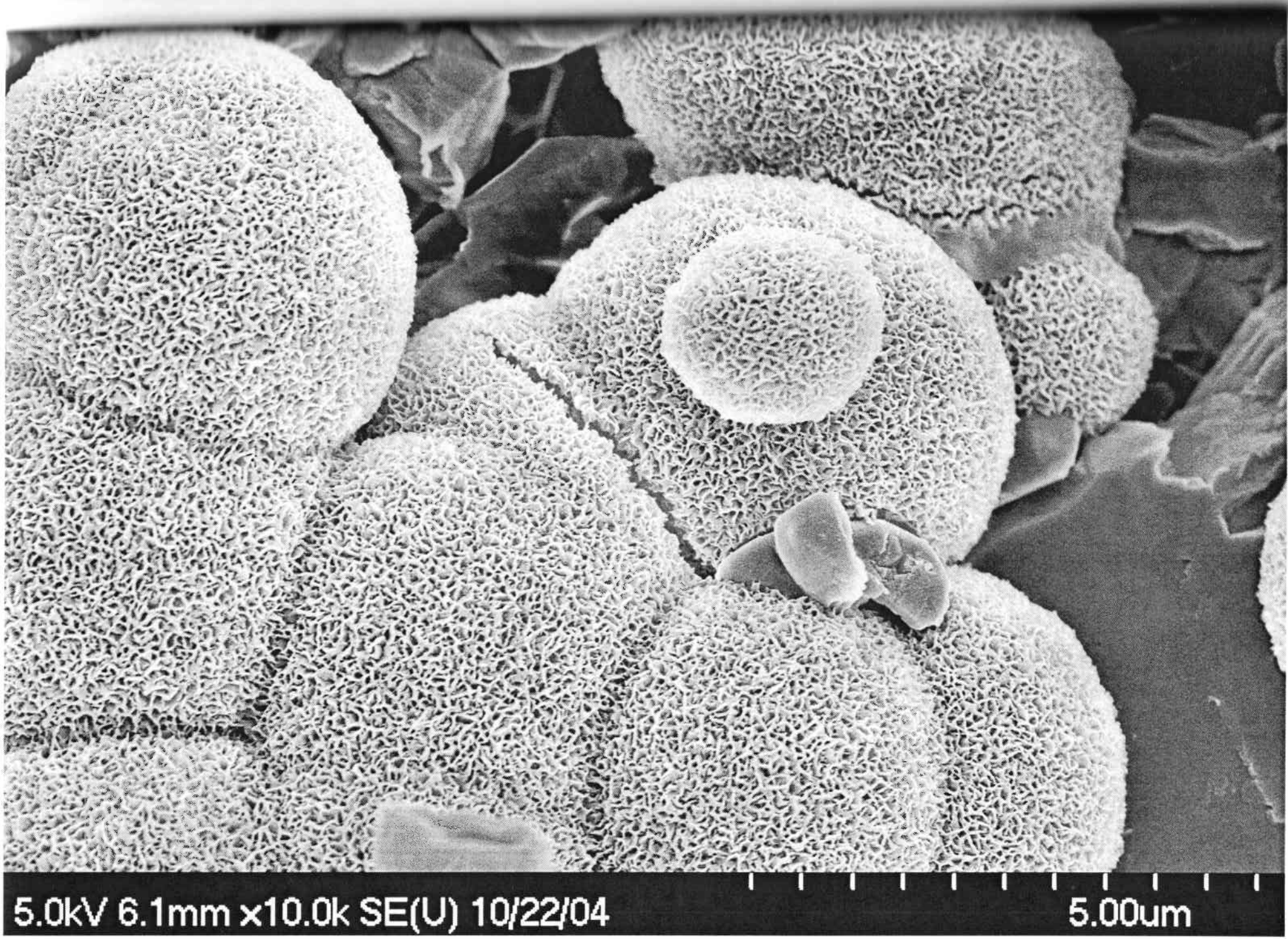
5.0kV 6.1mm x10.0k SE(U) 10/22/04
5.00um

4. Conclusions

A simple chemical etching process was applied to introduce surface irregularities on alumina surfaces. Micron size cavity formations and nano size surface irregularities, which eventually increase the available surface area, increased the number of attached cells on the surface. Additionally, chemical etching caused a thin sodium β-alumina film formation on the surfaces. The formed thin film on the surface greatly increased the apatite inducing ability of alumina surfaces. Attempts to use biomimetic coating procedures to coat Al_2O_3 were failed due to non-reactive surfaces. It is believed that sodium β-alumina on the surface increased the surface reactivity of alumina and allowed successful biomimetic coating on the alumina surface.

References

[1] K. Anselme, "Osteoblast adhesion on biomaterials," Biomaterials, 21 667-681 (2000)

[2] B. D. Boyan, C. H. Lohmann, D. D. Dean, V. L. Sylvia, D. L. Cochran, Z. Schwartz, "Mechanisms involved in osteoblast response to implant surface morphology," Annual Reviews Materials Research, 31 357-371 (2001)

[3] J. C. Keller, J.G. Collins, G. G. Niederauer, T. D.D McGee, "*In vitro* attachment of osteoblast-like cells to osteoceramic materials," Dental Materials 13 62-68 (1997)

[4] D. Buser, R. K. Schenk, S. Ssteinemann, J. P. Fiorellini, C. H. Fox, H. Stich, "Influence of surface characteristics on bone integration of titanium implants. A histomorphometic study in miniature pigs," Journal of Biomedical Materials Research 25 889-902 (1991)

[5] A. Wennerberg, A. Ektessabi, T. Albreksson, C. Johnsson, B. Andersson, "A 1-year follow up of implants of differeng surface roughness placed in rabbit bone," International Journal of Oral Maxillofac Implants 12 486-494 (1997)

[6] R. M. Pillar, D. A. Deporter, P. A. Watson, N. Valiquette, "Dental implant design: Effect of bone modeling," Journal of Biomedical Materials Research 25 467-483 (1991)

[7] R. L. Price, L.G. Gutwein, L. Kaledin, F. Tepper, T. J. Webster, "Osteoblast function on nanophase alumina materials: influence of chemistry, phase, and topography," Journal of Biomedical Materials Research 67(A) 1284-1293 (2003)

[8] M. Kamal, A. Oden, A. Wennerberg, K. Hultenby, K. Arvidson, "The influence of surface topography of ceramic abutments on the attachment and proliferation of human oral fibroblasts," Biomaterials 26 373-381 (2005)

[9] K. Hayashi, N. Matsuguchi, K. Uenoyama, Y. Sugioki, "Re-evaluation of the biocompatibility of bioinert ceramics *in vivo*," Biomaterials 13(4) 195-200 (1992)

[10] I. Dion, L. Bordenave, R. Lefebre, R. Bareille, C. H. Baquey, J. R. Monties, P. Havlik, "Physico-chemistry and cytotoxicity of ceramics," Journal of Materials Science- Materials in Medicine 5(1) 18-23 (1994)

[11] L. L. Hench, "Bioceramics," Journal of the American Ceramic Society 81(7) 1705-1728 (1998)

[12] H. Mittelmeir, J. Heisel, "Sixteen-years' experience with ceramic hip prostheses," Clinical Orthopedics and Related Research 282 64-72 (1992)

[13] J. M. Dorlot, "Long-term effects of alumina components in total hip prostheses," Clinical Orthopedics and Related Research 282 47-51 (1992)

[14] K. S. Tweden, G. I. Maze, T. D. McGee, C. L. Runyon, Y. Niyo, "Evaluation of the tissue response of organic, metallic, ceramic, and osteoceramic tooth roots," Materials Research Forum 293 17-36 (1999)

[15] R. Z. Chen, W. H. Tuan, "Thermal etching of alumina," . American Ceramic Society Bulletin 79(10) 83-86 (2000)

[16] I. O. Owate, R. Freer, "Thermochemical etching methods for ceramics," Journal of the American Ceramic Society 75(5) 1266-1268 (1992)

[17] M. G. Lawson, F. S. Pettit, J. R. Blachere, "Hot corrosion of alumina," Journal of Materials Research 8(8) 1964-1971 (1993)

[18] M. Schacht, N. Boukis, E. Dinjus, "Corrosion of alumina ceramics in acidic aqueous solutions at high temperatures and pressures," Journal of Materials Science 35 6251-6258 (2000)

[19] K. R. Mikeska, S. J. Bennison, S. L. Grise, "of ceramics in aqueous hydrofluoric acid," Journal of the American Ceramic Society 83(5) 1160-1164 (2000)

[20] J. G. Ameen, D. G. McBride, G. C. Phillips, "Etching of high alumina ceramics to promote copper adhesion," Journal of the Electrochemical Society: Electrochemical Science and Technology 120(11) 1518-1522 (1973)

[21] G.V. Elmore, R. F. Hershberger, "Molten alkali treatment of alumina surfaces for bonding to electroless copper," Journal of the Electrochemical Society: Electrochemical Science and Technology 121(1) 107-108 (1974)

[22] J. D. Kartz, G. Hurley, "Etching alumina with molten vanadium pentoxide," Journal of the American Ceramic Society 73(7) 2151-2152 (1990)

[23] P. Li, C. Ohtsuki, T. Kokubo, K. Nakanishi, N. Soga, K. D. Groot, "The role of hydrated silica, titania, and alumina in inducing apatite on implants," Journal of Biomedical Materials Research 28 7-15 (1994)

[24] M. Uchida, H. M. Kim, T. Kokubo, M. Nawa, T. Asano, K. Tanaka, T. Nakamura, "Apatite-forming ability of a zirconia/alumina nano-composite induced by chemical treatment," Journal of Biomedical Materials Research 60 277-282 (2002)

[25] A. C. Tas, "Synthesis of biomimetic Ca-hydroxyapatite powders at 37°C in synthetic body fluids," Biomaterials 21 1429-1438 (2000)

[26] D. Bayraktar, A. C. Tas, "Chemical preparation of carbonated calcium hydroxyapatite powders at 37C in urea-containing synthetic body fluids," Journal of the European Ceramic Society 19 2573-2579 (1999)

[27] G. Eriksson, P. Wu, A. D. Pelton, "Critical evaluation and optimization of the thermodynamic properties and phase diagrams of the MgO-Al_2O_3, MnO- Al_2O_3, FeO- Al_2O_3, Na_2O- Al_2O_3, and K_2O- Al_2O_3 systems," CALPHAD 17(2) 189-205 (1993)

[28] R. C. DeVries, W. L. Roth, Journal of the American Ceramic Society 52(7) 367 (1967)

[29] K. E. Spear, M. D. Allendorf, "Thermodynamic analysis of alumina refractory corrosion by sodium or potassium hydroxide in glass melting furnaces," Journal of the Electrochemical Society 149(12) B551-559 (2002)

[30] T. Sato, S. Sato, A. Okuwaki, S. Tanaka, "Corrosion behavior of alumina ceramics in caustic alkaline solutions at high temperatures," Journal of the American Ceramic Society 74(12) 3081-3084 (1991)

[31] S. Szmukler-Moncler, T. Testori, J. P. Bernard, " Etched implants: A comparative surface analysis of four implant systems," Journal of Biomedical Materials Research Part B 69B 46-57 (2004)

[32] M. Wong, J. Eulenberger, R. Schenk, E. Hunziker, "Effect of surface topography on the osseointegration of implant materials in trabecular bone," Journal of Biomedical Materials Research 29 1567-1575 (1995)

[33] D. H. Li, S. J. Ferguson, T. Beutler, D. L. Cochran, C. Sittig, H. P. Hirt, D. Buser, "Biomechanical comparison of the sandblasted and acid-etched and the machined and acid-etched titanium surface for dental implants," Journal of Biomedical Materials Research 60 325-332 (2002)

[34] S. F. Hulbert, F. A. Young, R. S. Mathews, J. J. Klawitter, C. D. Tlabert, F. H. Sterlling, "Potential of ceramic materials as permanently implantable skeletal prostheses," Journal of Biomedical Materials Research 4 43-456 (1970)

[35] M. Karlsson, E. Palsgard, P. R. Wilshaw, D. L. Silvio, "Initial in vitro interaction of osteoblasts with nano-porous alumina," Biomaterials 24 3039-3046 (2003)

[36] H. M. Kim, F. Miyaji, T. Kokubo, T. Nakamura, "Preparation of bioactive Ti and its alloys via simple chemical surface treatment," Journal of Biomedical Materials Research 32(3) 409-417 (1996)

[37] T. Kokubo, H. M. Kim, M. Kawashita, T. Nakamura, "Bioactive materials: preparation and properties," Journal of Materials Science: Materials in Medicine 15 99-107 (2004)

[38] Y. E. Greish, P. W. Brown, "Characterization of bioactive glass reinforced HAP-polymer composites," Journal of Biomedical Materials Research 52 687-694 (2000)

[39] E. I. Dorozhkina, S. V. Dorozhkina, "Surface mineralization of hydroxyapatite in modified simulated body fluid (mSBF) with higher amounts of hydrogencarbonate ions," Colloidal Surface A 210 41-48 (2002)

CHAPTER III

COATING OF ALUMINA WITH CALCIUM PHOSPHATES

Abstract

Alumina (Al_2O_3) ceramics are in successful clinical use as bionert, load-bearing implant materials, especially in hip revision surgery. When needed, the most preferred routes of ceramic deposition over such ceramic substrates have been the thermal spray, dip-coating and laser deposition methods. However, these methods suffered from the resultant heterogeneous coat layers of low adhesion strength, or undesired phase decomposition observed in the coatings.

In this study, dilute precursor solutions (calcium nitrate tetrahdyrate and triethyl phosphate) were first prepared and then the alumina substrates were directly placed into these solutions, followed by slow heating in an air atmosphere up to 600°C. This new process resulted in a deposit of chemically attached calcium phosphates on the substrates. Soaking of these samples in an SBF solution (Tris-buffered, 27 mM HCO_3^-) at 37°C converted the calcium phosphate deposits into carbonated, bonelike apatite. Samples were characterized by XRD, SEM, FTIR and cell culture tests.

1. Introduction

Bone consists of an organic compound (20-25% weight), an inorganic compound (70%) and a water component (5%). The organic compound is largely type I collagen but also includes bone cells (Osteoblast, osteocyte and osteoclast) and a small amount on noncollagenous protein. The inorganic portion of the bone and teeth consist of Hydroxyapatite (HA), predominantly, the impure calcium phosphate (CaP) form. Having the chemical formula of $Ca_{10-x}(HPO_4)_x(PO_4)_{6-x}(OH)_{2-x}$, it is also known as calcium hydroxyapatite. Besides magnesium, sodium, and potassium, the chief constituent of the hard tissues (bones) is the poorly crystalline, carbonate containing apatite phase. Calcium HA is biocompatible and bioactive in human body. It is compatible with different tissue types and can form bond directly to osseous, soft, and muscular tissue without an intermediate layer of a modified tissue (fibrous tissue) [1-3]. HA also displays an osteconductivity: the process of bone migration and attachment along a biocompatible surface [4]. Despite its excellent properties as a biomaterial, the inherent mechanical properties of HA, such as poor tensile strength, impact resistance, and brittleness have restricted its usage in load bearing applications. Therefore, HA coated implant materials, which combine the advantages of the mechanical properties of implant material with the excellent biocompatibility and bioactivity of the HA, was developed and considered to be the most promising group of implant materials. In the present study, alumina was selected as the substrate material because of its bioinertness [5], non-cytotoxicity [6] and almost an excellent record of clinical usage for dental and orthopedic restorations for several decades [7,8]. Al_2O_3 has a much higher mechanical strength compared to that of sintered

HA, and the HA surface coating can ensure a high bioactivity for bone growth. However, there are only a limited number of attempts made to coat HA on bioinert substrates (like alumina and zirconia) compared to metal substrates (titanium, tantalum and Ni-Ti alloys) [13-15].

Bioactivity and durability of the HA coatings depend on some critical quality specifications including phase purity, crystallinity, microstructure, Ca/P ratio, porosity, surface roughness, thickness, implant shape and surface texture which also lead to different mechanical properties, such as cohesive and bond strength, tensile strength, shear strength, Young's modulus and residual stress [16]. Various coating methods were proposed to deposit HA coatings to increase the bioactivity and hence accelerate and improve early bone-implant bonding, such as plasma spraying [17-19], electrophoretic deposition [20,21], ion-beam implantation [22,23], dip coating-sintering [24-26], spin coating [27,28], and solution deposition [29,30]. To the present date, there are no known methods which totally satisfy those criteria above. For example, high temperature procedures like, thermal spraying, can degrade mechanical properties of implants and lead to low bonding strength and impurity of HA. Meanwhile, low temperature processes, such as solution deposition, low adhesion strength of the coating and the maximum applicable thickness of the coatings are the main drawbacks. Nevertheless, plasma spraying is the only commercial technique available.

Coating of hydroxyapatite through sol-gel method uses relatively low temperatures for calcium phosphate coating formation. This process includes the use of appropriate calcium and phosphate containing precursor solutions [31]. Solutions of metal alkoxides and/or salts dissolved in organic solvents are mixed together to yield a

number of different combinations between these calcium and phosphorus precursors for sol-gel processes [32]. For instance, Weng *et al.* used phosphorus pentoxide and calcium nitrate as the calcium and phosphorus precursors [33]. Where else, calcium nitrate and phosphoric acid were used to prepare dipping solution [34, 35]. Typically, reactions involved in the sol-gel route, independent of the starting chemicals, are hydrolysis and condensation.

In hydrolysis process a hydroxo ligand substitutes an alkoxy group. The mechanism of hydrolysis is simply nucleophilic substitution of alkyl groups by hydroxyl groups bonded to the metal atom (M). Alcohol molecules are released as a byproduct. The reaction may simply be written as [36]:

$$M(OR)_Z + H_2O \rightarrow M(OH)\,(OR)_{Z-1} + ROH$$

Condensation/polymerization is a result of either olation or oxolation reactions in aqueous solutions. In either cases, the reaction between M-(OH) molecules leads to the formation of M-O-M bond and alcohol or water as byproduct:

$$M\text{-}(OH) + M\text{-}(OH) \rightarrow M\text{-}O\text{-}M + H_2O$$

Condensation includes aging of the sol solution followed by a gelation. However, a long period of aging time, i.e. 24 hrs or longer, required to form a monophasic HA [37].

The resultant sol can also be used to coat substrates using spin-, dip-coating, and aerosol-gel processes. Generally, sol-coated substrates are dried in an oven and pre-fired to higher temperatures (~500°C). To obtain desired thickness, the above procedure might be repeated several times. Gan *et al.* [38] compared two phosphate precursors, namely triethyl phosphate and ammonium dihydrogen phosphate, which reacted with calcium nitrate tetrahydrate to form HA coating on Ti_6Al_4V alloy substrates by dip coating. They reported both films resulted with sub-micron particle size crystalline, carbonated HA films at 500°C. They observed that ammonium hydrogen phosphate route displayed more irregular surface texture and formed a less dense coating. Kim *et al.* produced hydroxyapatite and fluoro-hydroyapatite thin films on a Ti substrate using triethyl phosphite, calcium nitrate tetrahydrate and ammonium fluoride as the starting chemicals. They reported formation of a phase-pure, uniform and dense coating on Ti substrate by spin-coating and subsequent heat treatment process [39,40]. Haddow *et al.* used triethyl phosphite and calcium ethoxide to prepare coating sol which was later deposited on quartz samples by dip-coating and fired above 900°C. The results showed the diphasic (β-TCP/HA) nature of the coating after firing at greater than 900°C [41]. These findings were supported by Kim *et al.* where hydroxyapatite and phosphate glass composites were spin-coated on a zirconia substrate. They reported the formation of triphasic calcium phosphates (HA/TCP/DCP) and glassy phases after heat treatment over 800°C [42]. Gross *et al.* investigated the effect of aging time on coatings produced by spin-coating. They concluded that the coatings produced from sols aged less than 24 hours yielded calcium oxide in addition to HA [43].

Alternatively, sol solution can be used to produce HA powders after gelation (drying) and calcination. Hsieh *et al.* investigated the effect of fast gelation on the synthesis of HA powders. Calcium nitrate tetrahydrate and triethyl phosphate were used as starting solutions [44]. They reported the formation of HA at 600°C. They applied a fast drying route. However, this resulted in a minor amount of CaO due to the non-reacted calcium nitrate decomposition during the calcination. Liu *et al.* found that an HA phase appeared as low as 350°C when calcium nitrate and triethyl phosphite was used as the starting chemicals [45]. These authors also investigated the affect of ethanol and distilled water as solvents. Remarkably, they observed very similar behaviors for ethanol-based gels and aqueous-based gels.

All the methods mentioned above point out to the importance of aging (sol-formation) regardless of the starting chemicals to obtain monophasic HA coatings and/or powder. Typical aging times are 24 hours. Present study investigates the possibility of a high quality coating (i.e. phase purity, texture and adhesion strength) on alumina substrate through the elimination of calcium and phosphorus precursors aging time. The steps involved in this approach can be outlined as follows. Hydrolysis of the phosphorus and calcium precursors is followed by polymerization. Heating of the coating sol caused condensation. At the end direct pyrolysis of the polymeric molecules resulted in the formation of the Ca-P coating on the substrate.

2. Materials and Methods

2.1. Substrate preparation

99.8% purity alumina substrates were supplied by Coorstek® (CoorsTek Inc. CO, USA) as slip cast 2 mm thick plates. Chemical analysis of the substrates was obtained from the supplier and shown in Table 3.1. XRD analysis of as-received alumina plates indicated that α-alumina is the only phase existed (ICDD card # 46-1212). In order to prepare the samples for X-ray diffraction (XRD), scanning electron microscopy (SEM), Fourier transform infrared spectroscopy.(FT-IR), square samples (1 cm X 1cm X 2 mm) were cut by a diamond saw. Adhesion strength measurement samples were polished manually to obtain flat-surfaced substrates prior to coating deposition. All samples were then degreased with acetone, and washed by distilled water in an ultrasonic bath.

Table 3.1 Chemical Analysis of Alumina Substrates

Constituent	Al_2O_3	SiO_2	Fe_2O_3	MgO	Na_2O
Weight Percent (%)	99.82	0.02	0.01	0.07	0.08

2.2. Coating deposition

Calcium nitrate tetradydrate ($Ca(NO_3)_2{\cdot}4H_2O$, Fisher Scientific Inc. GA, USA) and triethyl phosphate ($(C_2H_5O)_3PO$, Alfa Aesar Inc. MA, USA) was used as the calcium and phosphate precursors. Triethyl phosphate (0.0148 mol) was first hydrolyzed in 25 ml deionized water by stirring vigorously at room temperature for 30 minutes. Meanwhile, 0.0265 mol (Ca/P: 1.67) of calcium nitrate tetrahydrate was dissolved in 25 ml deionized water separately. The two solutions were then mixed with one another in a dropwise manner, and then stirred for another 1hour. At the end of 1 Hour the solution was still clear and the pH was measured as 5.35. Alumina substrates then placed on the bottom of a Pyrex® beaker and subsequently heated up to 565°C in a lab furnace without allowing any aging. This provided direct deposition of the Ca-P coating on alumina surface. Table 3.2 is the heat treatment scheme of the coating deposition used in present study.

Additionally, a set of calcium phosphate coated samples were soaked in Simulated Body Fluid (SBF) for a period of one week in order to convert the Ca-P coating into carbonated, non-stoichiometric, poorly crystalline apatitic calcium phosphate (biological apatite).

The SBF solution was prepared as suggested by Tas [46-47]. To accelerate the coating procedure, the values were multiplied by the factor of 1.50 in preparing the SBF-coating solutions. Samples were placed onto a 45° inclined stainless steel net platform and the samples were above the solution precipitation settling range. It was done to prevent the loosely attached precipitates on the surface, mostly seen if the substrates placed at the bottom of the bottles. The bottles were then sealed tightly and kept at 37°C, replenishing the SBF solution every 48 hours during soaking period.

Table 3.2 Heat Treatment Scheme for Coating Deposition.

Temperature(°C)	Step Time (min.)
RT-110	120
110	60
110-200	30
200	150
200-250	30
250	90
250-565	30
565	10 hrs.

2.3. Coating characterization techniques

Thermogravimetric analyses (TGA/DTA) of the solution was performed using a thermal analyzer (TGA, Mettler Corp. CT, USA) from room temperature to 750°C under an air flux of 50 ml/min ramping at 3°C/min. A XDS 2000 (XRD, Scintag Corp.) equipped with a monochromated Cu K_α radiation source was used to characterize the crystalline structure of the coatings. The scanning parameters used were as follows; scan range (2θ): 10-50°, step size: 0.03°, step time: 10 s. Scanning electron microscopes (Hitachi S3500, and Hitachi S4700 field emission-SEM, Hitachi Ltd. Tokyo, Japan) were used to examine the surface morphology of the coatings. The presence of functional groups was analyzed by a Nicolet Magna-IR 550 Fourier transform infrared spectroscopy (FT-IR) system. KBr pellets were pressed by a uniaxial press with a powder-KBr ratio of 1/100. Spectra were obtained at 4 cm^{-1} resolution and 32 scans in transmission mode. The collected spectra were processed by Omnic software package provided with the system.

2.4. *In vitro* study

Details of the In vitro study is given in chapter 2, section 2.5.

3. Results & Discussion

3.1. Thermal analysis

A thin layer of coating was applied by a simple evaporation-condensation-pyrolysis process within a laboratory furnace. DT/TGA analysis established the Ca-P coating formation temperature as 565°C (Figure 3.1). The endothermic peak at 100°C indicated the evaporation of the water, leaving behind the organic species and nitrate compounds. Majority of the weight loss (~ 40 %) was occurred in this stage. Shortly after the evaporation of water, condensation reaction began with in the temperature range of 110-250°C. Together with the TGA trace, which did not indicate significant mass loss, a plateau between 110°C and 250°C represented a thermally stable, highly viscous and clear gel. It is assumed that P-O-Ca linkage formation started at 110°C and further heating caused an accelerated thermal decomposition and polymerization/condensation between derivative units. This resulted in the formation of more P-O-Ca containing bonds in the gel. It is believed that partial pyrolysis also took place during this stage and completed at the soaking temperature. The small exothermic peak at around 565°C was assumed to be the removal of nitrate species from the system and accepted as Ca-P coating formation temperature. Samples were soaked at 565°C for an additional 10 hours to allow complete pyrolysis. Experiments conducted below this temperature (i.e. 550°C) resulted in highly unstable coatings due to nitrate group presence.

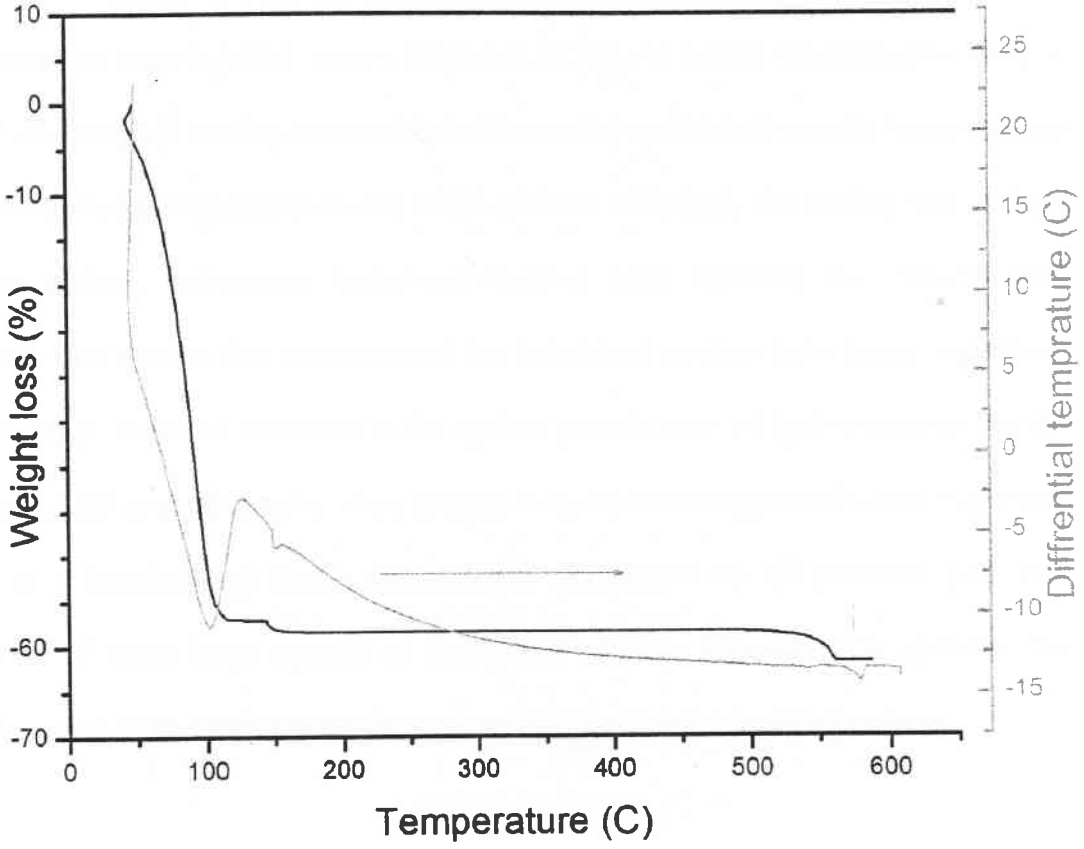

Figure 3.1 DT/TGA Trace of the Starting Materials

3.2. SEM analysis

Figure 3.2a represents a scanning electron micrograph of a Ca-P coated alumina substrate. The coating appeared to be uniform, almost crack free, and completely covered the substrate as seen in SEM images (Figure 3.3a, b). At higher magnification images, Figure 3.2b, the Ca-P coating appeared to be formed by individual crystals fused together in a fashion more or less perpendicular to the surface. Although, the coating was uniform upon the surface, sub-micron horizontal stacking gaps between the platelets were noticeable. The images also demonstrated the individual crystals have hexagonal crystal structure which might be attributed to the typical growth habit of hydroxyapatite. On the other hand, SBF soaked samples show (Figure 3.4a, b), not unexpectedly, round globules consisting of interlocking, needle like, calcium phosphates on the substrate [29]. Full conversion of those large crystals of hexagonal calcium phosphates to globular, the needle like, nanosize calcium phosphates completed in about a week of soaking.

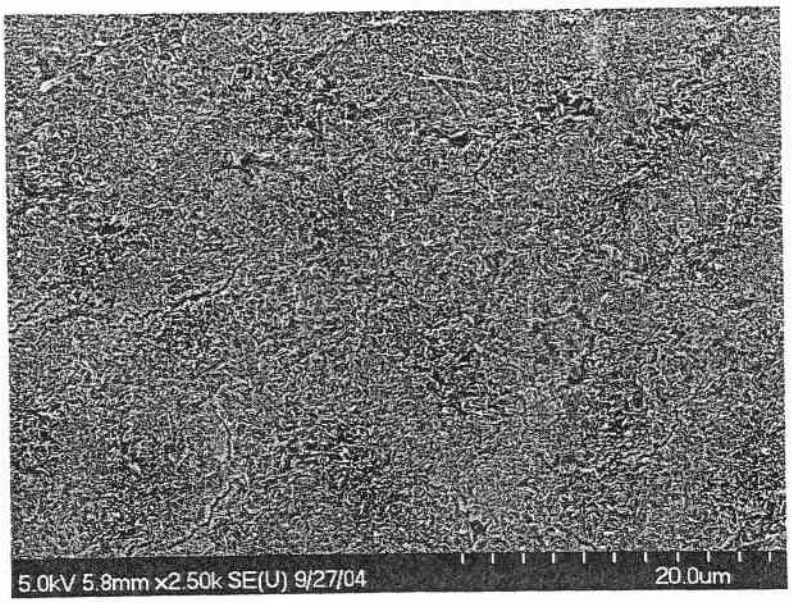

(a)

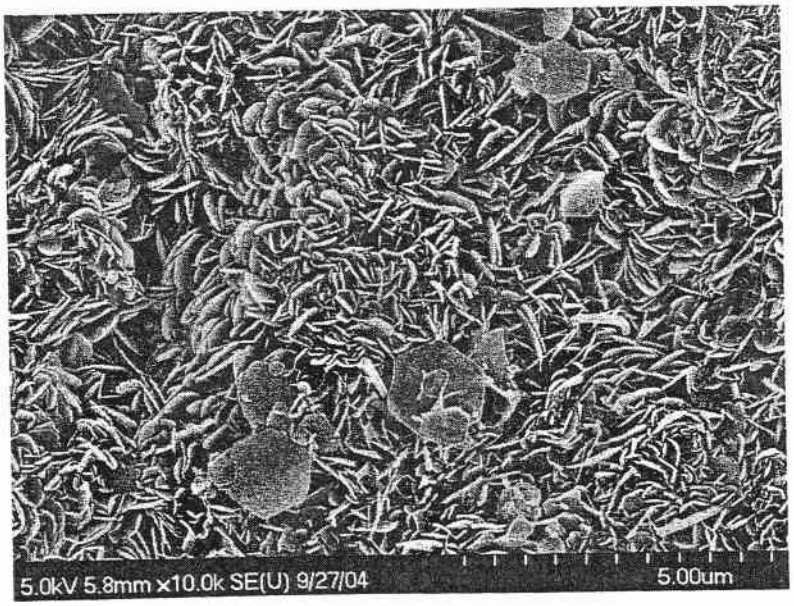

(b)

Figure 3.2 FE-SEM Micrographs of Ca-P Coating on the Surface of Alumina (a) Low Magnification (b) High Magnification

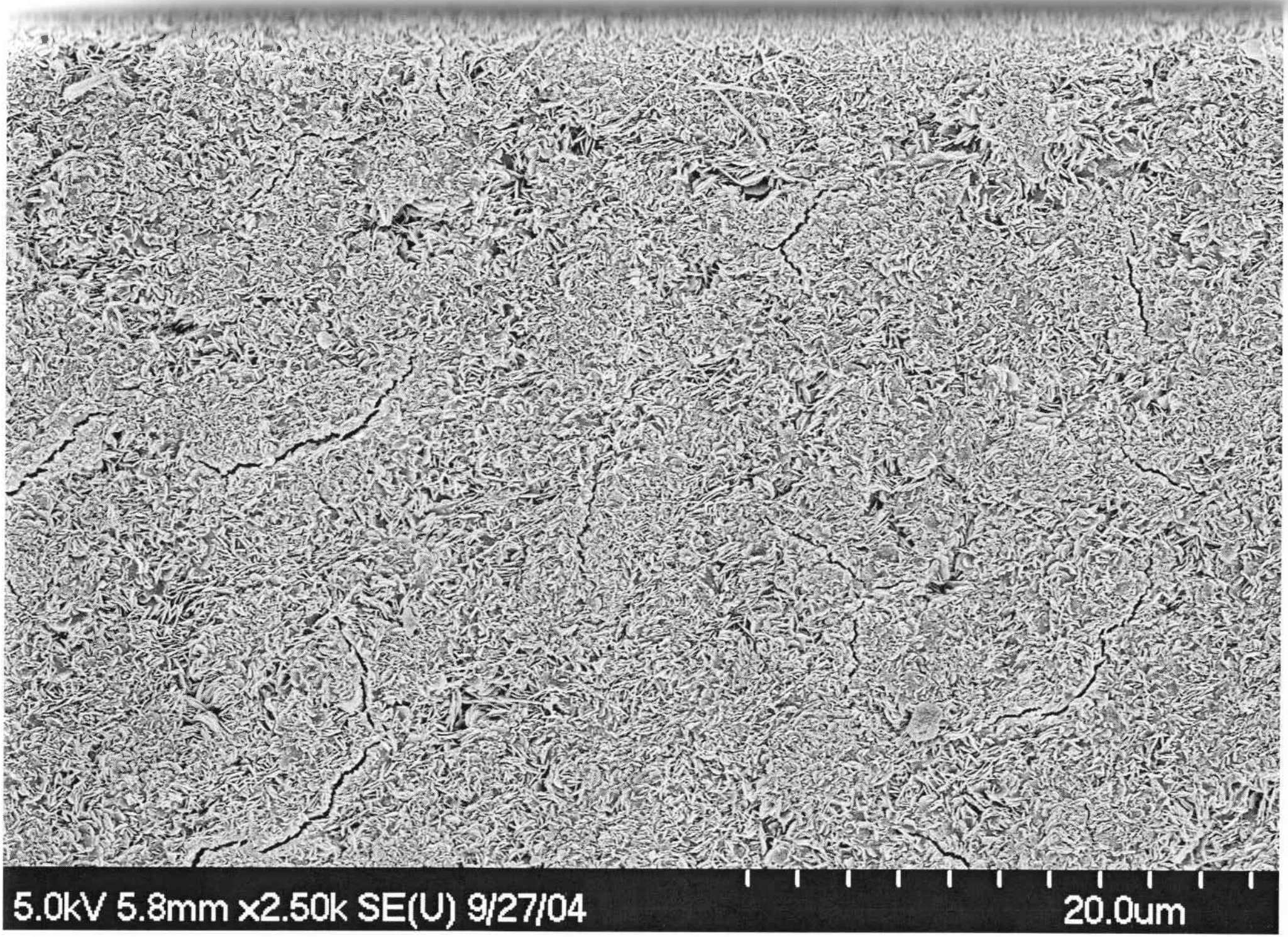
5.0kV 5.8mm x2.50k SE(U) 9/27/04
20.0um

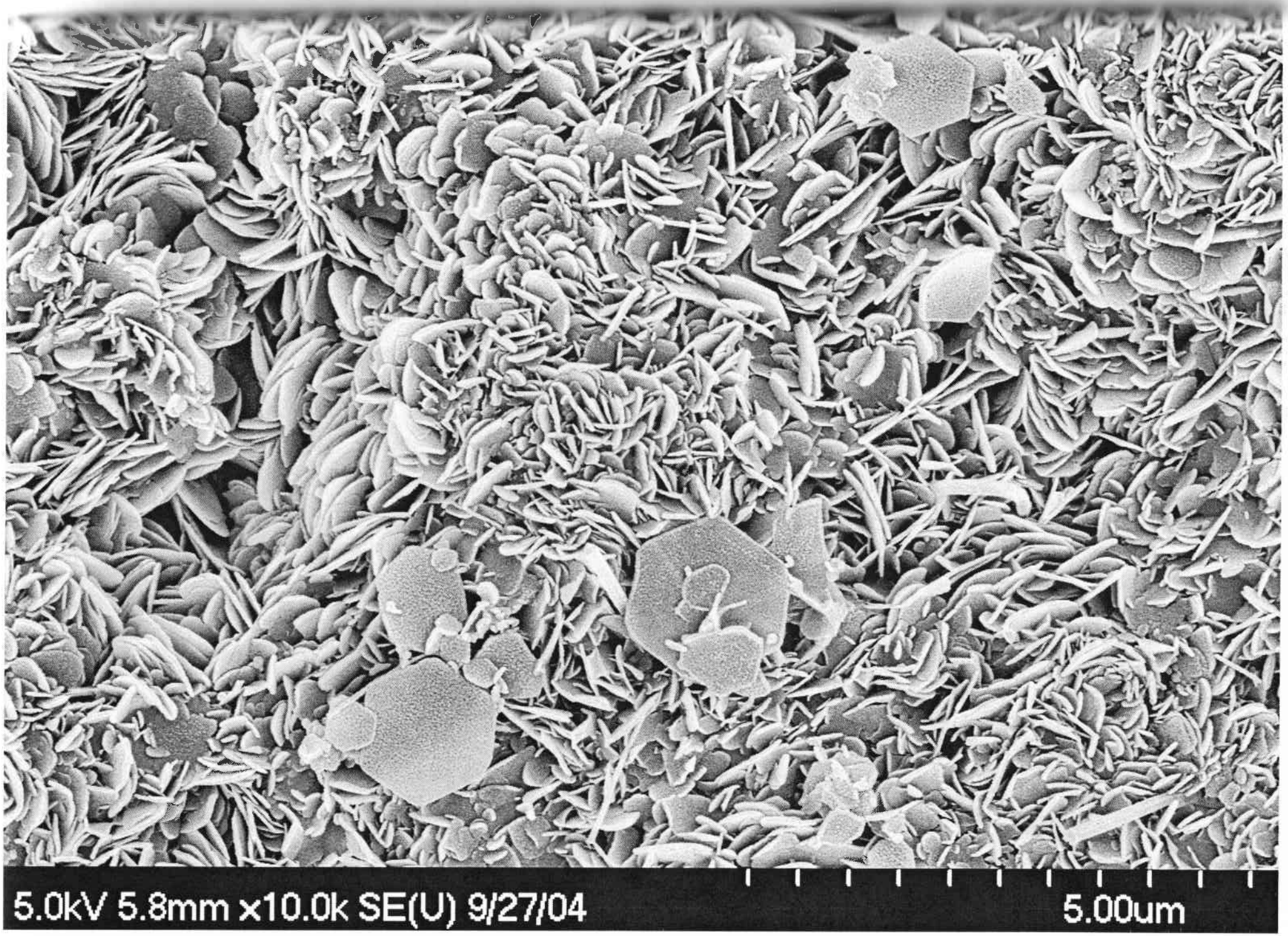
5.0kV 5.8mm x10.0k SE(U) 9/27/04
5.00um

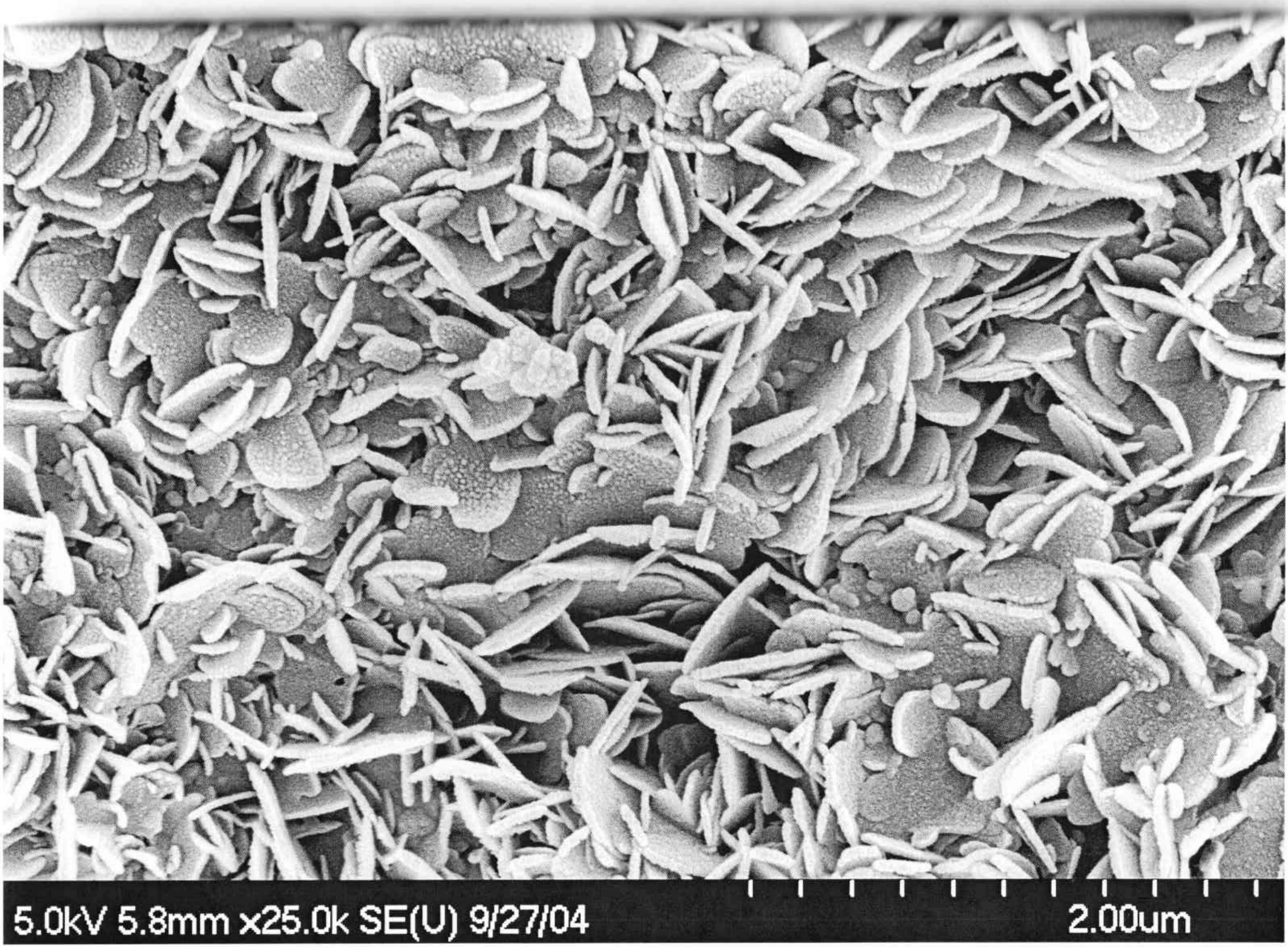
5.0kV 5.8mm x25.0k SE(U) 9/27/04
2.00um

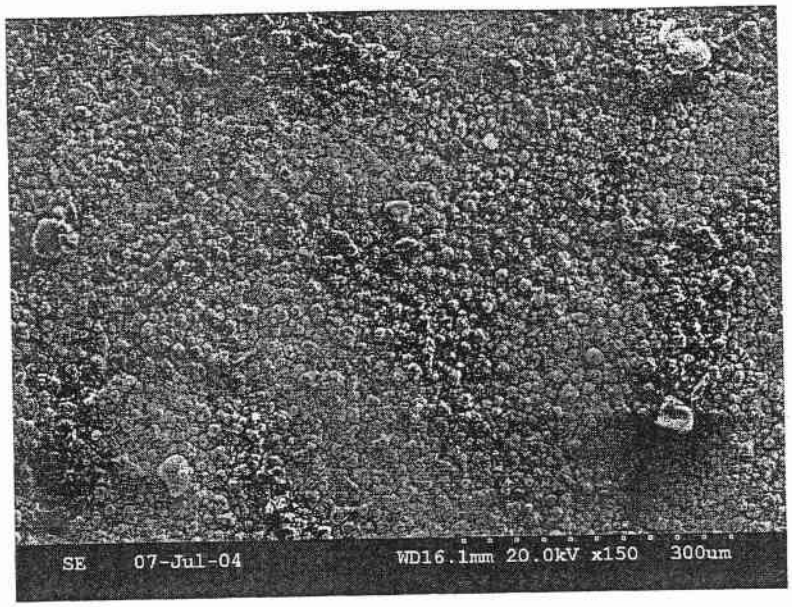

(a)

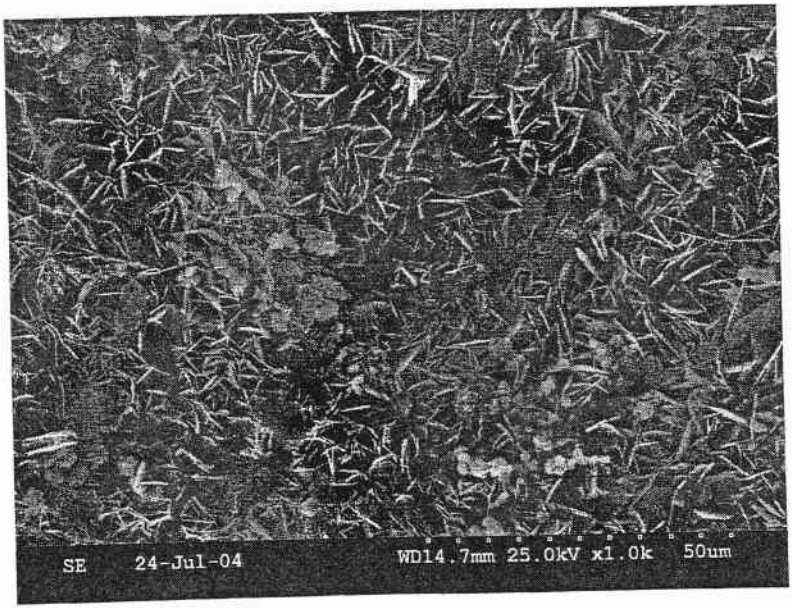

(b)

Figure 3.3 SEM Micrographs of Ca-P Coating on the Surface of Alumina (a) Low Magnification (b) High Magnification

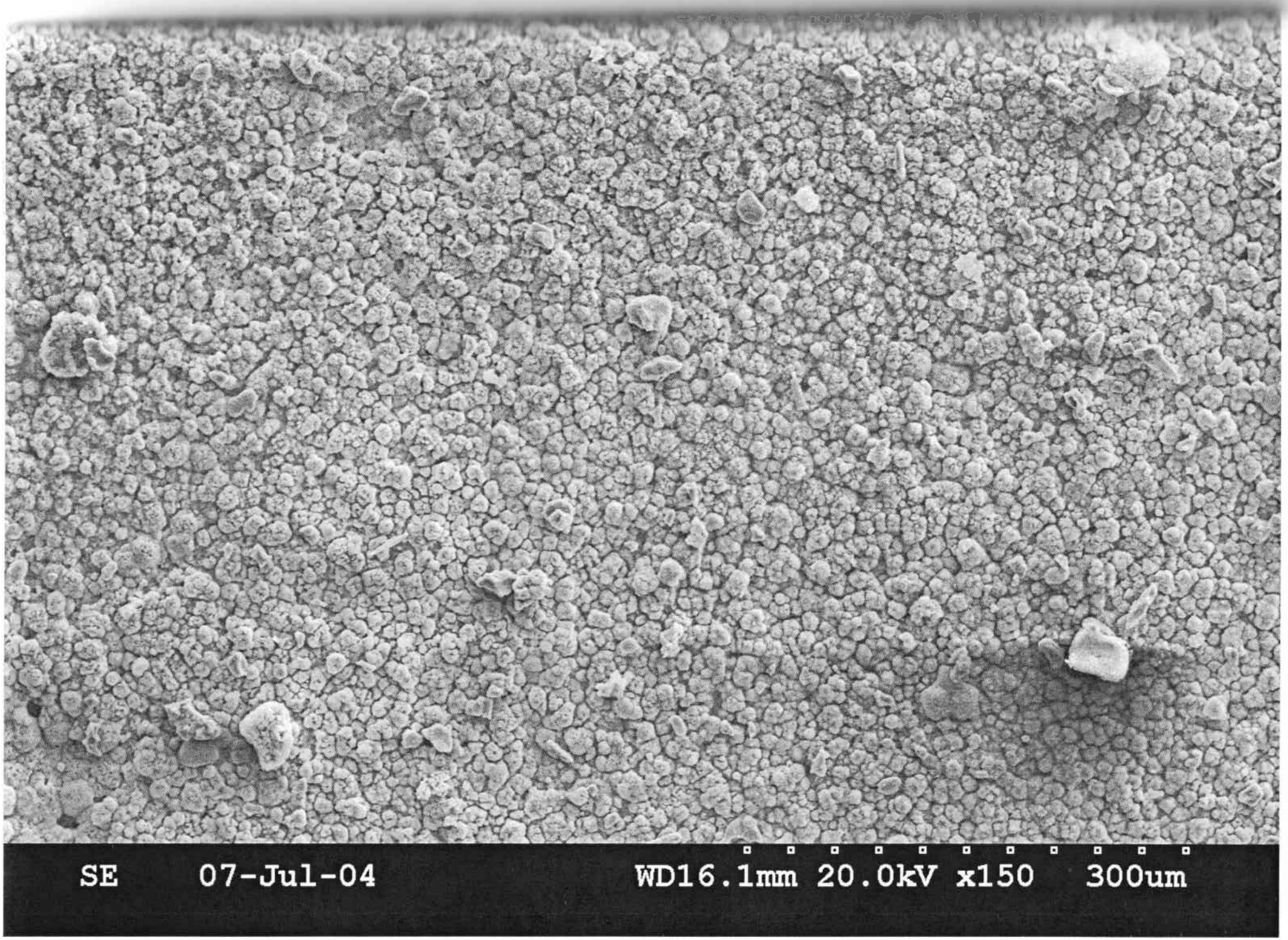
SE 07-Jul-04 WD16.1mm 20.0kV x150 300um

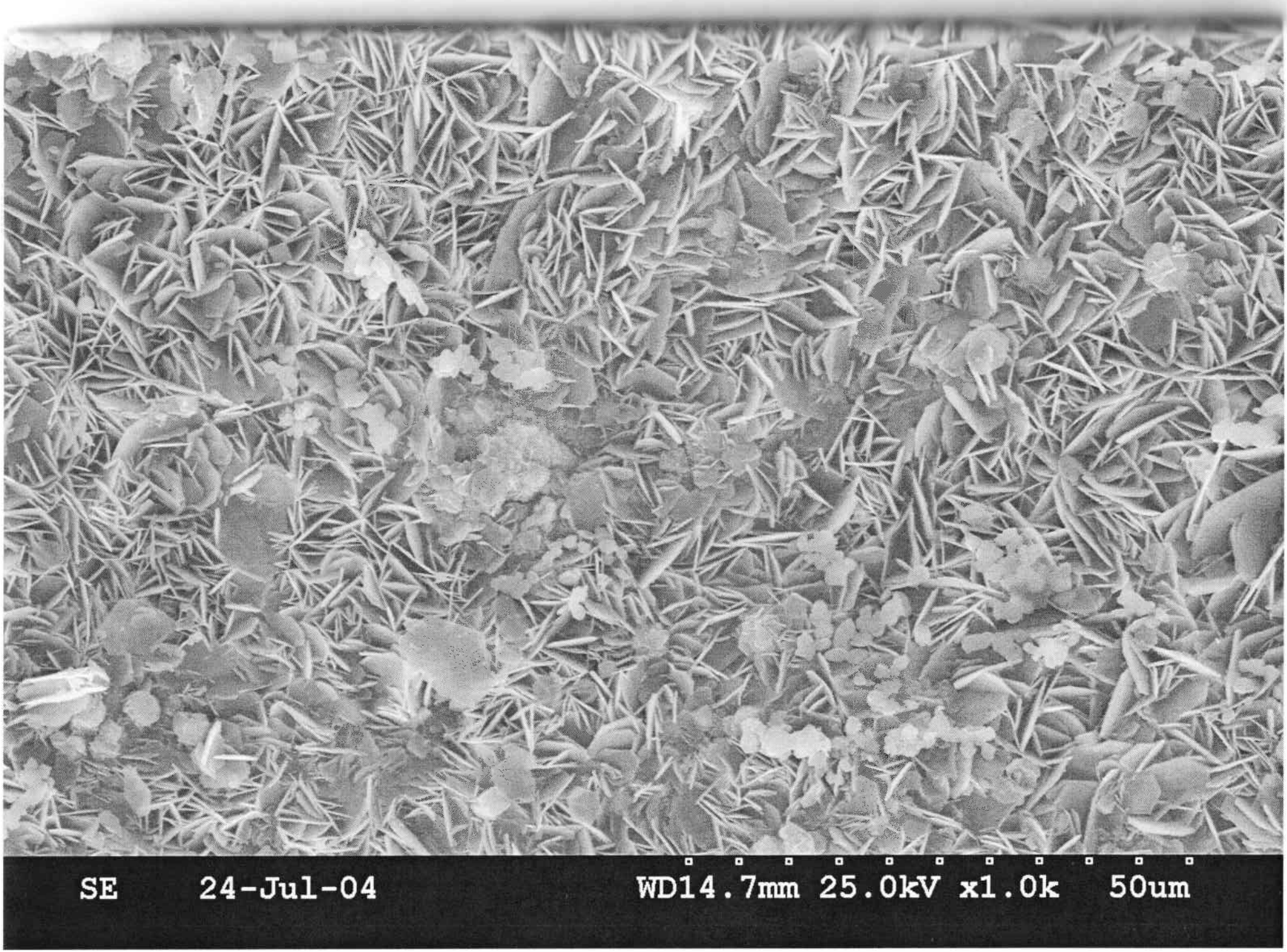
SE 24-Jul-04
WD14.7mm 25.0kV x1.0k 50um

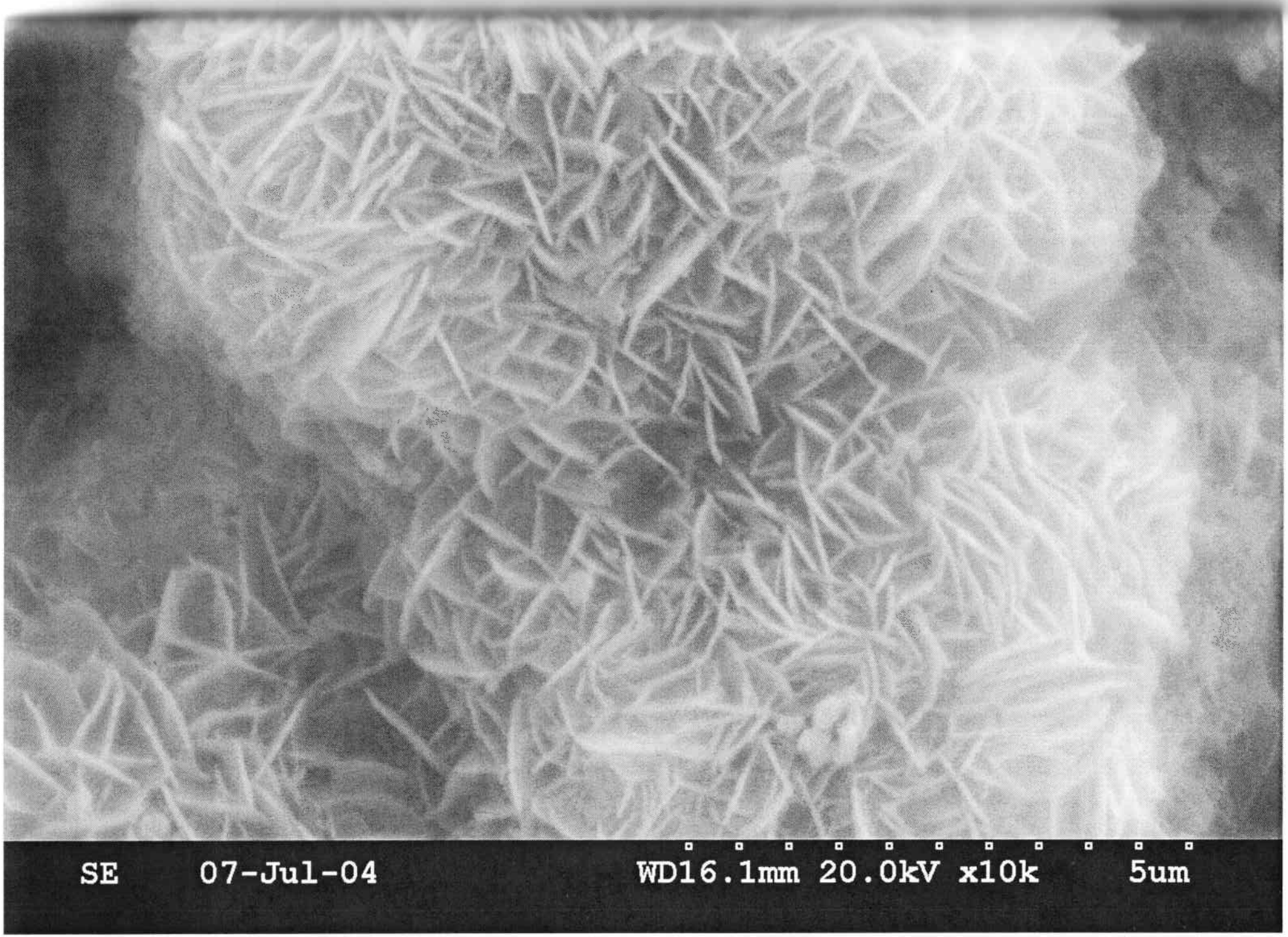
SE 07-Jul-04 WD16.1mm 20.0kV x10k 5um

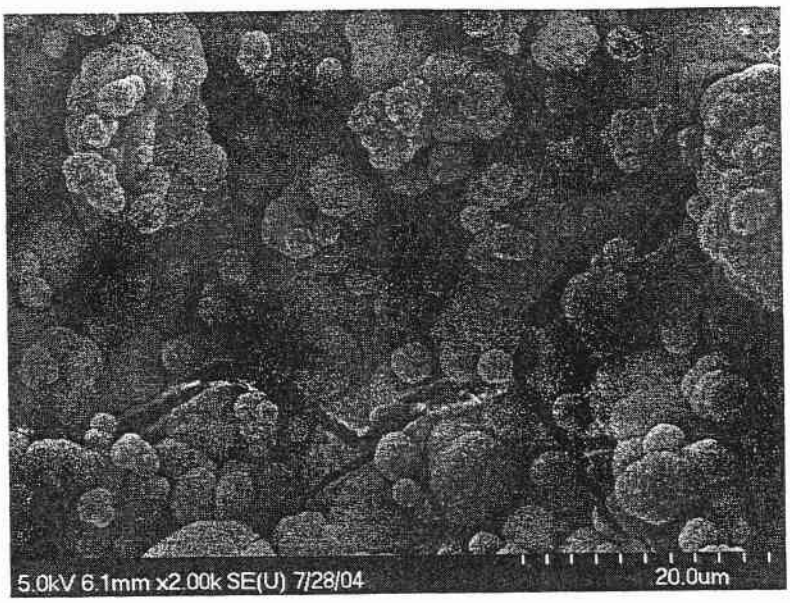

(a)

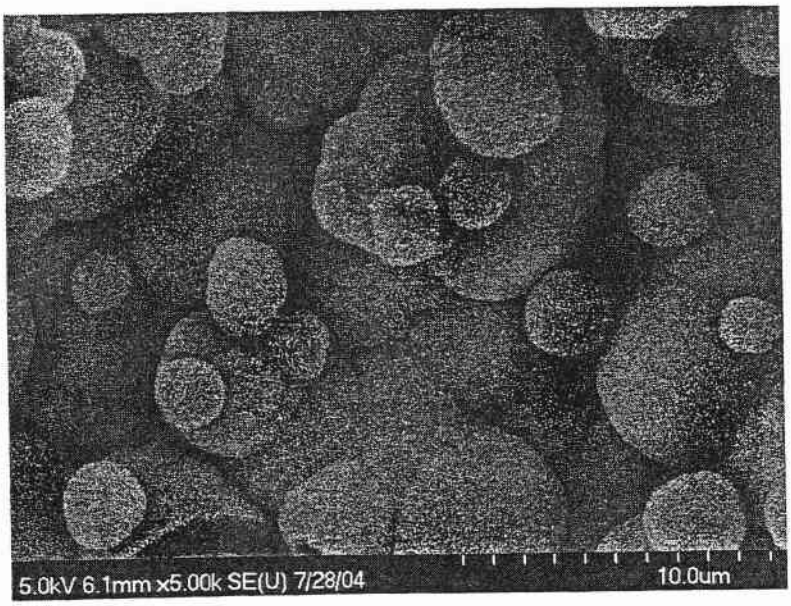

(b)

Figure 3.4 FE-SEM Micrographs of 1-week SBF Soaked Ca-P Coatings. (a) Low Magnification (b) High Magnification

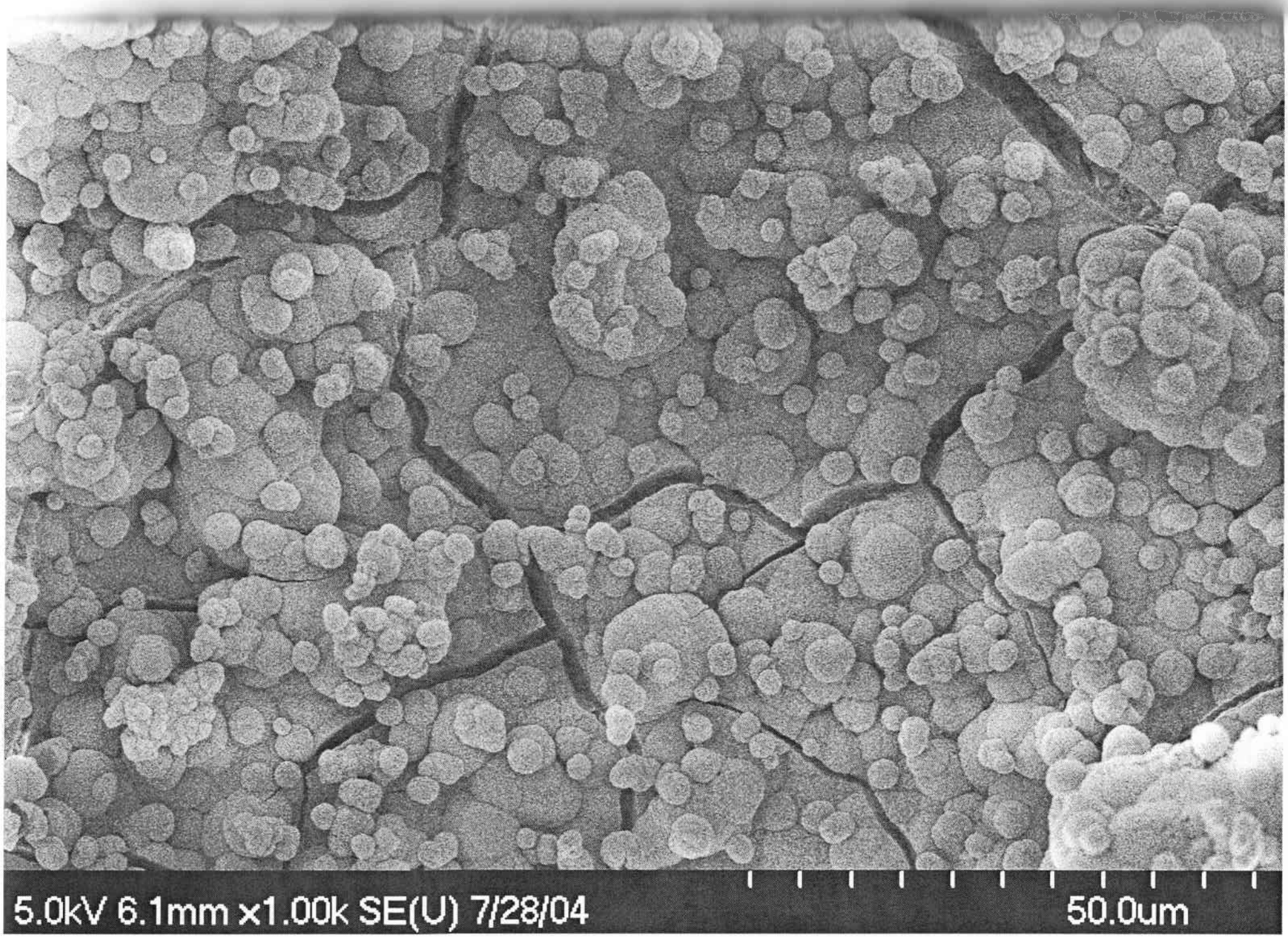
5.0kV 6.1mm x1.00k SE(U) 7/28/04
50.0um

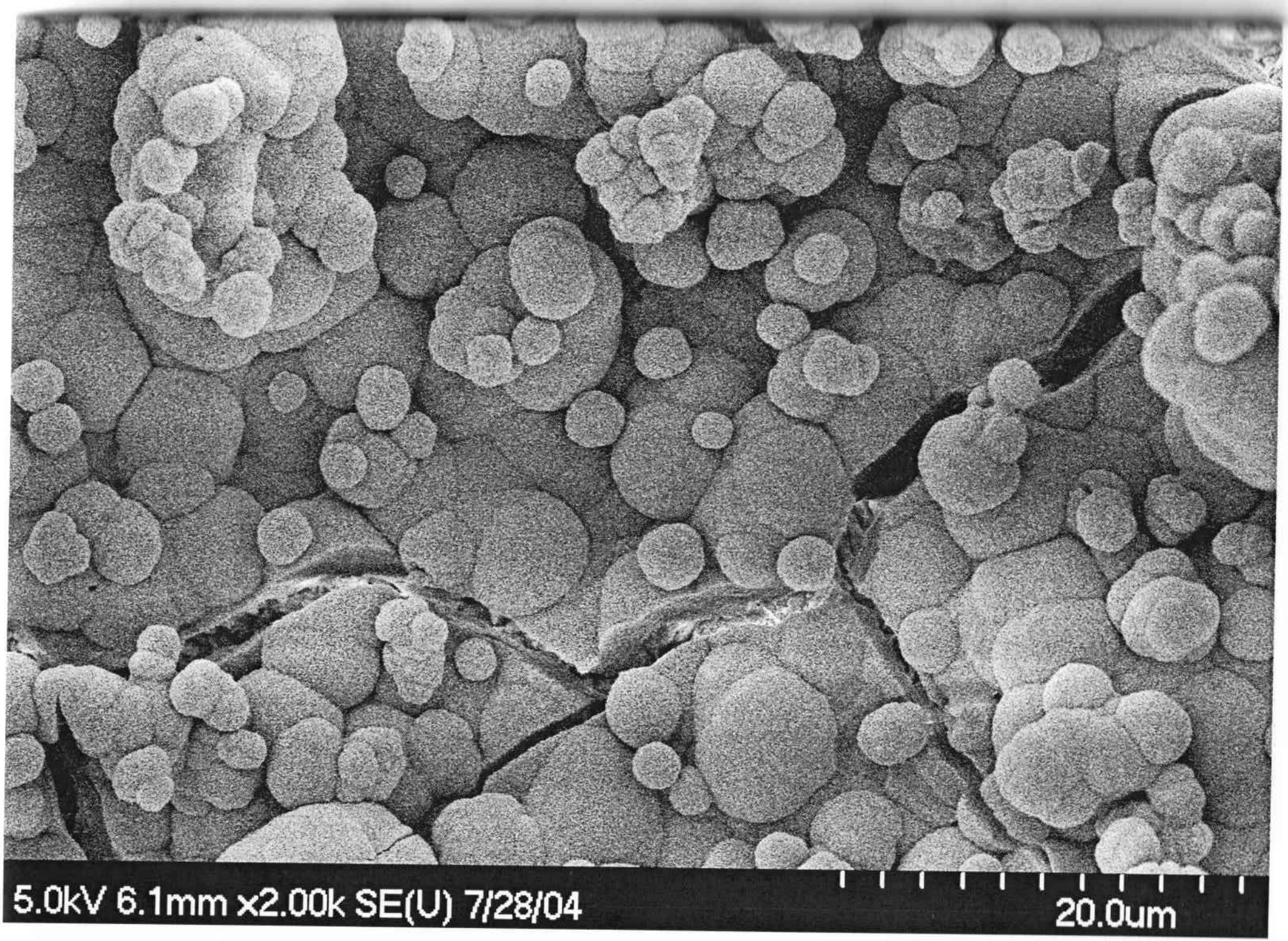
5.0kV 6.1mm x2.00k SE(U) 7/28/04
20.0um

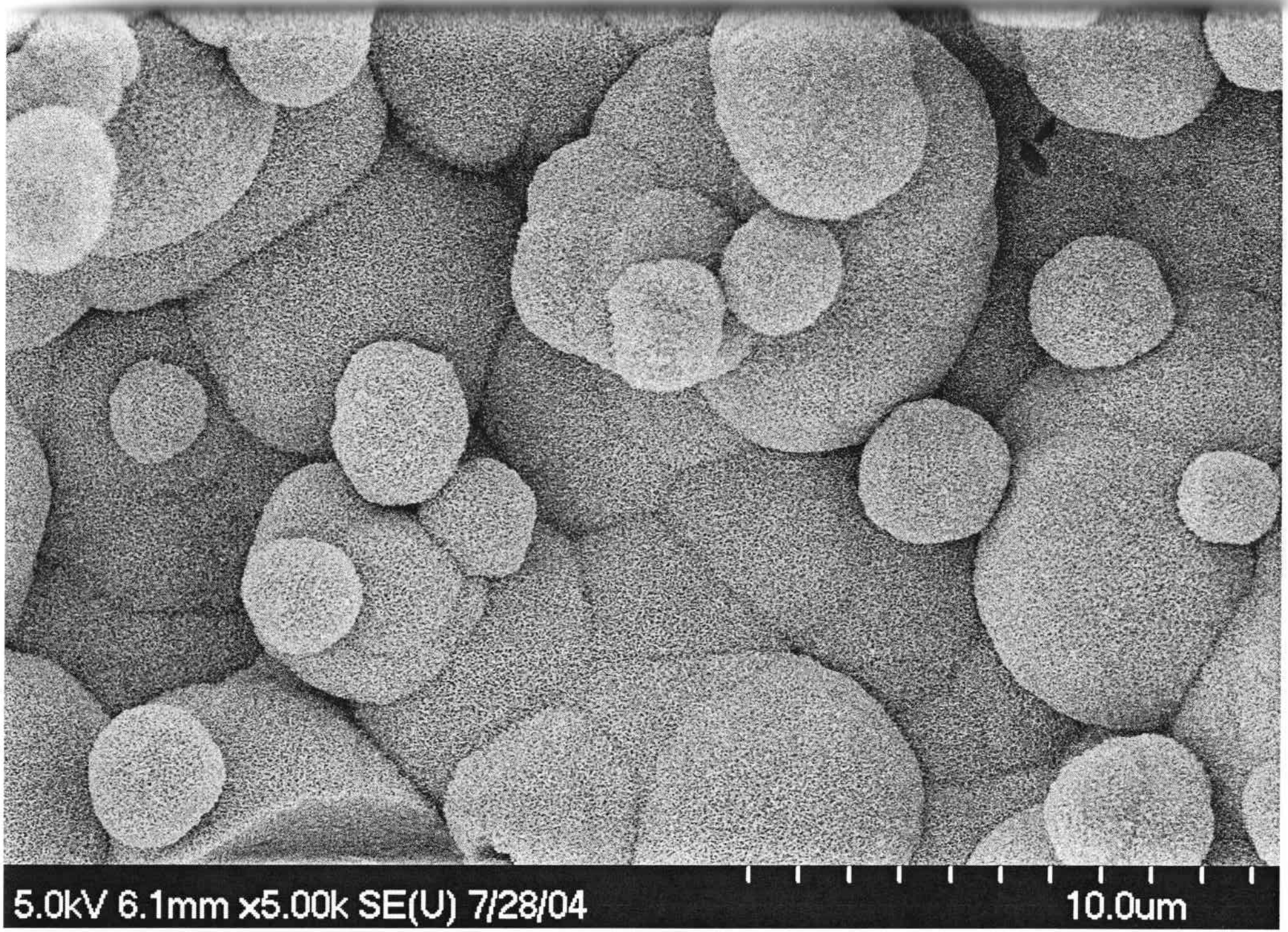
5.0kV 6.1mm x5.00k SE(U) 7/28/04
10.0um

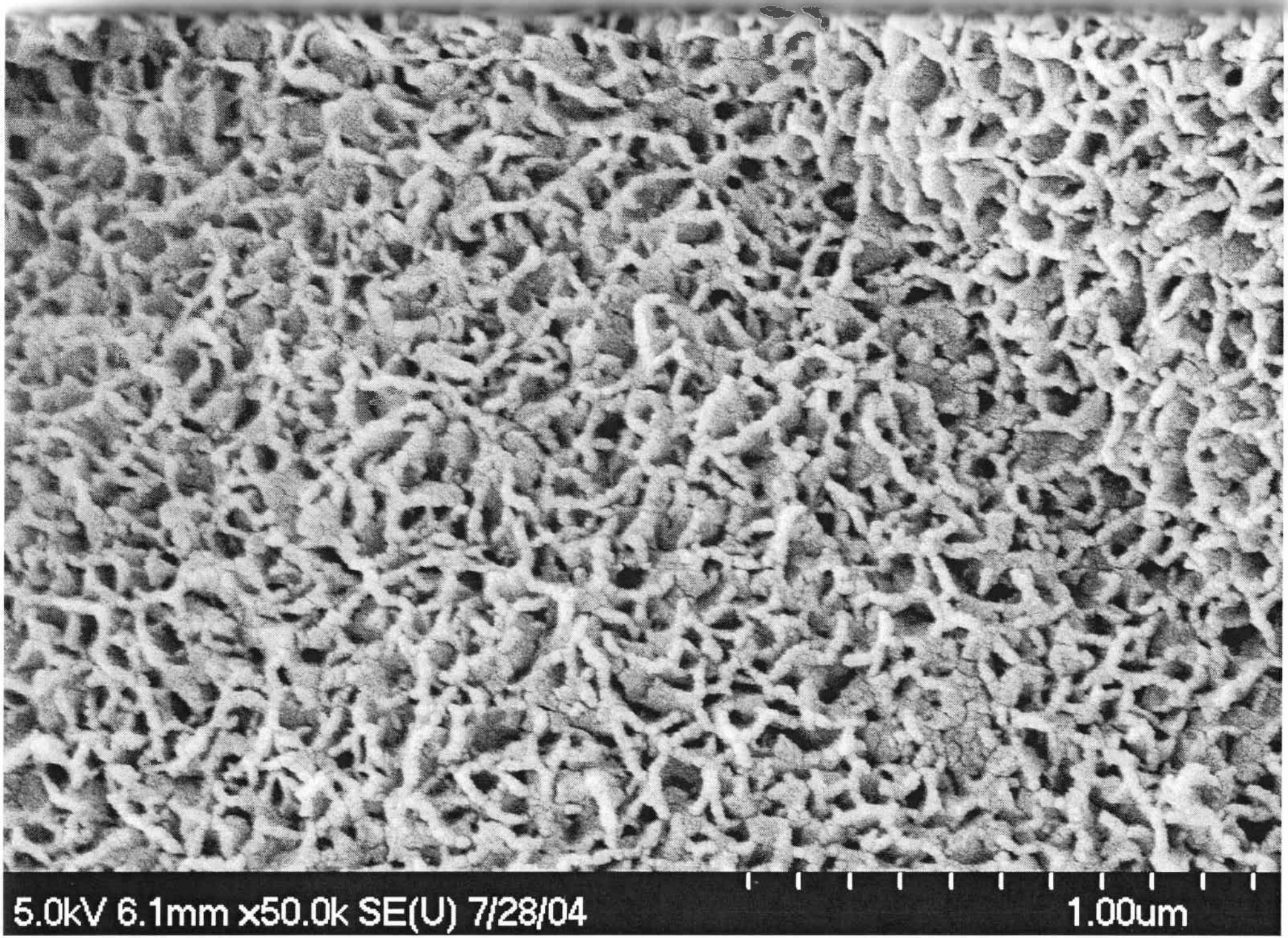
5.0kV 6.1mm x50.0k SE(U) 7/28/04
1.00um

3.3. XRD & FT-IR Analysis

XRD pattern of the scraped coating (Figure 3.5) from the substrate showed the presence of HA as the major phase where the peak positions match with the synthetic HA pattern (ICDD PDF card# 9-432). The peak located around 30° indicated the presence of the tricalcium phosphate (TCP) and CaO (peak at 37.5°) as a result of the available Ca^{+} ions in the system by the formation of TCP. TCP formation was generally attributed to the high temperature decomposition of HA. Hsieh *et al.* reported that CaO phase formation for the fast drying of the as-prepared precursors (16 hrs. aged sol at 80-90°C) under reduced pressure [44]. Their results did not reveal presence of TCP phase even after calcining powders at 600°C. They concluded that the presence of the CaO is due to the decomposition of undesirable $Ca(NO_3)_2$ precipitate during calcining. However, our results can not be explained by simple decomposition of the non-reacted calcium nitrate. Similar results reported by Liu *et. al.* for low temperature formation of HA by sol-gel synthesis. They proposed that amorphous Ca-P containing intermediate phases might already exist and transformed to crystalline phase (TCP) during the heat treatment [48]. An amorphous Ca-P containing intermediate phase was found by Hsieh *et al.* using solid sate nuclear magnetic resonance (NMR) spectroscopy. They showed that the gels converted into a 'glassy phosphate' at 350°C, then into the HA ceramic at 600°C [49].

Intensity changes for (100) and (200) planes are believed to be due to the platelets orientation. SEM images revealed the shrinkage along the c-axis which caused the intensity increase. Intensity abnormalities due to the crystal orientation have also been reported for HA whiskers where there was an elongation in the *c*-direction [50]. The

broadening of the peaks attributed to (100) and (200) planes might be explained either due to residual strains as a result of rapidly formed coatings or some lattice distortion [51].

Figure 3.5 shows the X-ray pattern of 1 week SBF soaked sample. The results confirmed the complete transformation of crystalline calcium phosphate chemistry to a poorly crystalline calcium deficient hydroxyapatite, which is almost identical with a human bone XRD pattern as shown in Figure 3.5 (inset). Coating Ca-P on alumina substrates using SBF had been attempted by Li *et al.* [15]. Previously, alumina surfaces subjected to an alkaline treatment (NaOH) prior to biomimetic process. Results showed a poor coating on the surface due to positively charged surface. Unlikely, in the present study we introduced a low crystalline (relative to sintered coatings at 1000°C) and reactive intermediate coating prior to the biomimetic process which was readily converted into bone-like apatite in SBF.

Conversion of a crystalline HA phase to a poorly crystalline calcium deficient apatite might be explained due to the defective crystal structure, reactivity and low crystallinity of the Ca-P coating deposited onto the surface. Stoichiometric HA has a very limited solubility in super saturated solutions but non-stoichiometric (or defective) HA may cause this conversion due to faster ion exchange. Driving force and activation energy required for this reaction take place is clearly explained by Shi *et al.* It was found that an increase in crystallinity greatly reduces the reactivity and so does Ca^{+} release [52].

FT-IR spectra of Ca-P coating is shown in Figure 3.6a. The spectra indicated phosphate (1090, 1050, 962, 602, and 571 cm^{-1}), carbonate (1410 and 876 cm^{-1}) and hydroxyl (3310-3580 cm^{-1}) groups in the coating. The peaks at 1050 and 1090 cm^{-1}

correspond to the ν_3 vibration mode of PO_4^{3-} indicating the stoichiometric apatite [53]. These bands are the ν_3 fundamental vibration mode of PO_4^{3-} tetrahedral corresponding to the triply degenerate asymmetric P-O stretching modes [54]. The band at about 962 cm^{-1} belong to the ν_1 symmetric P-O stretching vibration of the PO_4^{3-} [53]. The remaining two PO_4^{3-} peaks (602, and 571 cm^{-1}) correspond to the ν_4 domain [55].

The 878 cm^{-1} band represents ν_2 mode carbonate ions occupying the monovalent anionic sites of the apatite structure (type A carbonate) [56]. Type A refers to the substitution of the OH- group in the crystal lattice by CO_3^{2-} in the apatite structure where else, Type B is the substitution of the PO_4^{3-} in the lattice [57]. The broad band between 1400-1600 cm^{-1} corresponds to the ν_3 CO_3^{2-}. The peak at 1380 cm^{-1} is believed to be belonging to an unstable carbonate species appear at the early stages of formation (low temperature formation) and disappear with the crystallinity increases [54].

The hydroxyl band in the spectrum showed a sharp OH^- stretching $Ca(OH)_2$ peak at 3640 cm^{-1} [46]. On the other hand, the presence of $Ca(OH)_2$ was not detected by XRD analysis. It might be explained by the previously reported CaO FT-IR spectra with $Ca(OH)_2$ and carbonate impurities [58] which shows a sharp stretching peak at 3640 cm^{-1} with very similar intensity. The two broad H_2O absorption peaks (3310-3580, and 1610-1630 cm^{-1}) may be related to the surface morphology of the coating. As shown in the Figure 3.2b, the coating appeared porous (horizontal stacking gaps) thus, allowing more water molecule absorption on its surface [38].

FT-IR spectra for the one week SBF soaked sample was shown in Figure 3.6b. Distinguished changes occurred after the SBF soaking. The OH^- peak at 3640 cm^{-1} corresponds to $Ca(OH)_2$ disappeared and the absorbed water at 3400-3600 cm^{-1} became

more visible as a broad peak. The intensity of v_3 CO_3^{2-} peak at 1480 cm^{-1} decreased and it became broader. No noticeable changes occurred to $v_1$and v_3 domain PO_4 ions.

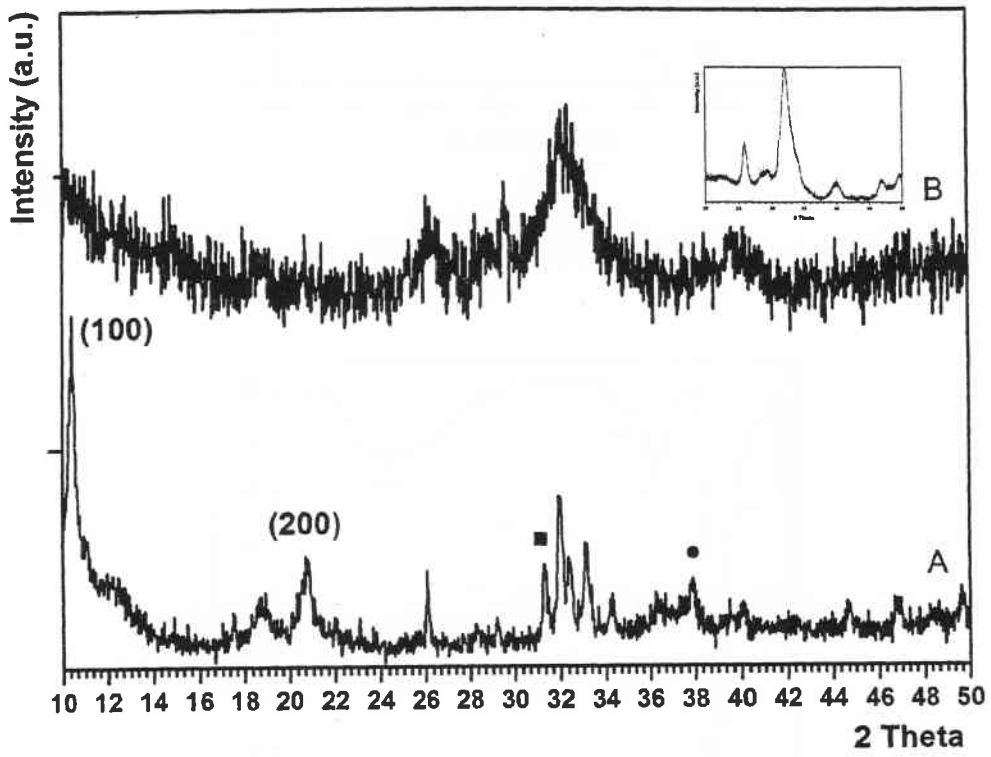

Figure 3.5 X-ray Diffraction Patterns of (A) Ca-P Coating on Al_2O_3(B) 1-week SBF Soaked Ca-P Coating. Inset; X-ray Diffraction of Human Bone.
(•)CaO, (■)TCP, others HA

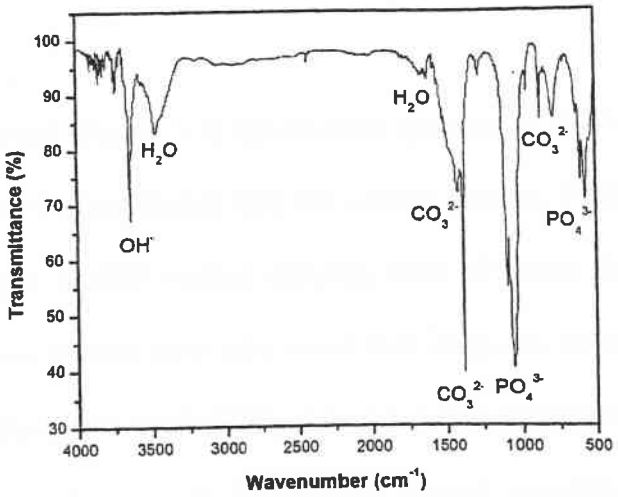

(a)

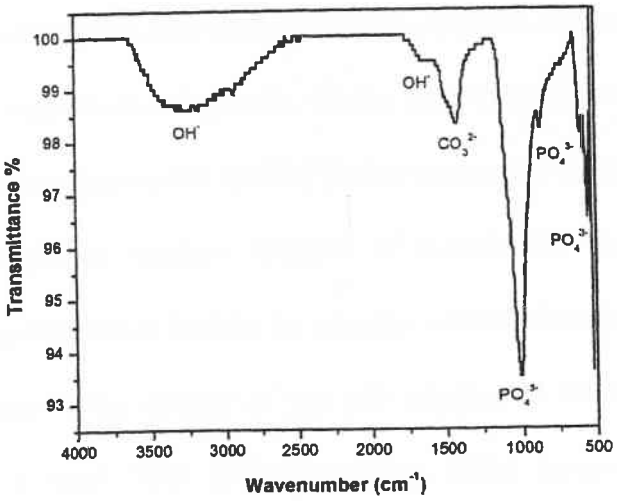

(b)

Figure 3.6 (a) FT-IR Spectra of Ca-P Coating. (b) FT-IR Spectra of 1-week SBF Soaked Ca-P Coating.

3.4. *In-Vitro* study

Cell viability test (Figure 3.7) showed that the amount of the cells attached to Ca-P coated samples was 4 times higher then the control sample. While, number of the cells attached to the surface of SBF soaked samples were 10 times higher then the alumina control sample. Those results were also consistent with the total protein concentration assay (Figure 3.8). Up to two weeks SBF soaked samples showed the highest total protein concentrations compared to Ca-P coated and control samples. The results can be correlated to the coating chemistry where SBF soaked samples have the closest chemical formula to the human bone.

The Ca-P coating produced on the substrate samples certainly provided a friendly environment for the osteoblast cell growth. On the other hand, poorly crystalline, calcium deficient hydroxyapatite (biological apatite) further increased the growth rate of the cells. Moreover, the nanoporous surface features of biomimetic application favored the increase of the cell proliferation besides its superior surface chemistry.

Figure 3.9 shows the quality of the cell attachment on the surfaces of control, Ca-P coated, and 1 week SBF soaked samples. SEM images showed an increase metabolic activity on the control, Ca-P coated, and SBF soaked samples, relatively. For instance vinculin adhesion plaques were in contact with HA platelets associated with stress fibers (filipodia) on Ca-P coated sample (Figure 3.10a). Additionally, SEM images of SBF soaked samples showed spread actin cytoskeleton on the globules associated with vinculin adhesion plaques (Figure 3.10b, c).

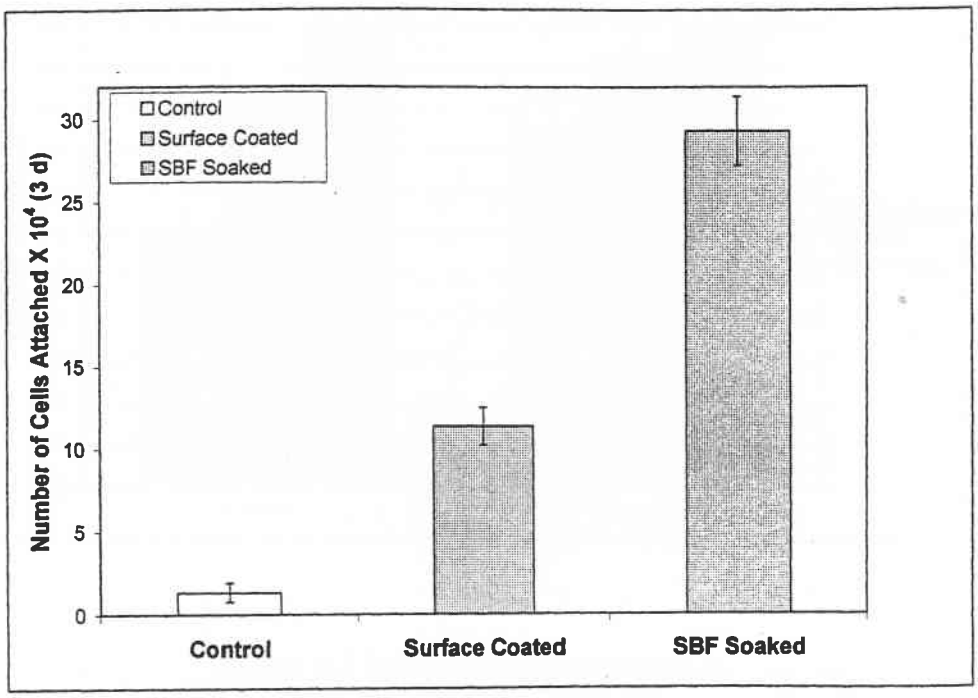

Figure 3.7 Cell Viability Results.

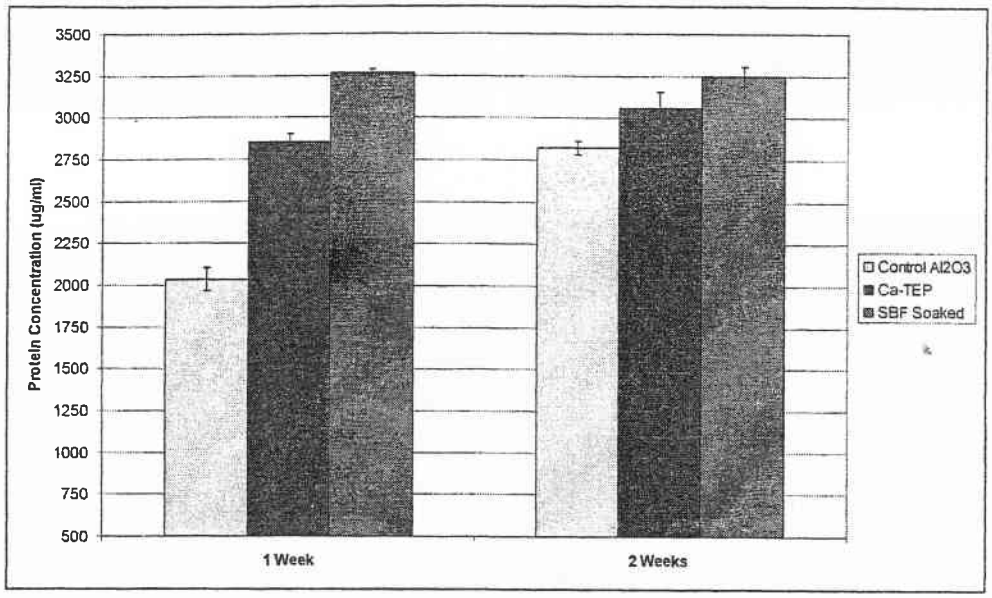

Figure 3.8 Total Protein Concentration.

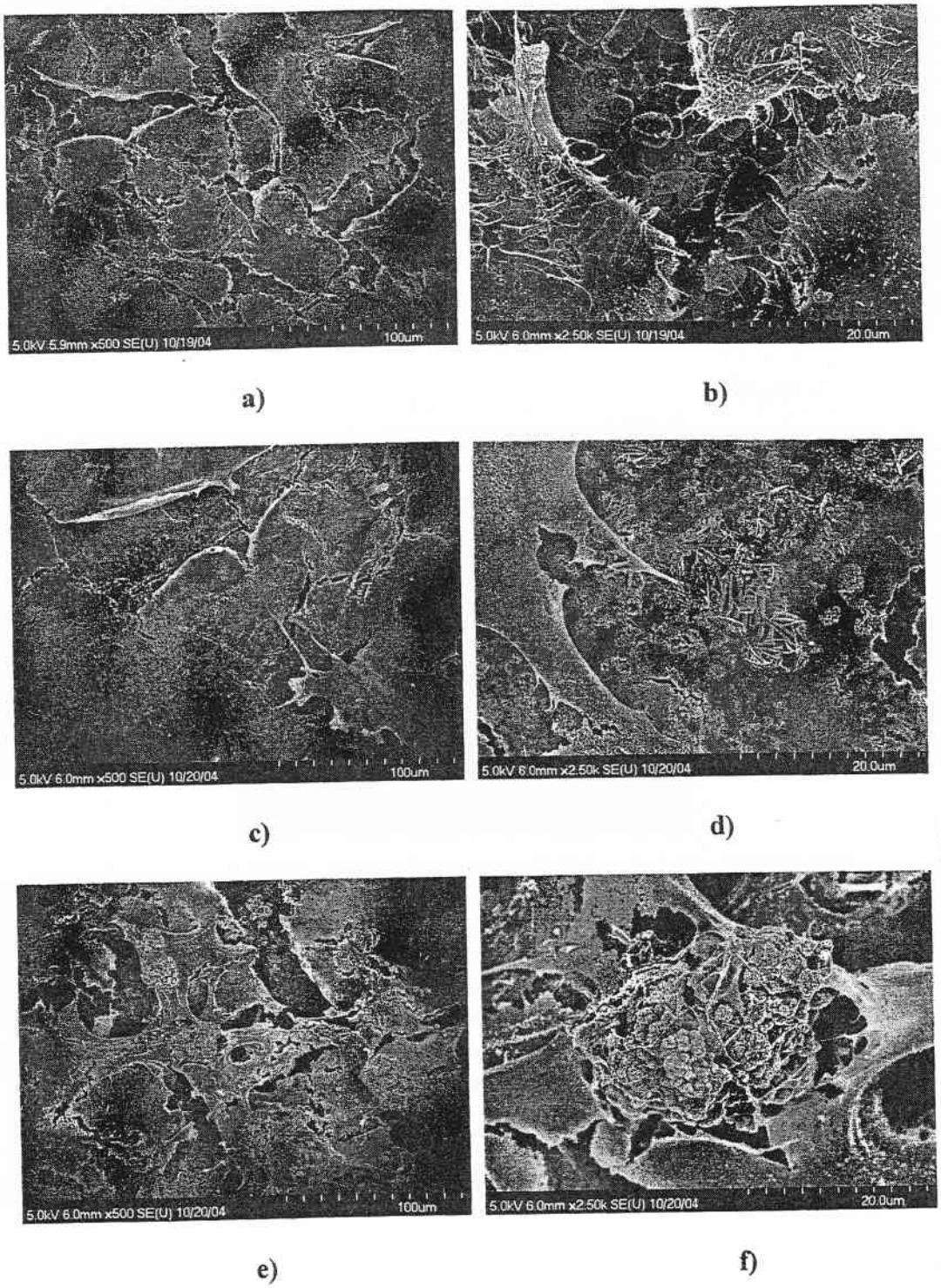

Figure 3.9 SEM Micrographs of Cell Attachment on the (a, b) Alumina Control Sample (Low Mag. and High Mag.) , (c, d) Ca-P Coated Sample (Low Mag. and High Mag.), (e,f) SBF Soaked Sample (Low Mag. and High Mag.)

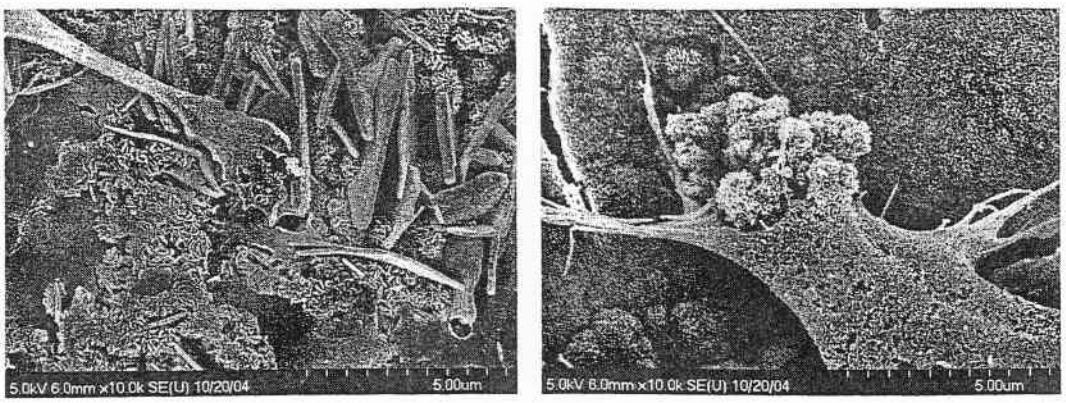

(a) (b)

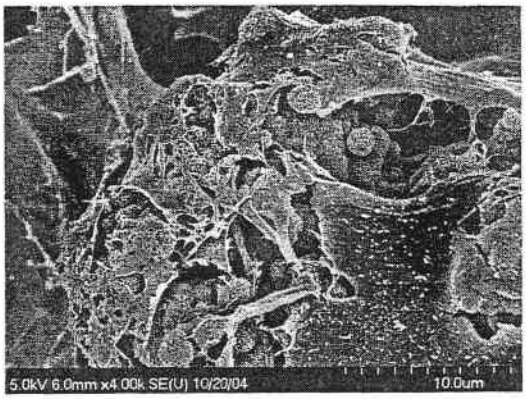

(c)

Figure 3.10 FE-SEM Micrographs of (a) Vinculin Adhesion Plaque Attached to the HA Platelet on Ca-P Coated Sample, (b) Vinculin Adhesion Plaques in contact with HA Globules Associated with Stress Fibers (Filipodia) on SBF Soaked Sample, (c) Spread Actin Cytoskeleton on the Globules Associated with Vinculin Adhesion Plaques on SBF Soaked Sample.

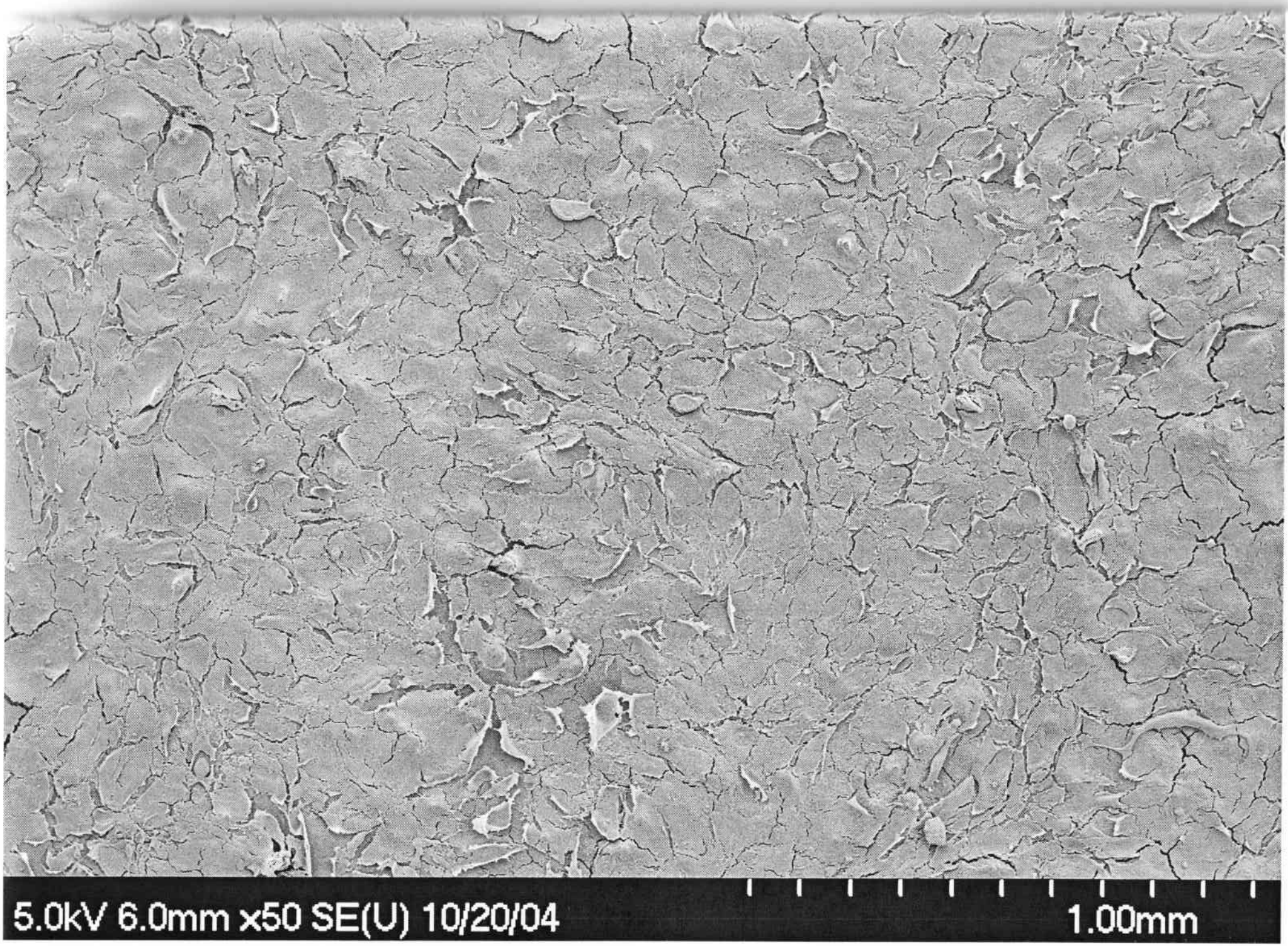
5.0kV 6.0mm x50 SE(U) 10/20/04
1.00mm

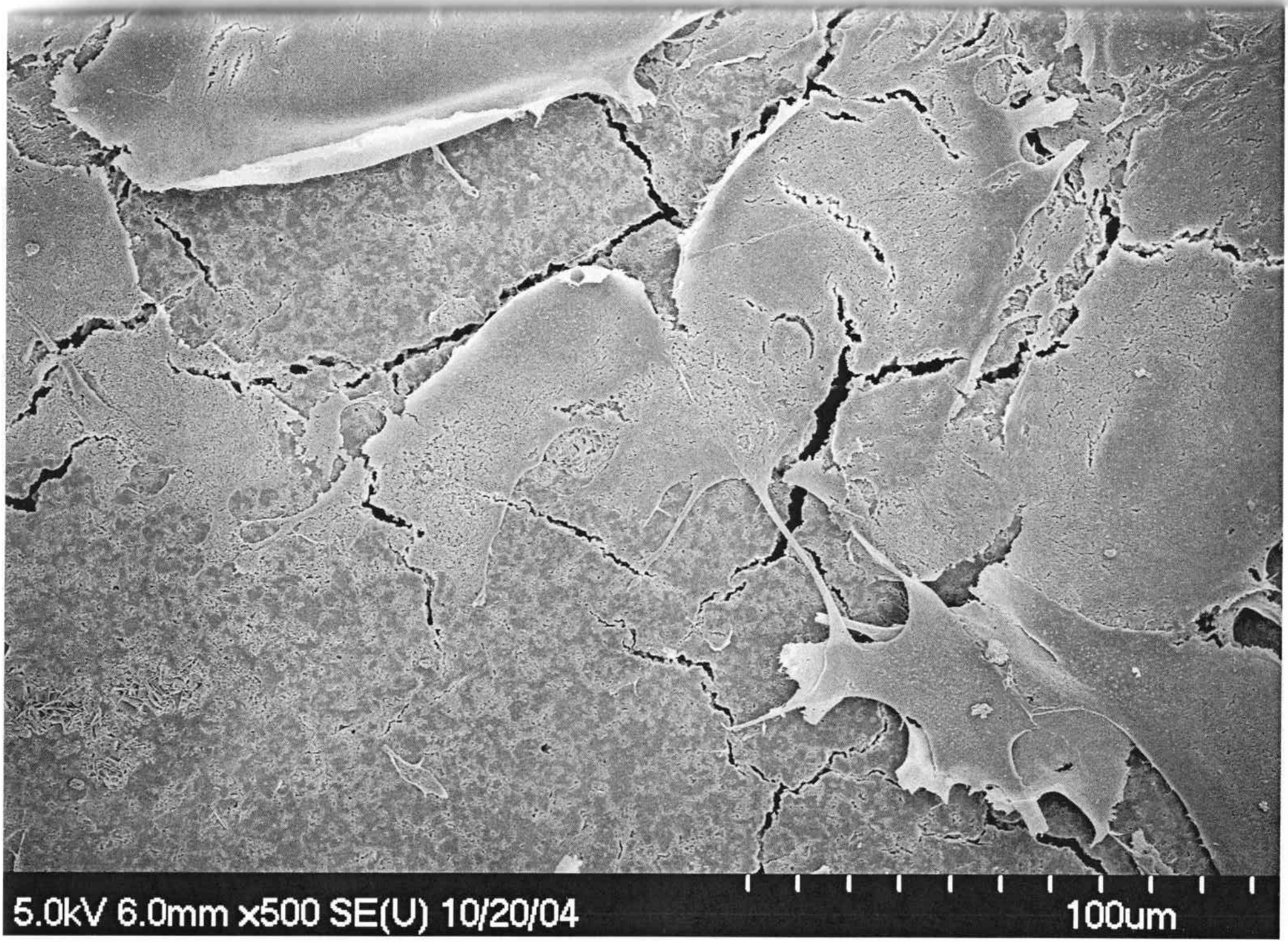
5.0kV 6.0mm x500 SE(U) 10/20/04
100um

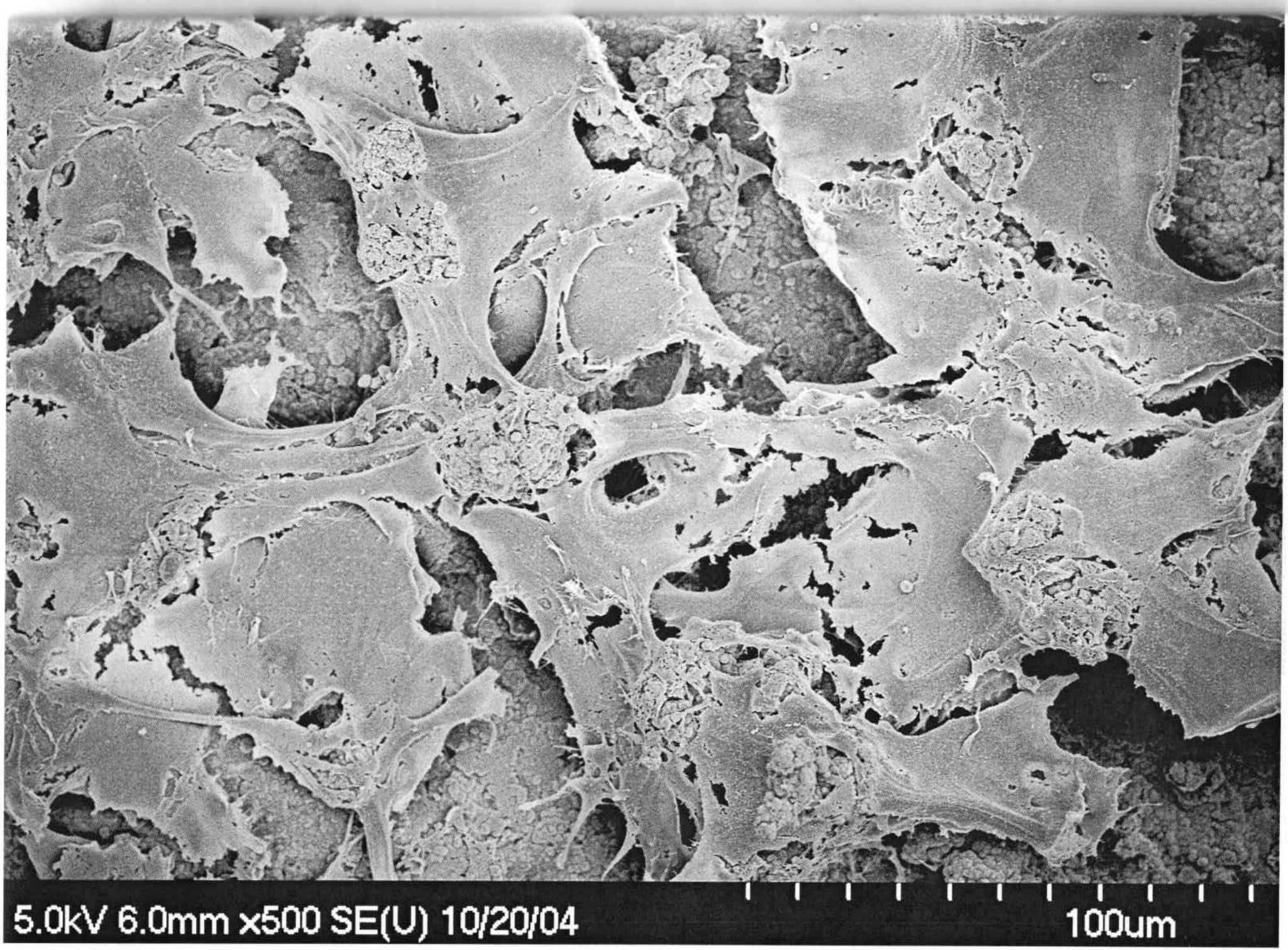
5.0kV 6.0mm x500 SE(U) 10/20/04
100um

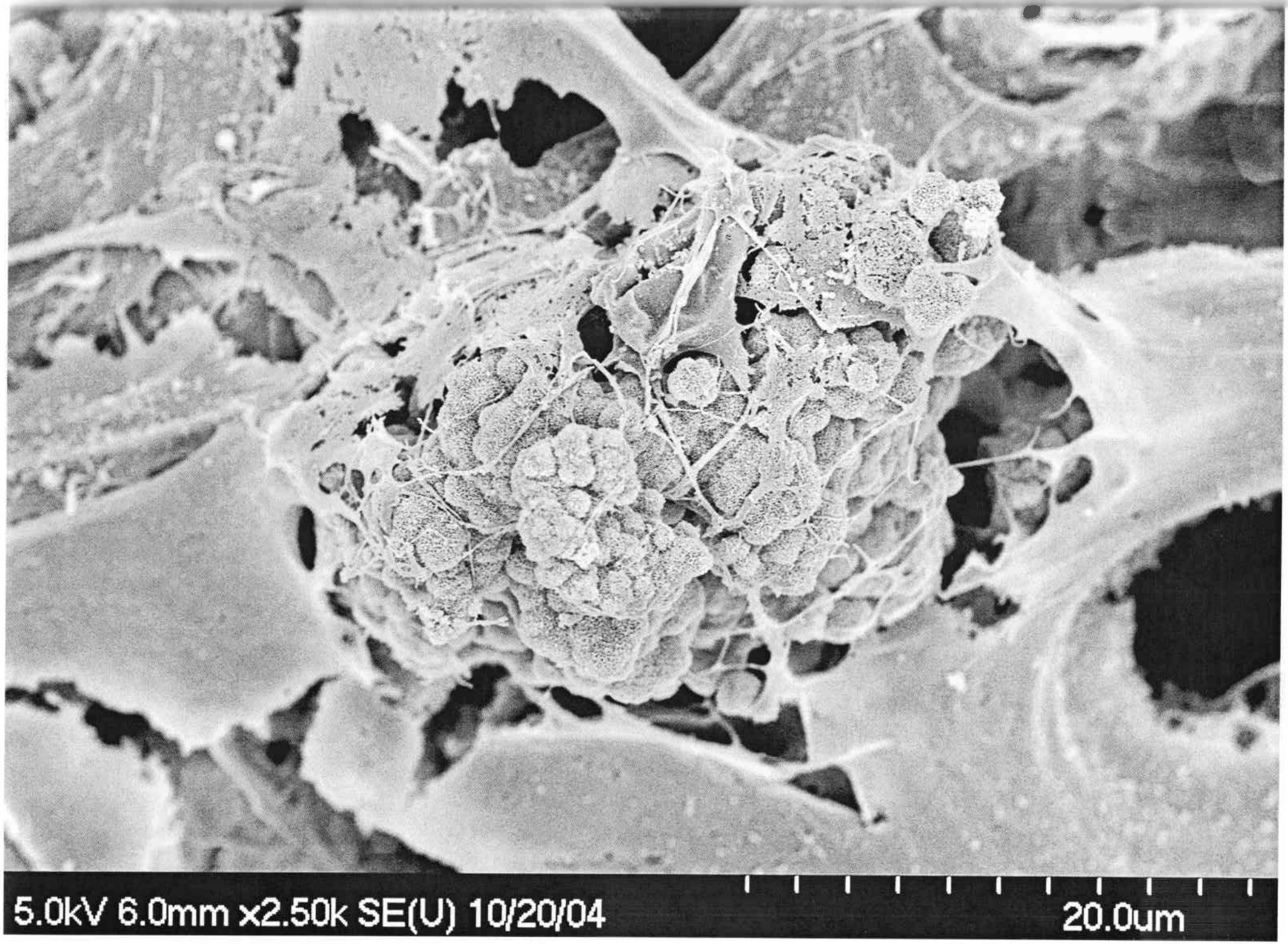
5.0kV 6.0mm x2.50k SE(U) 10/20/04
20.0um

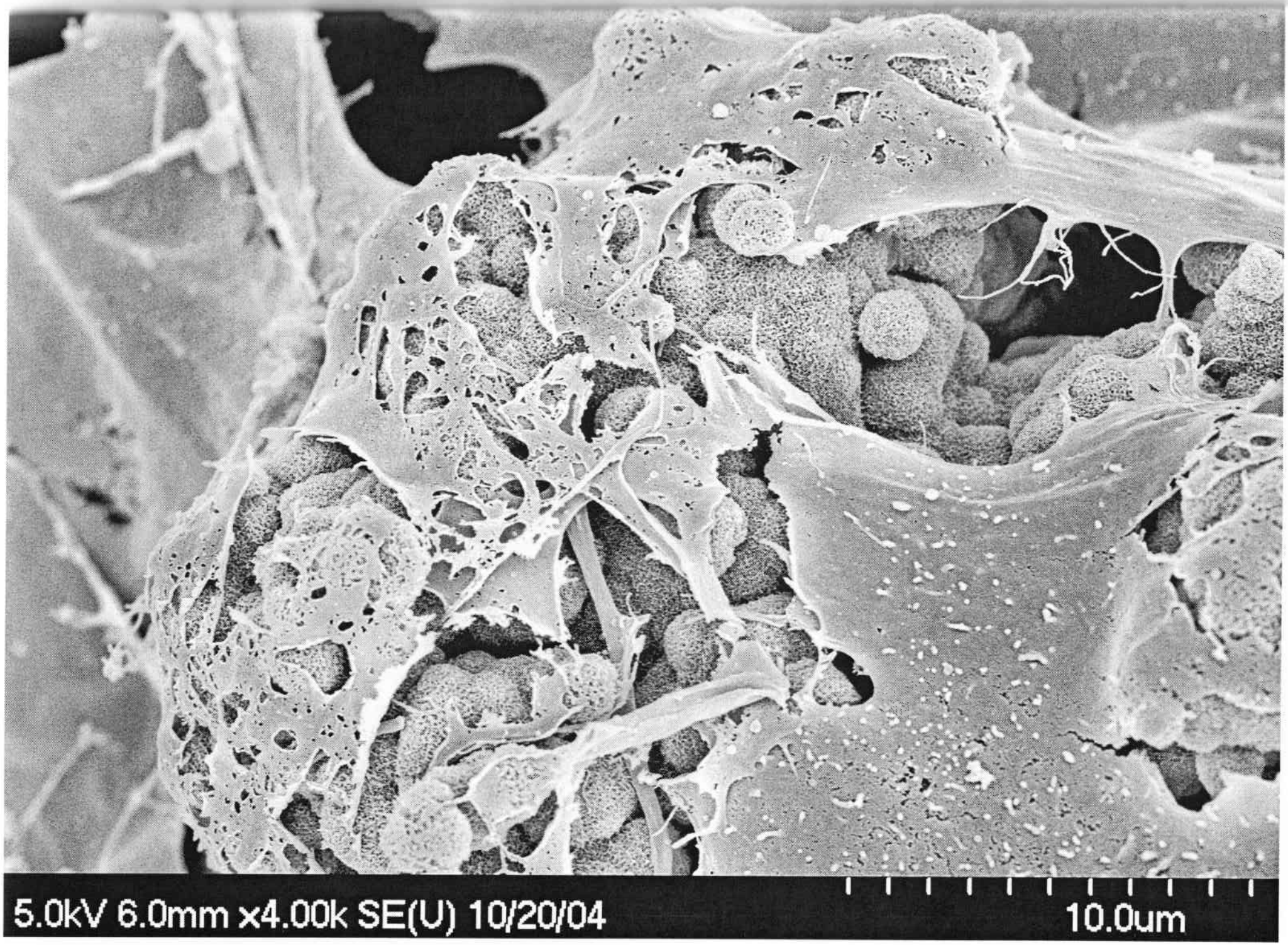
5.0kV 6.0mm x4.00k SE(U) 10/20/04
10.0um

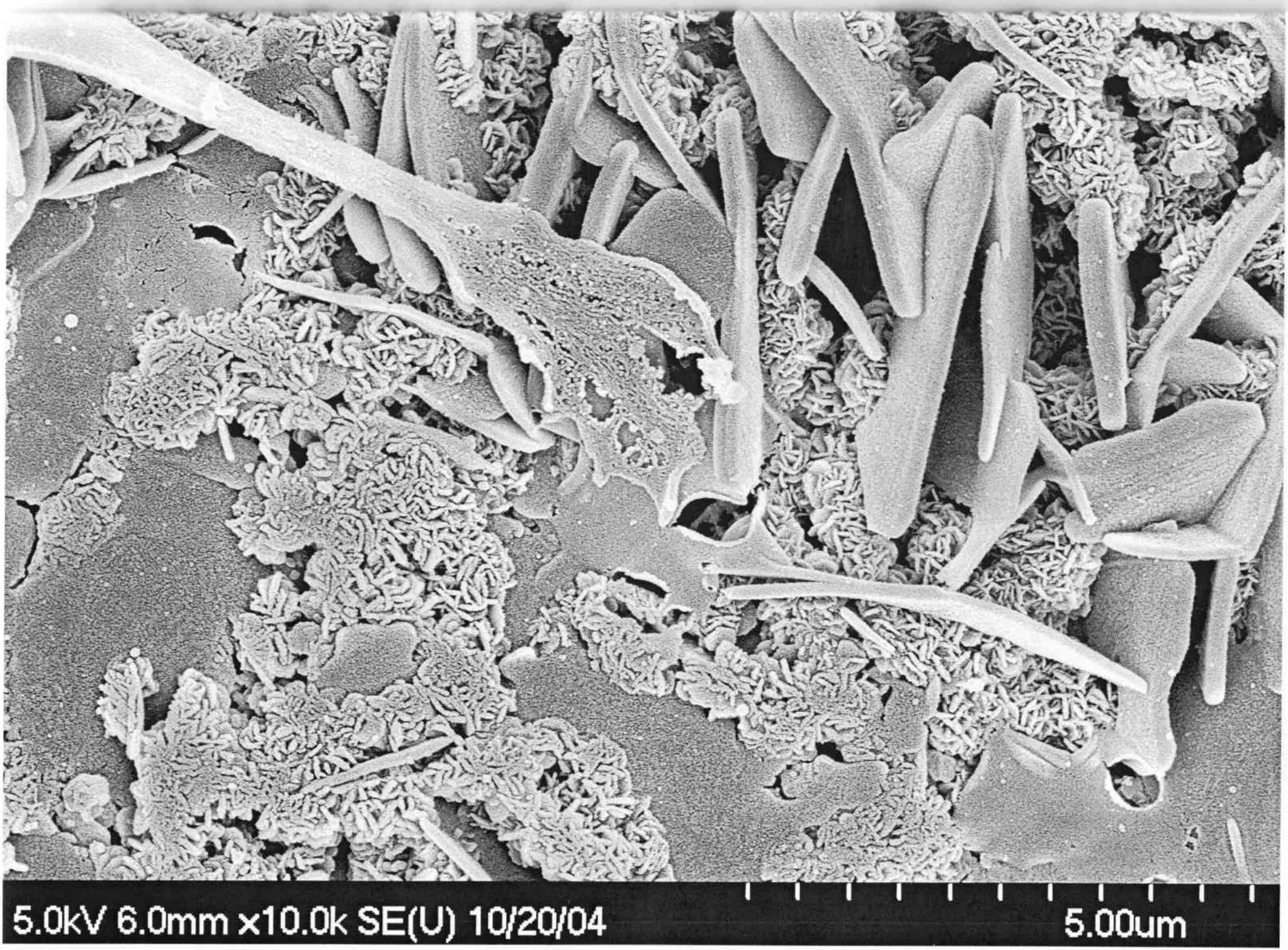
5.0kV 6.0mm x10.0k SE(U) 10/20/04
5.00um

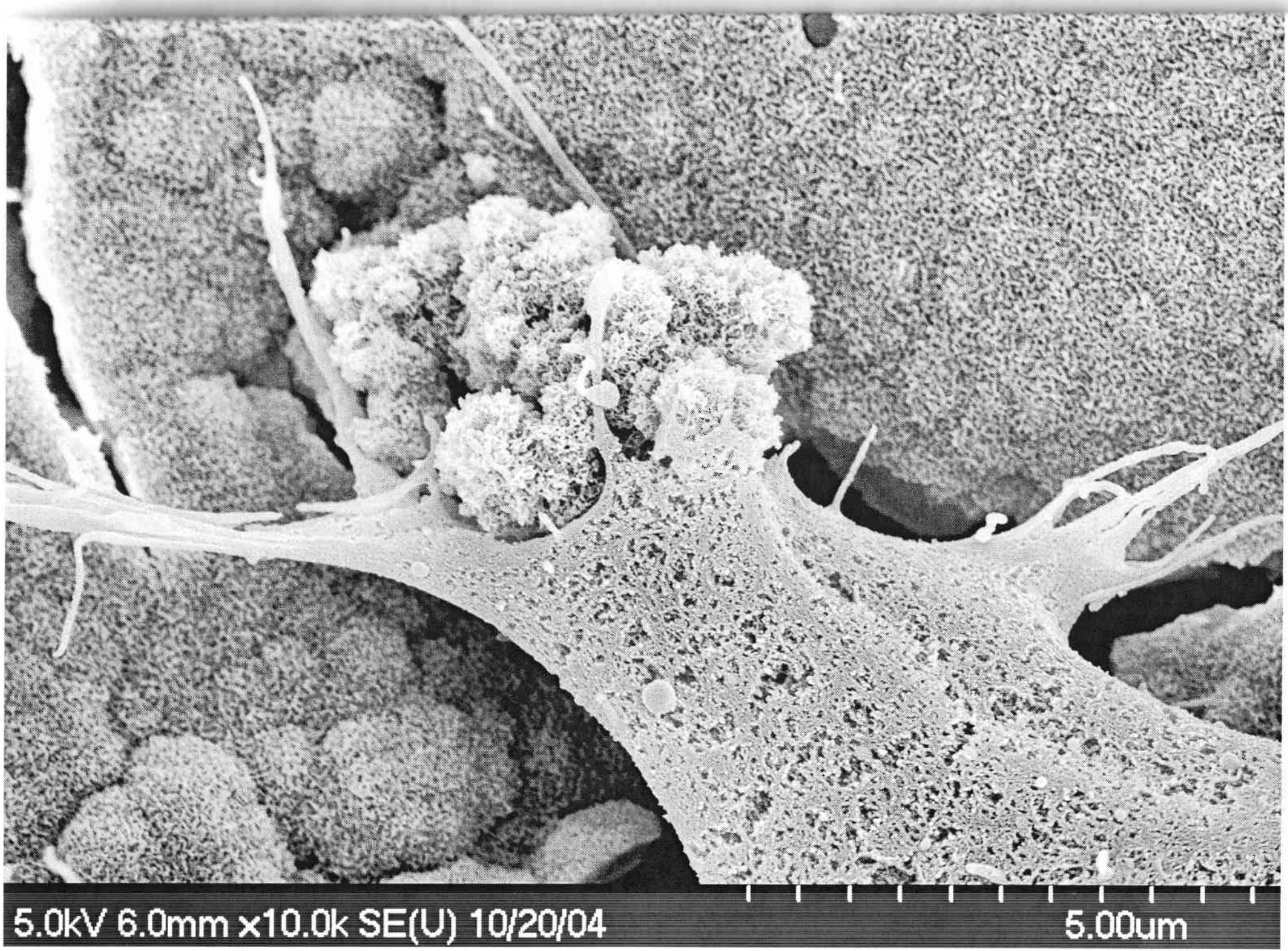
5.0kV 6.0mm x10.0k SE(U) 10/20/04
5.00um

4. Conclusion

It has been shown that Ca-P coatings can even be produced on pristine Al_2O_3 surfaces, which did not receive any prior treatment (like alkaline treatment). In the present study Ca-P coating applied by direct pyrolysis of these transparent solutions to about 250 to 565°C directly on the immersed substrates without ageing the coating sol. The aim of this direct pyrolysis process was just to impart the surface of a bionert ceramic with an intermediate layer of Ca-P's. Ca-P surfaces can then readily be coated/converted into carbonated, apatitic calcium phosphates by soaking in supersaturated Ca-P solutions, such as SBF. SBF soaking of the CaP-coated samples changed the chemistry and morphology of the coating into carbonated calcium deficient hydroxyapatite. *In vitro* study was established the preferred pyhsico-chemical surface characteristics for the osteoblast cell growth.

References

[1] J. B. Park (ed.), "Biomaterials; princibles and applications," CRC press 21-55 (2003)

[2] P. Ducheyne, Q. Qui, "Bioactive ceramics: the effect of surface reactivity on bone formation and bone cell function," Biomaterials 20(23-24) 2287-2303 (1999)

[3] J. B. Park, "Biomaterials; an introduction," Plenum Press 117-140 (1992)

[4] L. L. Hench, "Sol-gel materials for bioceramic applications," Current Opinion in Solid State & Materials Science 2 604-610 (1997)

[5] K. Hayashi, N. Matsuguchi, K. Uenoyama, Y. Sugioki, "Re-evaluation of the biocompatibility of bioinert ceramics *in vivo*," Biomaterials 13(4) 195-200 (1992)

[6] I. Dion, L. Bordenave, R. Lefebvre, R. Bareille, C. H. Baquey, J. R. Monties, P. Havlik, "Physico-chemistry and cytotoxicity of ceramics," Journal of Materials Science- Materials in Medicine 5(1) 18-23 (1994)

[7] H. Mittelmeir, J. Heisel, "Sixteen-years' experience with ceramic hip prostheses," Clinical Orthopedics and Related Research 282 64-72 (1992)

[8] J. M. Dorlot, "Long-term effects of alumina components in total hip prostheses," Clinical Orthopedics and Related Research 282 47-51 (1992)

[9] W. Suchanek, M. Yoshimura, "Processing and properties of hydroxyapatite-based biomaterials for use as the hard tissue replacement implants," Journal of Materials Research 13(1) 94-117 (1998)

[10] K. S. Katti, "Biomaterials in total joint replacement," Colloids and Surfaces B: Biointerfaces 39 133-142 (2004)

[11] I. J. McColm, "Ceramic hardness," Plenum Press 255-264 (1990)

[12] W. H. Gitzen, (ed.), "Alumina as ceramic material," The America Ceramic Society 43-62 (1970)

[13] H. W. Kim, H. E. Kim, J. C. Knowles, "Hard-tissue-engineered zirconia porous scaffolds with hydroxyapatite sol-gel and slurry coatings," Journal of Biomedical Materials Research Part B-Applied Biomaterials 70B(2) 270-277 (2004)

[14] G. W. Jiang, D. L. Shi, "Coating of hydroxyapatite on porous alumina substrate through a thermal decomposition method," Journal of Biomedical Materials Research 48(2) 177-120 (1999)

[15] P. J. Li, C. Ohtsuki, T. Kokubo, K. Nakanishi, N. Soga, K. DeGroot, "The role of hydrated silica, titania, and alumina in inducing apatite on implants," Journal of Biomedical Materials Research 28(1) 7-15 (1994)

[16] K. Soballe, S. Overgaard, "The current status of hydroxyapatite coating of prostheses," Journal of Bone and Joint Surgery 78B 689-691 (1996)

[17] L. M. Sun, C. C. Berndt, K. A. Gross, A. Kucuk, "Material fundamentals and clinical performance of plasma-sprayed hydroxyapatite coatings: A review," Journal of Biomedical Materials Research 28(5) 570-592 (2001)

[18] S. Overgaard, "Calcium phosphate coatings for fixation of bone implants," Acta Orthopedia Scandinavia 71(Suppl. 297) 1-59 (2000)

[19] L. M. Sun, C. C. Berndt, K. A. Khor, N. H. Cheang, K. A. Gross, "Surface characteristics and dissolution behavior of plasma-sprayed hydroxyapatite coating," Journal of Biomedical Materials Research 62(2) 228-236 (2002)

[20] R. Wang, Y. X. Hu, "Patterning hydroxyapatite biocoating by electrophoretic deposition," Journal of Biomedical Materials Research Part A 67(A) 270-275 (2003)

[21] J. Ma, C. H. Liang, L. B. Kong, C. Wang, "Colloidal characterization and electrophoretic deposition of hydroxyapatite on titanium substrate," Journal of Materials Science –Materials in Medicine 14(9) 797-801 (2003)

[22] V. Nelea, H. Pelletier, D. Muller, N. Broll, P. Mille, C. Ristoscu, I. N. Mihailescu, "Mechanical properties improvement of pulsed laser-deposited hydroxyapatite thin films by high energy ion-beam implantation," Applied Surface Science 186 483-489 (2002)

[23] J. M. Choi, H. E. Kim, I. S. Lee, "Ion-beam-assisted deposition (IBAD) of hydroxyapatite coating layer on Ti-based metal substrate," Biomaterials 21 469-473 (2000)

[24] B. Mavis, A. C. Tas, "Dip coating of calcium hydroxyapatite on Ti6Al4V substrates," Journal of the American Ceramic Society 83(4) 989-991 (2000)

[25] M. Manso, M. Langlet, C. Jimenez, J. M. Martinez-Duart, "Hydroxyapatite coatings obtained by the thermal activation of polymeric sols," International Journal of Inorganic Materials 3 1153-1155 (2001)

[26] H. W. Kim, H. E. Kim, V. Salih, J. C. Knowles, "Hydroxyapatite and titania sol-gel composite coatings on titanium for hard tissue implants; Mechanical and *In Vitro* biological performance," Journal of Biomedical Materials Research part B-Applied Biomaterials 72(B) 1-8 (2005)

[27] H. W. Kim, Y. H. Noh, L. H. Li, S. Lee, H. E. Kim, "Hydroxyapatite coating on titanium substrate with titania buffer layer processed by sol gel method," Biomaterials 25 2533-2538 (2004)

[28] H. W. Kim, Y. M. Kong, C. J. Bae, Y. H. Noh, H. E. Kim, "Sol gel derived fluor-hydroxyapatite biocoatings on zirconia substrate," Biomaterials 25 2919-2926 (2004)

[29] S. Jalota, "Evaluation of apatite inducing ability of SBF solutions on titanium alloys, calcium phosphate nanowhiskers and TTCP powders," Ms Thesis, Clemson University, SC. (2004)

[30] P. Habibovic, "Biomimetic hydroxyapatite coating on metal implants," Journal of the American Ceramic Society 85(3) 517-522 (2002)

[31] H. Q. Nguyen, D. A. Deporter, R. M. Pillar, N. Valiquette, R. Yakubovic, "The effect of the sol-gel-formed calcium phosphate coatings on bone ingrowth and osteoconductivity of porous-surfaced Ti alloy implants," Biomaterials 25 865-876 (2004)

[32] C. S. Chai, B. Ben-Nissan, "Bioactive nanocystalline sol-gel hydroxyapatite coatings," Journal of Materials Science-Materials in Medicine 10 465-469 (1999)

[33] W. Weng, J. L. Batista, "Preparation and characterization of hydroxyapatite coatings on Ti6Al4V alloy by sol-gel method," Journal of the American Ceramic Society 82(1) 27-32 (1999)

[34] K. Hwang, Y. Lim, "Chemical and structural changes of hydroxyapatite films by using a sol-gel method," Surface & Coating Technology 115 172-175 (1999)

[35] M. Manso, M. Langlet, C. Jimenez, J. M. Martinez-Duart, "Microstructural study of aerosol-gel derived hydroxapatite coatings," Biomolecular Engineering 19 63-66 (2002)

[36] A.C. Pierre, "Introduction to sol-gel processing," Kluwer Academic Publishers 50-70 (1998)

[37 C. S. Chai, K. A. Gross, B. Ben-Nissan, "Critical aging of hydroxyapatite sol-gel solutions," Biomaterials 19 2291-2296 (1998)

[38] L. Gan, R. M. Pillar, "Calcium phosphate sol-gel-derived thin films on porous-surfaced implants for enhanced osteoconductivity. Part I: Synthesis and characterization," Biomaterials 25 5303-5312 (2004)

[39] H. W. Kim, H. E. Kim, J. C. Knowles, "Hydroxyapatite and fluor-hydroxyapatite layered film on titanium processed by a sol-gel route for hard-tissue implants," Journal of Biomedical Materials Research part B-Applied Biomaterials 71B(1) 66-76 (2004)

[40] H. W. Kim, H. E. Kim, J. C. Knowles, "Fluor-hydroxyapatite sol gel coating on titanium substrate for hard tissue implants," Biomaterials 25 3351-3358 (2004)

[41] D. B. Haddow, P. F. James, R. V. Noort, "Sol-gel derived calcium phosphate coatings for biomedical applications," Journal of Sol-Gel Science and Technology 13 261-265 (1998)

[42] H. W. Kim, G. Georgiou, J. C. Knowles, Y. H. Noh, H. E. Kim, "Calcium phosphates and glass composite coatings on zirconia for enhanced biocompatibility," Biomaterials 25 4203-4213 (2004)

[43] K. A. Gross, C. S. Chai, G. S. K. Kannanga, B. Ben-Nissan, L. Hanley, "hydroxyapatite coatings via sol-gel synthesis," Journal of Materials Science: Materials in Medicine 9 839-843 (1998)

[44] M. F. Hsieh, L. H. Perng, T. S. Chin, H. G. Perng, "Phase purity of sol-gel derived hydroxyapatite ceramic," Biomaterials 22 2601-2607 (2001)

[45] D. M. Liu, T. Troczynski, W. J. Tseng, "Water based sol-gel synthesis of hydroxyapatite: process development," Biomaterials 22 1721-1730 (2000)

[46] A. C. Tas, "Synthesis of biomimetic Ca-hydroxyapatite powders at 37°C in synthetic body fluids," Biomaterials 21 1429-1438 (2000)

[47] D. Bayraktar, A. C. Tas, "Chemical preparation of carbonated calcium hydroxyapatite powders at 37C in urea-containing synthetic body fluids," Journal of the European Ceramic Society 19 2573-2579 (1999)

[48] D. M. Liu, T. Troczynski, D. Hakimi, "Effect of hydrolysis on the phase evolution of water based sol-gel hydroxyapatite and its application to bioactive coatings," Journal of Materials Science: Materials in Medicine 13 657-665 (2002)

[49] M. F. Hsieh, T. S. C hin, L. H. Perng, H. G. Perng, "Gel-to-ceramic conversion during hydroxyapatite synthesis," Journal of the American Ceramic Society 84(9) 2123-2125 (2001)

[50] A. C. Tas, "X-Ray diffraction data for flux-grown calcium hydroxyapatite whiskers," Powder Diffraction 16(2) 102-106 (2001)

[51] A. A. Braig, J. L. Fox, R. A. Young, Z. Wang, J. Hsu, W. I. Higuchi, A. Chettry, H. Zhuang, M. Otsuka, "Relationships among carbonated apatite solubility, crystalline size, and microstrain parameters," Calcified Tissue International 64 437-449 (1999)

[52] D. L. Shi, G. W. Jiang, J. Bauer, "The effect of structural characteristics on the in vitro bioactivity of hydroxyapatite," Journal of Biomedical Materials Research 6(1) 71-78 (2002)

[53] S .J. Gadaleta, E. P. Paschalis, F. Betts, R. Mendolsohn, A. L. Boskey, "Fourier transform infrared spectroscopy of the solution-mediated conversion of amorphous calcium phosphate to hydroxyapatite: new correlations between X-Ray diffraction and infrared data," Calcified Tissue International 58 9-16 (1996)

[54] A. Beganskiene, "Water based sol-gel synthesis of hydroxyapatite," Materials Science 9(4) 383-386 (2003)

[55] C. Rey, M. Shimizu, B. Collins, B. Glimcher, "Resolution-enhanced Fourier transform infrared spectroscopy study of the environment of phosphate ion in the early deposits of a solid phase of calcium phosphate in bone and enamel and their evolution with age: 2. investigations in the v_3 PO_4 domain," Calcified Tissue International 49 383-388 (1991)

[56] C. Rey, V. Renugopalakrishnan, B. Collins, B. Glimcher, "Fourier transform infrared spectroscopic study of the carbonate ions in bone mineral during aging," Calcified Tissue International 49 251-258 (1991)

[57] E. P. Paschalis, E. DiCarlo, F. Betts, P. Sherman, R. Mendelsohn, A. L. Boskey, "FTIR microspectroscopic analysis of human osteonal bone," Calcified Tissue International 59 480-487 (1996)

[58] R. A. Nyquist, "Infrared spectra of inorganic compounds," Academic Press 206-207 (1971)

THESIS

SURFACE MODIFICATIONS OF THE ALUMINA CERAMIC FOR BIOMEDICAL APPLICATIONS

Baris Kokuoz